MIDWESTERN UNIVERSITIES RESEARCH ASSOCIATION

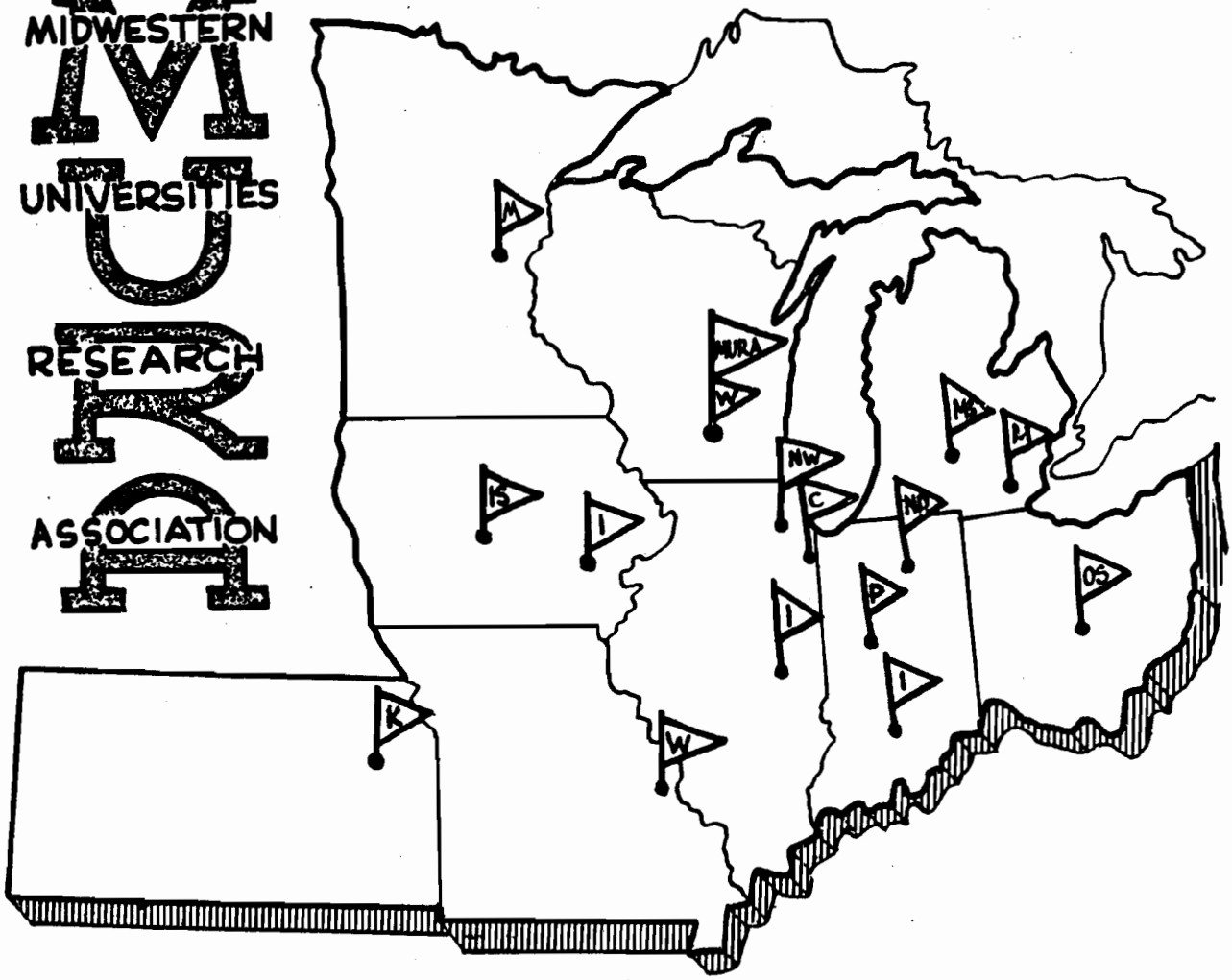

NONLINEAR AZIMUTHAL SPACE CHARGE EFFECTS IN PARTICLE ACCELERATORS

R. A. DORY

REPORT NUMBER 654

LEGAL NOTICE

This report was prepared as an account of Government sponsored work. Neither the United States, nor the Commission, nor any person acting on behalf of theCommission:

A. Makes any warranty or representation, expressed or implied, with respect to the accuracy, completeness, or usefulness of the information contained in this report, or that the use of any information, apparatus, method, or process disclosed in this report may not infringe privately owned rights; or

B. Assumes any liabilities with respect to the use of, or for damages resulting from the use of any information, apparatus, method, or process disclosed in this report.

As used in the above, "person acting on behalf of the Commission" includes any employee or contractor of the Commission, or employee of such contractor, to the extent that such employee or contractor of the Commission, or employee of such contractor prepares, disseminates, or provides access to, any information pursuant to his employment or contract with the Commission, or his employment with such contractor.

Printed in USA. Price $2.50. Available from the

Office of Technical Services
U. S. Department of Commerce
Washington 25, D. C.

NONLINEAR AZIMUTHAL SPACE CHARGE EFFECTS IN PARTICLE ACCELERATORS

BY

R. A. DORY

A thesis submitted in partial fulfillment of the requirements for the degree of

DOCTOR OF PHILOSOPHY
(Physics)

at the

UNIVERSITY OF WISCONSIN

1962

MURA-654
UC-28: Particle Accelerators and
High Voltage Machines
TID-4500 (16th Edition)

MIDWESTERN UNIVERSITIES RESEARCH ASSOCIATION*
2203 University Avenue, Madison, Wisconsin

NONLINEAR AZIMUTHAL SPACE CHARGE EFFECTS IN PARTICLE ACCELERATORS

R. A. DORY
August 10, 1962

ABSTRACT

Numerical methods have been developed to simulate solution of the Vlasov equation governing the (one-dimensional) azimuthal motion of particles in circular accelerators. Unlike previous analytical solutions, these are not restricted to consideration of small perturbations. The numerical methods are used to analyze particle distributions thought to be representative of those to be found in existing accelerators. The results are found to be in accord with recent experimental data, in that the following features were found. Above transition energy, the Coulomb interaction of the particles causes formation of long-lived bound clusters of particles. Such clusters tend to follow single-particle orbits in synchrotron phase space, even when radio-frequency acceleration fields are present. When clusters interact, they can coalesce and orbit as entities about one another in the phase space. Below transition, beam bunching may occur because of nonlinear instabilities of the beam, or with a fairly simple mechanism, there develop two-stream velocity distributions which can be unstable. A symmetry principle is discussed, showing the equivalence of the "negative-mass" instability and the two-stream instability.

*AEC Research and Development Report. Research supported by U. S. Atomic Energy Commission Contract No. AT(11-1)-384.

NONLINEAR AZIMUTHAL SPACE CHARGE

EFFECTS IN PARTICLE ACCELERATORS

CONTENTS

INTRODUCTION 1

I. THE THEORY AND EXPERIMENTAL OBSERVATIONS 4

Background 4

The Space Charge Field 8

The Vlasov Equation 13

Linearization and Dispersion Theory 14

Stationary States 18

Nonlinear Motion 24

Resume of Physical Experiments 28

II. COMPUTER EXPERIMENTS 29

Mesh Solution of the Vlasov Equation 29

Following the Motion of Particles 32

Stability of Clusters Above Transition Energy 40

Limiting Energy Spreads 43

Space Charge Clusters in RF Buckets 44

Following the Motion of Boundaries 46

Beams above Transition Energy 50

Beams below Transition Energy 52

CONCLUSIONS 58

ACKNOWLEDGEMENTS 62

APPENDIX I. AN APPROXIMATION TO THE RELATIVISTIC FIELD 63

APPENDIX II. THE PARTICLE FOLLOWING PROGRAM 67

APPENDIX III. THE BOUNDARY FOLLOWING PROGRAM 100

FIGURE INDEX

The following table lists the figures by number, giving the location of the page which the figure follows and a brief identification of the figure. Further details appear in the figure captions and in the text.

Figure	Page	Description
1	9	Cutaway view of vacuum tank.
2	16	A two-stream velocity distribution.
3	19	Three stationary nonuniform distributions.
4	33	Typical kernel (physical).
5	38	Typical kernel (computational).
6	38	Evolution of monoenergetic beam above transition.
7	38	Growth rate of negative instability as function of time.
8	41	Sample histogram from particle following program.
9	44	Relation between initial and final energy spreads in negative-mass-unstable uniform beam.
10	47	Topology of phase boundaries.
11	48	Sample giving failure of area computation.
12	50	Boundary motion, zero field.
13	50	Boundary motion, weak field.
14	50	Boundary motion, medium field.
15	51	Boundary motion, cluster formation.

Figure	Page	Description
16	51	Boundary motion, cluster formation.
17	52	Boundary motion, cluster evolution.
18	52	Boundary motion, cluster evolution.
19	54	Distribution at injection.
20	55	Beam bunching below transition.
21	55	Beam bunching below transition.
22	56	Beam bunching below transition.
23	57	Bunched beam below transition, initial state.
24	57	Bunched beam below transition, evolved state.
25	70	Phase trajectories from particle following program.
26	70	Phase distribution from particle following program.

REFERENCES

1. M. Q. Barton and C. E. Nielsen, Proceedings of the Brookhaven International Conference on High Energy Accelerators (Brookhaven, New York, 1961).
2. C. E. Nielsen, A. M. Sessler, and K. R. Symon, Proceedings of the International Conference on High Energy Accelerators (CERN, Geneva, 1959), p. 239.
3. C. E. Nielsen and A. M. Sessler, Rev. Sci. Instr. 30, 80 (1959).
4. D. C. Morin, Jr., Ph.D. Thesis, University of Wisconsin, 1962.
5. D. C. Morin, Jr., (private communication).
6. E. M. Rowe, MURA Technical Note TN-296, 1962 (unpublished).
7. M. S. Livingston and J. P. Blewett, Particle Accelerators (McGraw-Hill Book Co., Inc., New York, 1962).
8. K. R. Symon and A. M. Sessler, Proceedings of CERN Symposium on High Energy Accelerators and Pion Physics (CERN, Geneva, 1956), Vol. 1, p. 44.
9. L. W. Jones, C. H. Pruett, K. R. Symon, and K. M. Terwilliger, Proceedings of the International Conference on High Energy Accelerators (CERN, Geneva, 1959), p. 58.
10. A. Becher, MURA Report No. 458, 1959 (unpublished). MURA reports are available from the Office of Technical Services, U. S. Department of Commerce, Washington 25, D. C.

11. R. L. Mills and A. M. Sessler, MURA Report No. 433, 1958 (unpublished).

12. M. Mitchner, Radiation and Waves in Plasmas, (Stanford University Press, Stanford, California, 1961) Chapter I.

13. H. G. Hereward, Bevatron Internal Report BEV-524, 1960 (unpublished).

14. M. Seidl, Proceedings of the International Conference on High Energy Accelerators (CERN, Geneva, 1959), p. 327.

15. D. W. Kerst et al., Rev. Sci. Instr. 31, 1076 (1960).

16. A. V. Haeff, Proc. Inst. Radio Engrs. 37, 1024 (1949).

17. A. M. Sessler, MURA Report No. 442, 1959 (unpublished).

18. C. E. Nielsen and A. M. Sessler, MURA Report No. 480, 1959 (unpublished).

19. R. S. Christian (private communication).

20. R. D. Richtmyer, Difference Methods for Initial Value Problems (Interscience Publishers, Inc., New York, 1957).

21. C. Lanczos, Applied Analysis (Prentice Hall, Inc., Englewood Cliffs, New Jersey, 1961).

22. E. M. Rowe (private communication).

23. P. M. Morse and H. Feshbach, Methods of Theoretical Physics (McGraw-Hill Book Co., Inc., New York, 1953).

24. Bateman Manuscript Project, Tables of Integral Transforms (McGraw-Hill Book Co., Inc., New York, 1954).

25. IBM Form C28-6106 (International Business Machines Corporation, White Plains, New York, 1961).

26. IBM Form A22-6500-3 (International Business Machines Corporation, White Plains, New York, 1960).

27. G. A. Westlund, MURA Report No. 580, 1960 (unpublished).

28. G. A. Westlund, MURA Report No. 536, 1959 (unpublished).

29. G. A. Westlund, MURA Report No. 562, 1960 (unpublished).

30. G. A. Westlund, MURA Report No. 550, 1960 (unpublished).

31. R. S. Christian (to be available as a MURA report).

32. California Computer Products, Inc., Downey, California, Digital Incremental Recorder Model 563.

33. G. A. Westlund and V. W. Pratt, MURA Report No. 607, 1961 (unpublished).

34. G. A. Westlund, MURA Report No. 601, 1961 (unpublished).

35. V. K. Neil, D. L. Judd, and L. J. Laslett, Rev. Sci. Instr. 32, 267 (1961).

INTRODUCTION

Recent experiments at the Cosmotron by Barton and Nielsen[1] have indicated that the theory of the longitudinal or azimuthal motion of a circular accelerator beam under the influence of its own Coulomb (space charge) field as carried out by Nielsen, Sessler, and Symon,[2] is a substantially good approximation to the physical behavior of the system. However, because the theory has been limited so far to a linearized calculation, a number of the experimentally observed phenomena have not been well understood.

The theory neglects all interaction of the azimuthal motion with radial and vertical degrees of freedom except insofar as these are counted upon to provide a beam consisting of a toroidal tube of charge with not too great spread in energy or position transverse to the beam direction. It is desirable to know which of the observed phenomena can be explained by the mathematical model when it is not restricted to linear effects.

The general result of a longitudinal instability is an increase in the energy spread of the circulating beam, and because the energy spread which can be tolerated without substantial loss of particles is generally limited to values not far different from those injected into an accelerator, it seems clear that more theoretical understanding of the instabilities

is needed. The linear theory by its nature cannot predict the final energy spread attained in an unstable case. Similarly, it cannot predict or describe the type of resonance often found in the presence of large disturbances in complex systems. Because the perturbations on actual accelerator beams need not be small, the excitation of such nonlinear resonances cannot be neglected.

The analytical extension to the nonlinear region has thus far proved to be very difficult, and only a very few general results have been obtained. For this reason, two simple but fairly effective representations of the mathematical model have been developed. Using numerical techniques and a high speed digital computer, these allow the nonlinear motion to be studied.

These representations use all the simplifying assumptions made in the previous work except that the interaction of a disturbance with itself may be neglected. One major assumption is that the parameters of the machine do not vary with time. As noted by Nielsen and Sessler,[3] time variations which are small in times of the order of the characteristic times of the azimuthal motion, will not change the results significantly. This is exactly true in FFAG (fixed-field alternating-gradient) machines of type designed by MURA, and is reasonably accurate for the Cosmotron.

With the numerical calculations, we find that many of the experimental phenomena are observed and to a certain extent explained, on the

basis of the longitudinal motion alone. In order to further understand the entire physical system, extensions are currently being made at MURA on the related problem of the effects of space charge on the motion transverse to the beam;[4] and, with not too much success so far, on the interaction between the azimuthal and transverse collective motions.[5]

In Section I of this paper the linear theory is briefly explained, some supplementary information found during this investigation is given, and pertinent results of the Cosmotron experiment[1] and recent studies made with the MURA 50 Mev test model[6] are discussed.

In Section II are presented a short discussion of previous numerical calculations of the nonlinear dynamics, explanation of the two numerical procedures used in the present study, descriptions of the results, and comparisons with the experimental phenomena.

Appendix I contains an extension of the space charge field calculation into the relativistic region.

Appendices II and III present the actual computer codes used, and enough description to allow them to be deciphered by someone familiar with the Fortran programing system.

I. THE THEORY AND EXPERIMENTAL OBSERVATIONS

We outline the mathematical model of the azimuthal motion of charged particles under the influence of their own collective Coulomb field and of possible radio-frequency (RF) fields applied externally. A complete and rigorous discussion of most of these results is given by Nielsen, Sessler, and Symon.[2]

Background. The properties of the external magnetic guide fields in the circular accelerator are neglected, except that the fields are required to vary appropriately in the radial, azimuthal, and vertical directions, so that a family of particle orbits which are bounded by the vacuum tank exists. Generally then, for a given particle energy, there is an equilibrium orbit which is stable against small perturbations and is characterized as being closed, or periodic in the azimuthal angle with period 2π. A particle on an equilibrium orbit has a known frequency of revolution which is given as a function $f(E)$ of the particle energy. Within well known stability limits, a particle perturbed from an equilibrium orbit will follow an orbit with different periodicity, but will remain close to the equilibrium orbit. Comprehensive discussions of orbit theory may be found in many books about accelerators.[7]

The azimuthal motion of a particle may be described in terms of an equivalent angular distance θ along an equilibrium orbit. This is

closely equal to the azimuthal position of the particle in the vacuum tank, the deviation of the orbits from circles being neglected in the analysis. A variable w related to the single particle energy may be defined, allowing a Hamiltonian formulation of the equations for the longitudinal motion. The equations are

$$\begin{aligned} d\theta/dt &= \omega(w), \\ dw/dt &= 2\pi e R\, \mathcal{E}_\theta(\theta,t), \end{aligned} \tag{1}$$

where

$$\omega(w) = 2\pi f(E), \qquad \text{and} \qquad w(E) = \int_{E_0}^{E} dE' \, [f(E')]^{-1},$$

and E_0 is a convenient reference energy. Here R is the equivalent orbit radius, or the length of the orbit divided by 2π, and the azimuthal field $\mathcal{E}_\theta$ has two possible contributions, the space charge or beam self-interaction term and the term caused by the application of external radio-frequency (RF) accelerating fields. The RF term has little net effect except when the RF is in resonance with the rotation frequency of the particles and causing them to change energy rapidly. For detailed explanations of this the reader is referred to the paper by Symon and Sessler,[8] and for experimental verification to that by Jones et al.[9]

These motion equations are derivable from a Hamiltonian of the form

$$\mathcal{H}(w,\theta) = 2\pi E(w) + 2\pi e R\, U(\theta,t), \tag{2}$$

where

$$2\pi E(w) = \int \omega(w)\, dw \qquad \text{and} \qquad \mathcal{E}_\theta = -\frac{\partial}{\partial\theta} U(\theta,t)$$

In most sections of this paper, the particle beam will be taken to extend over a range in energy which is small enough to allow neglect of terms higher than order two in the w power series expansion of $E(w)$ about some point w_s. Then

$$E(w) \simeq E(w_s) + 2\pi\omega(w_s)(w-w_s) + \pi \left.\frac{d\omega}{dw}\right|_{w_s} \cdot (w-w_s)^2.$$

If we now measure angles in a coordinate system rotating with the beam at frequency $\omega(w_s)/2\pi$, the Hamiltonian becomes

$$\mathcal{H}(w,\varphi) \simeq \frac{1}{2} f \left.\frac{df}{dE}\right|_{w_s} (w-w_s)^2 + 2\pi e R\, U(\varphi + t\cdot\omega(w_s), t),$$

except for constants. Furthermore if $w-w_s$ is measured in the appropriate units, the number $f \left.\frac{df}{dE}\right|_{w_s}$ may be taken as ∓ 1. The minus or plus sign is to be taken if the beam is above or below transition energy, above which the number df/dE is negative, and since the motion changes radically under change of this sign, the alternatives will be carried specifically. Near transition energy, higher terms must be taken in the expansion of $E(w_s)$. We reserve the letters (W,φ) for measurements in this system and set of units. The Hamiltonian is

$$H(W,\varphi) = \mp\frac{1}{2} W^2 + 2\pi e R\, U(\varphi + t\cdot\omega(w_s), t), \tag{3}$$

and the motion equations are

$$\begin{aligned} d\varphi/dt &= \mp W, \\ dW/dt &= 2\pi e R\, \mathcal{E}_\theta(\varphi + t\cdot\omega(w_s), t). \end{aligned} \tag{4}$$

The negative sign in (3) can lead to a "negative mass instability," so-called on comparison of (3) with the Hamiltonian for a pair of non-relativistice particles of charge e and mass m in free space:

$$H = \tfrac{1}{2} m^{-1}(p_1^2 + p_2^2) + eU, \quad \text{where} \quad U \propto e/|\vec{r}_1 - \vec{r}_2|.$$

In the scaled coordinates, the effect of the RF fields may be easily included by adding to the azimuthal space charge field, a term

$$-\dot{W}_s + V \sin \varphi,$$

where $\dot{W}_s$ is the rate of change of w_s for a "synchronous" particle which stays in phase with the RF fields while these are frequency modulated to accelerate the particles. The value V is the maximum energy per turn which a particle can gain from the RF field.

If we choose the point w_s for expansion of the function $E(w)$, then the (W, φ) coordinate system is accelerated with a synchronous particle, so that particles which are not accelerated have their coordinate W decreased with time at an average rate $\dot{W}_s$. Particles accelerated will remain in the vicinity of $w = w_s$ or $W = 0$ and execute "synchrotron" oscillations about the synchronous point. Above the transition energy, the region of stable oscillations is bounded, in the absence of space charge fields, by the curve

$$W^2 = -2\dot{W}_s(\pi - \varphi) + 2V(1 + \cos \varphi),$$

and below transition energy by the curve

$$W^2 = -2\dot{W}_s(\varphi) + 2V(1 - \cos \varphi).$$

The stable region is called an RF "bucket." The acceleration has been assumed to be at the first harmonic of the particle revolution frequency, but this is inessential to our later arguments. The reader is again referred to Symon and Sessler[8] and to Nielsen and Sessler[3] for futher

details.

We will analyze the collective motion of a particle beam in terms of a distribution function Ψ in the two-dimensional μ space (W, φ). Then $\Psi(W,\varphi,t)\cdot\Delta W\cdot\Delta\varphi$ gives the number of particles at time t in the ΔW by $\Delta\varphi$ rectangle centered at W and φ. The distribution will be periodic in φ with period 2π, and will be taken to be identically zero outside the region of interest which is assumed to be bounded. Parts integration then is valid, and integrated terms are usually zero. When integrations over W are written, the limits implied are the edges of the region.

The Space Charge Field

For a given distribution of particles, we can calculate the space charge field. For completeness, we write the full relativistic wave equation and indicate how it can be solved, but we must soon specialize to the nonrelativistic limit to obtain tractable solutions.

We regard the beam as a collection of particles distributed throughout a thin tube extending around the accelerator at an average radius R. The particles are assumed to be on or oscillating about equilibrium orbits with random phases so that to good approximation, the beam is a tube of current. The azimuthal dependence of the charge density is given by $e\,\rho(\varphi,t)R^{-1}$ with the units charge/length, and in terms of the coordinates (x,y) which are transverse to the beam at the azimuth of observation, the true charge density is $e\,\rho(\varphi,t)Q(x,y)R^{-1}$.

The transverse distribution Q, of particles is held fixed in time and azimuth, and is taken to fall off quickly from its value at the center of the beam. The field used to find the average behavior of beam particles will be the actual field averaged over the distribution Q. The variation of particle orbit radii with energy in the beam may then be neglected. Figure 1 illustrates such a beam, and may clarify the coordinate system (x, y).

In terms of the operator

$$\nabla_2^2 \equiv \frac{\partial^2}{\partial x^2} + \frac{\partial^2}{\partial y^2},$$

which is so written to emphasize that little notice will be taken of the curvature of the vacuum tank, the wave equation for the field is

$$\left(\nabla_2^2 + \frac{1}{R^2}\frac{\partial^2}{\partial\theta^2} - \frac{1}{c^2}\frac{\partial^2}{\partial t^2}\right)\mathcal{E}_\theta(x,y,\theta,t) = \frac{4\pi}{R}\frac{\partial}{\partial\theta}P(x,y,\theta,t) + \frac{4\pi}{c^2}\frac{\partial}{\partial t}J(x,y,\theta,t), \quad (5)$$

where charge and current densities are

$$\begin{aligned} P(x,y,\theta,t) &= e\,Q(x,y)\int R^{-1}\,\Psi(w,\ \theta-\omega(w_0)t,t)\,dw, \\ J(x,y,\theta,t) &= e\,Q(x,y)\int \omega(w)\,\Psi(w,\theta-\omega(w_0)t,t)\,dw. \end{aligned} \quad (6)$$

The azimuthal charge density is

$$\rho(\varphi,t) = \int \Psi(w,\varphi,t)\,dw.$$

The boundary conditions are that $\mathcal{E}_\theta$ should vanish on the tank walls and should be periodic in θ with period 2π.

Since $Q(x,y)$ is taken as fixed, the transverse variation of $\mathcal{E}_\theta(x,y,\theta,t)$ may be separated and written down in terms of the

Fig. 1. Cutaway view of vacuum tank and circulating beam, showing coordinates used.

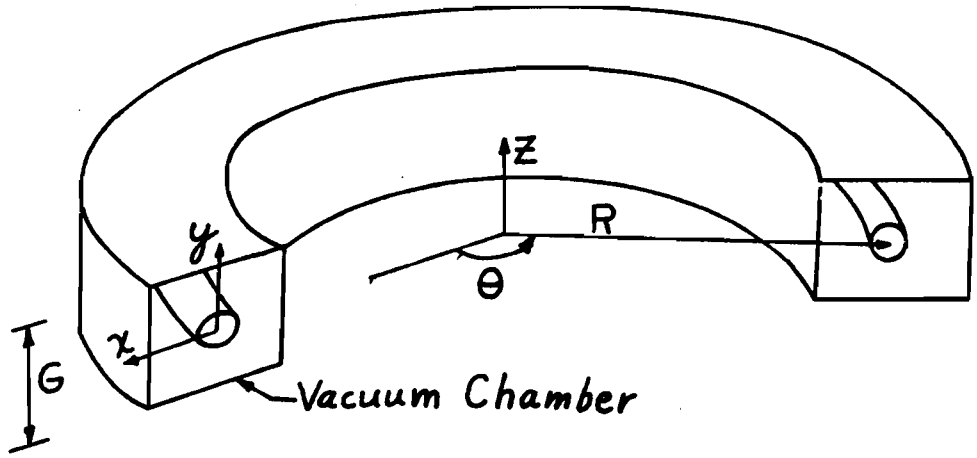

Figure 1

eigenfunctions g_j of ∇_2^2 and the corresponding eigenvalues $-K_j/R^2$. The subscript j symbolizes a two-parameter set of indices. As discussed in Nielsen, Sessler and Symon,[2] this separation is dependent upon the assumption that the radius R is very large. The general effect of this failure to separate exactly, is the possibility that the number K_j may be negative,[10] and that it is not completely independent of the variation of the field with θ. In terms of Fourier coefficients of index n, K_j depends upon n for very low values n.

The appropriate eigenfunction analysis of the remainder of the wave equation requires Fourier analysis in harmonics n, of the θ variation and Laplace transformation in frequencies iq, of the time dependence. If $F(x,y,\theta,t)$ is the source term on the right side of equation (5) and F_{jLF} and $\mathcal{E}_{jLF}$ are the full four-dimensional transformations of $F(x,y,\theta,t)$, and $\mathcal{E}_\theta(x,y,\theta,t)$, the wave equation becomes

$$\mathcal{E}_{jLF} = -F_{jLF} \cdot [n^2 + K_j - q^2\omega_0^{-2}]^{-1} R^2, \tag{7}$$

where $\omega_0 = c/R$ and $\mathcal{E}$ and $\partial\mathcal{E}/\partial t$ are zero at zero time.

Equation (7) may be inverted generally to yield $\mathcal{E}_\theta(x,y,\theta,t)$ when the charge and current densities are given. This result is not usable here, but shows the interesting behavior of fields in the geometry given. We will relegate the calculation to Appendix I and specialize to the more tractable nonpropagating limit.

As is pointed out in Nielsen, Sessler and Symon,[2] the simplest result of relativistic effects is the reduction of the space charge forces

by a factor γ^{-2}, where the momentum of a particle is γ times the classical value when the orbital radii of the particles are large compared to the transverse dimensions of the vacuum tank. We include this factor henceforth in the kernel which is to be calculated.

Since we must restrict ourselves to short wavelength perturbations in order that neglect of the curvature of the vacuum tank is accurate, the delay in propagation of field effects will be neglected also.

When propagation effects are neglected, the field calculation is an exercise in electrostatics. One correct method for performing the reduction to static fields is to take ω_0 in (7) as infinite and discard the term $q^2\omega_0^{-2}$ in the denominator. This is the latest point at which ω_0 may be made infinite without further worry about convergence in the process.

With this assumption, the solution for the field has been calculated by Nielsen and Sessler.[3] Thus, the Laplace transformation inversion is trivial and the Fourier series may be summed. We first note that F has reduced to $4\pi R^{-1}\partial/\partial\theta\, P(x,y,\theta,t)$, and $F_{jF}(t)$ to $4\pi R^{-1} in\, P_{jF}(t)$.

We may use the convolution theorem for Fourier series:

$$\left\{ \int_{-\pi}^{\pi} d\varphi' f(\varphi-\varphi') g(\varphi') \right\}_F = 2\pi \{f\}_F \cdot \{g\}_F , \tag{8}$$

and any table of Fourier series to perform the sum. Doing so, performing a symbolic inversion of the j transformation, and integrating over Q to get the average field seen by the beam, we obtain

$$\mathcal{E}(\varphi,t) \equiv \bar{\mathcal{E}}_\theta(\theta,t) = \int_{-\pi}^{\pi} d\varphi' \, \rho(\varphi-\varphi') K(\varphi'), \tag{9}$$

where the field kernel K has the Fourier transform

$$K_F = -in K_{UF} = -in \gamma^{-2} \cdot 2e \sum_j \bar{g}_j^2 / (K_j + n^2), \tag{10}$$

and is a sum of exponentials with characteristic widths $\Delta\varphi_j = (K_j)^{-1/2}$. We have defined K_{UF}, the Fourier amplitude of the kernel K_U with which $\rho(\varphi,t)$ must be convoluted to obtain the space charge potential U. Since the function $g^2/(\alpha^2+n^2)$ has the same behavior as K_{UF} for large and small values of n, we may expect that a rough estimate of the behavior of K_U is afforded by a single term in the sum on n. In that case, the kernel has the form

$$K(\varphi) \propto \frac{\varphi}{|\varphi|} \exp(-\alpha|\varphi|), \tag{11}$$

assuming that α is normally large, being of order of the ratio R/G, the machine radius divided by the vacuum tank height. This is clear simply from considering the shielding of electric fields by the vacuum tank. Thus, a charge will not have much effect on another at the same radius but an azimuth differing by more than G/R.

For comparison, the potential kernel for the one-dimensional solution to Laplace's equation is just proportional to $\varphi/|\varphi|$ which is the same as (11) with $\alpha = 0$.

The Motion Equation

In this section, the motion equation is discussed, a symmetry principle relating clusters of particles above transition and particle

deficiencies below is stated, the motion equation is linearized about the stationary uniform beam solution with $\rho(\varphi,t)$ constant, a dispersion relation is obtained, and simple instabilities are discussed. Other stationary states are described, and a prescription for finding useful eigenfunction expansions for them is demonstrated. Two examples are given where arguments may be made about the stability of states subjected to large perturbations.

<u>The Vlasov Equation.</u> We can now study the collective motion of particles since we have a method for approximating the fields.

In general, the equation governing the motion of particles is the Liouville equation in the $2N$ dimensional γ space $(W_1 - W_N, \varphi_1 - \varphi_N)$, where N is the number of particles. However, since we have tacitly assumed that close collisions of small numbers of particles may be neglected, an assumption justified by the calculations of Becher,[10] we can simplify the problem to solution of the Vlasov equation instead. This has been called the μ space (W,φ) Liouville equation and derived for the special case of accelerator beams by Mills and Sessler.[11] It is also equivalent to the collisionless Boltzmann equation since the only velocity dependent forces included in the theory are the electromagnetic ones. The general relationship between the Liouville and Vlasov equations is discussed by Simon.[12]

The equation is

$$\frac{d\Phi}{dt} = \frac{\partial\Phi}{\partial t} + 2\pi e R\, \mathcal{E}(\varphi,t)\, \frac{\partial\Phi}{\partial W} + \omega(W)\, \frac{\partial\Phi}{\partial\varphi} = 0. \tag{12}$$

A very important solution to this is given by

$$\Psi(W,\varphi,t) = \Psi^{\circ}(W,t), \tag{13}$$

which is a uniform distribution of particles around the machine. The density then is independent of φ, and the field is zero. The equation reduces to $\partial\Psi/\partial t = 0$, so that this state is stationary. It is this state which is attained by a coasting beam (no accelerating fields) if the particle density is sufficiently small and the energy spread is non-zero, because the particles have different circulating frequencies. If the density is slowly increased, or rather if in a number of experiments we increase the number of particles injected, the effect of perturbations on this stationary state can be large.

<u>Linearization and the Dispersion Theory.</u> Again following Nielsen, Sessler and Symon,[2] we may write out a first-order perturbation theory in the form of solution of (12) when it is linearized about the stationary uniform state.

If the perturbed system has the distribution $\Psi = \Psi^{\circ} + \psi$, where ψ is small compared to Ψ° at each point (W,φ), and $\mp W$ is written as $\omega(W)$, the equation takes the form:

$$\frac{\partial\psi}{\partial t} + 2\pi e R\mathcal{E}(\varphi,t)\,\frac{\partial\Psi^{\circ}}{\partial W} + \omega(W)\frac{\partial\psi}{\partial\varphi} = -2\pi e R\,\mathcal{E}(\varphi,t)\frac{\partial\psi}{\partial W}. \tag{14}$$

The right-hand side is of order ψ^2 while the left is of order ψ. The linearization consists of neglecting the second-order term. Laplace transformation of the time dependence and Fourier transformation of the azimuthal dependence are now natural. The entire procedure is

carried out in the reference last cited. One important result is the derivation of the dispersion relation for the system. This obtains quickly upon consideration of the harmonic trial solution

$$\psi(W,\varphi,t) = f(W)\ \exp(-in\varphi)\cdot \exp(-in\Omega t). \tag{15}$$

The field obtains from (9) in the form

$$\mathcal{E}(\varphi,t) = 2\pi i n\, K_{UF}\, \exp(-in\varphi)\exp(-in\Omega t)\int f(W')dW', \tag{16}$$

where $-in K_{UF}$ is the Fourier transform of the field kernel $K(\varphi)$ at harmonic n. The phase of K_{UF}, the transform of the potential kernel, has been chosen so that it is real. The trial solution then is a solution if

$$[\Omega + \omega(W)]f(W) - 2\pi e R\,\frac{\partial \Phi^0}{\partial W}\cdot 2\pi K_{UF}\int f(W')dW' = 0.$$

Isolating the f in the first term and integrating over W:

$$\int f(W)dW = 4\pi^2 e R K_{UF}\cdot\int f(W')dW'\cdot\int dW\,\frac{\partial \Phi^0}{\partial W}[\Omega + \omega(W)]^{-1}.$$

A non-trivial solution then must satisfy the dispersion relation

$$4\pi^2 e R K_{UF}\int dW\,\frac{\partial \Phi^0}{\partial W}[\Omega + \omega(W)]^{-1} = 1. \tag{17}$$

Solutions of this equation yield the normal modes.

If the signs of $\omega(W)$, $\partial\Phi^0/\partial W$, and Ω are all changed, equation (17) is not changed. A state subjected to this "inversion" then retains all its modes. Since $\omega(W)$ is $\mp W$, the inversion just displaces the system from above to below transition or the reverse, and interchanges the roles of particle excesses and particle deficiencies.

Nielsen, Sessler, and Symon[2] prove a theorem stating that the solutions Ω_i, of (17) occur in complex conjugate pairs. The inversion then interchanges the roles of damping and antidamping modes, and reverses the direction of propagating modes. The "symmetry" property is a special example of the invariance of (12) under the replacements of $\omega(W)$ by $-\omega(W)$, t by $-t$, and $\Psi(W,\phi,t)$ by $\text{constant} - \Psi(W,\phi,t)$. This symmetry principle is important because it says that each property of a particle beam above transition energy has one and only one analogue for a beam below.

We may see one consequence of the symmetry by choosing a simple initial distribution $\Psi^{\circ}(W)$ in the form of a set of step functions:

$$\Psi^{\circ}(W) = \begin{cases} 0 & \text{if} \quad W_2 < |W|, \\ \sigma & \text{if} \quad W_1 < |W| < W_2, \\ \sigma - S & \text{if} \quad 0 < |W| < W_1. \end{cases} \tag{18}$$

This is shown in Fig. 2. We may take $\partial\Psi^{\circ}/\partial W = \pm\sigma\,\delta(W \pm W_2) \mp S\,\delta(W \pm W_1)$ to obtain from (17), the expression:

$$\frac{\omega_2 \sigma r}{\Omega^2 - \omega_2^2} - \frac{\omega_1 S r}{\Omega^2 - \omega_1^2} = 1. \tag{19}$$

Here we have set $\omega(W_1) = \omega_1$ and $\omega(W_2) = \omega_2$, and assumed that $\omega(-W) = -\omega(W)$, recalling that when sufficiently far from transition energy, a beam with narrow energy spread has $\omega(W) = \mp W$. The number r is given by

$$r = 8\pi^2 e R K_{UF}.$$

Multiplication by $(\Omega^2 - \omega_2^2)\cdot(\Omega^2 - \omega_1^2)$ yields a polynomial quadratic in Ω^2 with solutions given by

Fig. 2. A two-stream velocity distribution $\Psi^{\circ}(w)$.

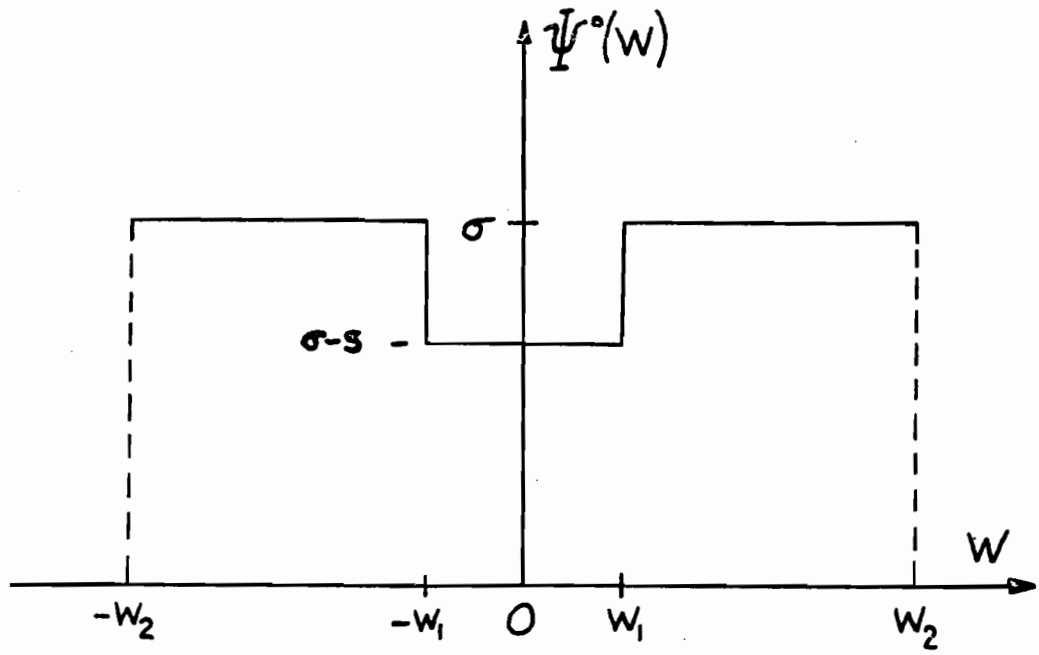

Figure 2

$$2\Omega^2 = [\omega_1^2 + \omega_2^2 + r(\omega_2\sigma - \omega_1 s)] +$$
$$\pm\{[\omega_1^2 - \omega_2^2 - r(\omega_2\sigma - \omega_1 s)]^2 + 4\omega_1 r s(\omega_2^2 - \omega_1^2)\}^{1/2}. \quad (20)$$

Stable modes are obtained if Ω is real, or the right side of (20) positive. Squaring this criterion does not introduce spurious solutions if $s < \sigma$ as it should be. The result may be expressed in terms of a threshold value r_0, of r above which the instability occurs:

$$\frac{1}{r_0} = \frac{s}{\omega_1} - \frac{\sigma}{\omega_2} \quad . \quad (21)$$

This expression gives simple thresholds for the two-stream instability below transition and for the negative-mass instability above transition. It also illustrates that the two are just different aspects of one instability. Above transition where $\omega(W) < 0$, we may take $\sigma = 0$ to obtain

$$\omega_1 = s r_0, \quad (22)$$

which yields a real threshold. This may be written as

$$W_1^2 \geq 2\pi e R N K_{UF} \quad (23)$$

for stability. This is the usual longitudinal space charge limit on the energy spread of the beam.[3]

Below the transition energy, taking $\sigma = 0$ yields that the energy spread which stabilizes a unimodal (single peak) distribution is negative so that such a beam is always stable. However, for a bimodal distribution (21) indicates that the two-stream instability can arise from a very shallow depression in the velocity distribution $f(W)$ if the depres-

sion is sufficiently narrow. For a very narrow depression, the growth rate is

$$\Gamma \simeq \omega_1 r s \cdot \omega_2^2 / (\omega_2^2 + N r / 4\pi), \tag{24}$$

which is very small compared to the characteristic frequency ω_2, of the system. Although mathematically unstable, a very narrow depression can cause no difficulties within times for which the entire theory may be regarded as a good approximation to the physical system. Further discussion of the two-stream instability will be found in a later discussion on interpretation of some recent experiments.

Stationary States. There are stationary beam distributions other than the uniform one. Of these, two especially interesting ones are the square-hump state and the triangular-hump state, so named for the form of the azimuthal density. The densities are given by

$$\rho_{SQ} \propto \Theta(\varphi+\varphi_2) - \Theta(\varphi-\varphi_2), \text{ and } \rho_{TRI} \propto \Theta(\varphi_2-|\varphi|)\cdot(\varphi_2-|\varphi|)/2\varphi_2.$$

Here, Θ is the unit step function, being zero for negative argument and unity for positive; and φ_2 is a constant. We will analyze these, assuming the beam is above transition energy.

Both of these may be stationary for the potential shape given, but only in the limit of zero range of interaction where the kernel width is made very small. The field then is proportional to the φ gradient of the density, the potential kernel being a delta function. The Fourier coefficients are now equal for all harmonics. For kernels of finite range it is clear physically that stationary distributions similar to the

two mentioned should exist, the difference being a smoothing of the discontinuities and rounding of corners. The zero range kernel allows very simple analysis with which we proceed, taking the potential kernel to be $K_0\ \delta(\varphi)$.

The square-hump potential, described by Hereward,[13] has the distribution $\Psi(W,\varphi) = \sigma$ a constant, in the region $|W| < W_2$ and $|\varphi| < \varphi_2$, where the reference angle $\varphi = 0$ is chosen at the center for convenience. See Fig. 3(a). The distribution is zero elsewhere. The potential then is $2\sigma K W_2$ for $|\varphi| < \varphi_2$, and zero elsewhere. The Hamiltonian may be written

$$H = -\tfrac{1}{2}W^2 + 4\pi e R \sigma K_0 W_2\, \Theta(\varphi_2 - |\varphi|).$$

A particle at φ in $(-\varphi_2, \varphi_2)$ and $W > 0$ remains at W and moves in the $-\varphi$ direction at the rate W until it reaches the point $-\varphi_2$ where it suffers a discontinuous velocity change ΔW given by

$$-\tfrac{1}{2}W^2 + 4\pi e R \sigma K_0 W_2 = -\tfrac{1}{2}(W + \Delta W)^2.$$

If $|\Delta W| > W$, the particle is trapped; if the inequality is in the other direction, it is not; and if equality holds, it is on the separatrix or line separating the trapped and untrapped regions. The separatrix then is given by

$$-\tfrac{1}{2}W^2 + 4\pi e R \sigma K_0 W_2 = 0,$$

or

$$W = \{2 \cdot e R N K_0\}^{1/2}.$$

This has a more familiar form if K_0 is replaced by $2\pi K_{0F}$. Then the separatrix falls at

Fig. 3. Stationary synchrotron phase space distributions: (a) Square bunch above transition. (b) Square hole below transition. (c) Triangular density bunch above transition.(The phase density is not uniform here.)

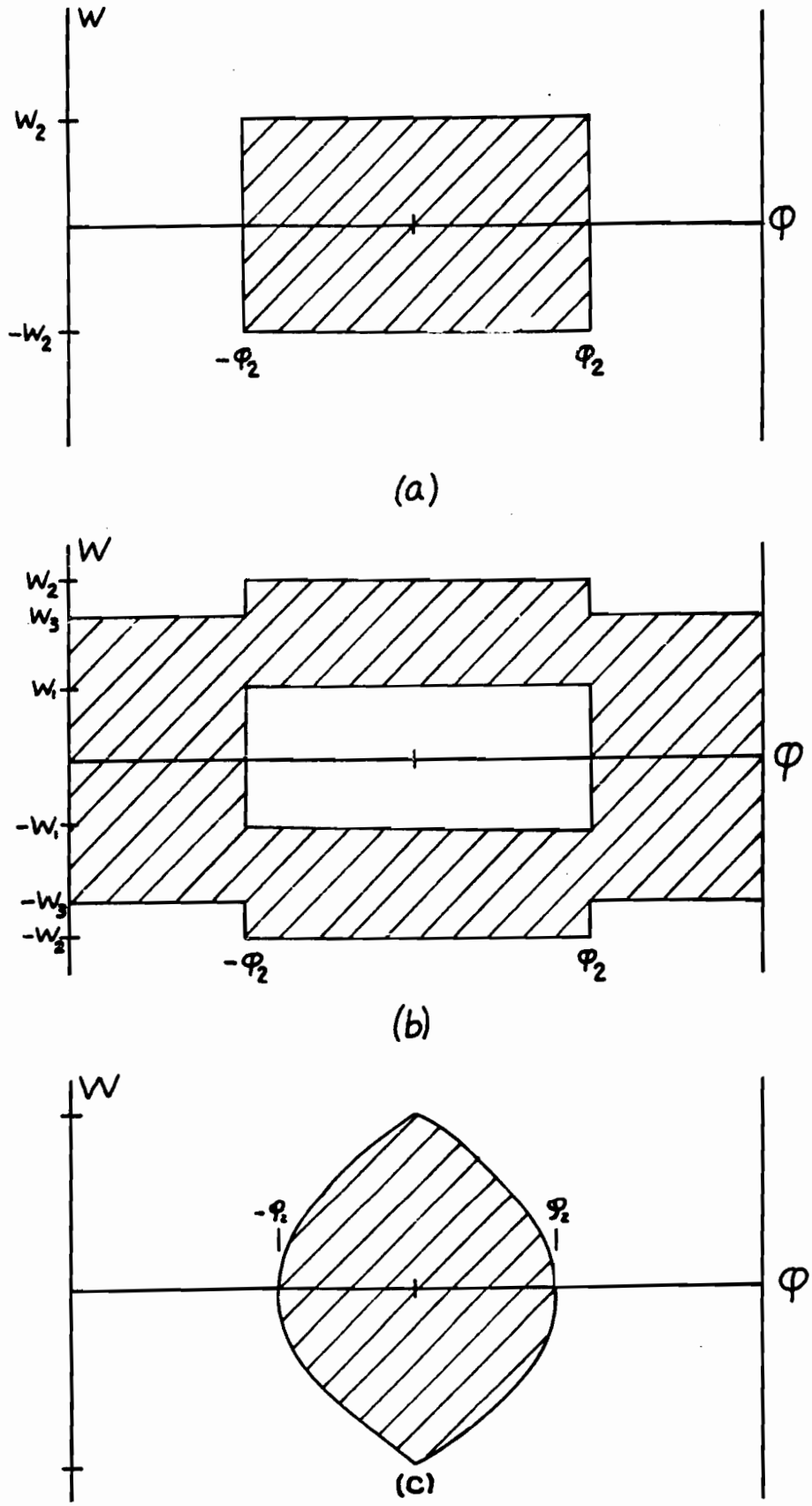
W
W_2
$-W_2$
φ
$-\varphi_2$
φ_2
(a)
W
W_2
W_3
W_1
$-W_1$
$-W_3$
$-W_2$
φ
$-\varphi_2$
φ_2
(b)
W
$-\varphi_2$
φ_2
φ
(c)

Figure 3

$$W = [2 \cdot 2\pi e R N K_{UF}]^{1/2}, \tag{25}$$

and if this value W is W_2, the state is self-consistent and stationary. Except for the factor $\sqrt{2}$, the right side is just the stable energy spread given by (23) for the uniform beam. The bunched state should then be stable against longitudinal instabilities, as well as stationary. A perturbation in phase density near the center of the bunch sees no effects of the ends and oscillatory motion should result.

If the energy spread is held fixed and the phase density σ is decreased throughout the bunch from the value implied by (25), the fields at the ends are no longer large enough to hold the bunch together. The streaming motion reduces the fields further, and the system quickly leaves the bunched configuration. Because the energy spread is greater than that critical for the uniform beam, it seems probable that the system will approach the uniform state after sufficient time. The opposite perturbation, where the phase density is increased from the stationary value, will tend to leave the beam bunched. If the field kernel is much narrower than the bunch, small filaments of filled phase space will be ejected. The streaming spreads these out in the azimuthal direction, and the fields are reduced. The main bunch may then approach the stationary bunched configuration, since this is a negative feedback. From numerical calculations, it appears that the bunch does not even lose the streamers, if σ was initially not too far from the stationary value.

We can apply the inversion symmetry result to the square-hump state and conclude that the unphysical state where all phase space is filled uniformly except for a square hole of the proper spread in W, is also a stationary state if below transition.

Actually, the entire phase space need not be filled to obtain a stationary and stable square hole distribution. With the same type argument as that used for the square hump, it is easy to show that the state shown in Fig. 3(b) is stable and stationary. The phase density is constant in the shaded region of the diagram. Using the parameters shown in the figure, the state is stationary if

$$W_2^2 = W_3^2 + W_1^2 \quad \text{and} \quad W_1^2 = 8\pi e R \sigma K_u (W_1 + W_3 - W_2). \tag{26}$$

When the first is satisfied, the triangle inequality shows that the second can be satisfied, and a stationary state actually exists. There is really a two-parameter continuous set of these states. Each such state could be susceptible to two-stream instabilities. The equation giving as a function of $\zeta = W_2/W_1$, the critical state which separates the stable from the unstable ones, obtains from (21) and (26) in the form

$$\zeta(\zeta-1)(\zeta^2-3\zeta+4)=0.$$

This has two real roots $\zeta = 0$ and $\zeta = 1$, which give trivial examples where there is no hole in the middle of the distribution or there is a hole but no distribution. The other two roots are imaginary so that a critical state fails to exist. An example $W_1 = 3$, $W_3 = 4$, and $W_2 = 5$, yields the stationary state requirement $8\pi^2 e R \sigma K_{uF} = 9/4$,

while two-stream stability requires that this number be less than $15/2$, so that all such stationary states are stable against two-stream instabilities.

We can obtain a very general criterion for testing distributions to see if they are stationary. Constructing such states however is a more difficult question and does not appear to admit of a general prescription.

Thus, it is well known that a distribution function depending on the canonical coordinate x and momentum p of a system only through a dependence upon the Hamiltonian $H(x,p)$, is a stationary distribution. We may show this as a special case of a formalism that yields the eigenfunctions of the operator

$$\mathcal{L} = \dot{x}\frac{\partial}{\partial x} + \dot{p}\frac{\partial}{\partial p},$$

which by the Vlasov equation gives the difference between $d\Phi/dt$ and $\partial\Phi/\partial t$ as $\mathcal{L}\Phi$. The canonical transformation to coordinates $P = H(x,p)$ and $Q = \tau(x,p)$, where $\tau(x,p) = t$ is assumed to be a solution to the Hamiltonian equations fulfilling the correct boundary conditions, yields a new Hamiltonian $K(Q,P) = P$, so that in these variables $\mathcal{L} = \frac{\partial}{\partial Q}$. The operator now has eigenfunctions $\psi_\lambda(P,Q)$ for which $\mathcal{L}\psi_\lambda = i\lambda\psi_\lambda$, the i being included because $\mathcal{L}$ is anti-Hermitian in the appropriate region and its eigenvalues are correspondingly imaginary. The general eigenfunction is

$$\psi_\lambda = f(P)\cdot \exp(i\lambda Q),$$

where f is an arbitrary function of its argument. Returning to the original coordinates x and p, we obtain

$$\mathcal{L} f[H(x,p)]\exp[i\lambda\tau(x,p)] = \mathcal{L} f e^{i\lambda\tau} = i\lambda f e^{i\lambda\tau}.$$

Stationary states are those for which $\lambda = 0$, which is just the result quoted.

The Fourier integral theorem guarantees that the ψ_λ form a complete set in the phase space (P, Q). These eigenfunctions will then span the space of functions of x and p. Thus for a harmonic oscillator, f may be taken as $H^{n/2}$ and λ as n'/ω, so that in polar coordinates A and φ in the phase space, the ψ_λ become $A^n e^{in'\varphi}$. These functions satisfy the correct periodicity conditions if n' is integral, and span the space of functions defined on the planes (x,p) or (A,φ). A similar result holds for the free particle Hamiltonian.

The theorem just made plausible can be useful because it tells what expansion process must be used to obtain decoupled equations when a solution is desired to the Vlasov equation linearized about some stationary state. For a free particle system with a periodic boundary condition on the variable φ, the theorem shows that $e^{in'\varphi}$ times an arbitrary function of momentum is the general form of the eigenfunction which should be used. If the φ period of the system is 2π, then n' must be integral, and we find a fairly fundamental reason for the useful-

ness of Fourier expansion in the uniform beam calculation, and the uselessness of the same expansion in analyzing the square-hump state stability.

A third type of stationary state is that calculated by Nielsen[1] to explain the existence of apparently stable bunches of particles above transition which are trapped on triangle-shaped potential humps. The essence of the calculation is that states which are stationary and have this potential must have phase trajectories which are formed of parabolae joined in a nonsmooth fashion at the azimuthal center of the bunch. The effect of giving the kernel a range here is to round off the corners of the potential and the phase curves. Figure 3(c) shows a region bounded by such a phase trajectory. Using the theorem on the (W, φ) dependence of stationary distribution functions, one may show that the dependence $\Psi \propto H^{1/2}$ is self-consistent with the required potential form.

<u>Nonlinear Motion.</u> The theory of nonlinear effects is very limited, but at least one argument may be made. It concerns the effect of strong interactions on a uniform beam above transition. It is quite nebulous and is an attempt to understand the results of digital calculations to be described later. The essence of the results was that if Ψ is taken to be the constant σ within the region bounded initially by the curves $W_{\pm}(\varphi) \equiv \pm W_B(\varphi) = \pm(\bar{W} + \delta \cos\varphi)$, and if the narrow portion $(\varphi = \pm\pi)$ of the region contracts at all in the first stages of the

system evolution, then the beam is pinched off almost completely at the narrow part, and a bunched beam results. The final result is strikingly close to the square-hump state described earlier.

In order to use this result and partially rationalize it we must know something about the time behavior of the density, at least at the initial time $t = 0$. Integration of the Vlasov equation over W yields the usual continuity equation

$$\frac{\partial}{\partial t} \rho(\varphi,t) = -\frac{\partial}{\partial \varphi} \int dW\, \omega(W)\, \Psi(W,\varphi,t). \tag{27}$$

Using the continuity equation and the Vlasov equation to evaluate $\int dW\, \partial^2\Psi/\partial t^2$ yields

$$\frac{\partial^2}{\partial t^2} \rho(\varphi,t) = \frac{\partial^2}{\partial \varphi^2} \int dW\, \omega^2(W)\, \Psi(W,\varphi,t) - 2\pi e R \frac{\partial}{\partial \varphi}\left[\bar{E}(\varphi,t) \int dW\, \omega(W) \frac{\partial \Psi}{\partial W}\right]. \tag{28}$$

which corresponds to the heat flow equations of magnetohydrodynamics. We evaluate this at zero time for the distribution given, assuming a zero range potential kernel as before, and taking $\omega(W)$ to be $-W$ (above transition):

$$\frac{\partial^2}{\partial t^2} \rho(\varphi,0) = 4\sigma (W_B')^2 (W_B - r\sigma) + 2\sigma W_B'' (W_B^2 - 2r\sigma W_B), \tag{29}$$

where r is $8\pi^2 e R K_{0F}$, and K_{0F} is the Fourier transform of the potential kernel. Here primes represent φ derivatives. The function $W_B(\varphi)$ is assumed to be positive in the region $-\pi \le \varphi \le \pi$.

At a local minimum point φ_0 in the curve $W^+ = W_B(\varphi)$, we have that $\partial\rho/\partial t$ is zero and

$$\partial^2 \rho / \partial t^2 = 2\sigma W_B''(W_B^2 - 2r\sigma W_B), \tag{30}$$

where W_B'' is positive. The local minimum in the curve $W^+(\varphi)$ and the local maximum in $W^-(\varphi)$ will then tend to become less pronounced if $W_B \geq 2r\sigma$ at φ_0. We will leave this result in the form

$$\text{minimum}\,(W_B/r\sigma) \geq 2, \qquad \text{for reduction of fields,} \tag{31}$$

which is seen to reduce to the stability criterion for the uniform beam (23) when δ is small.

The critical point is that the reaction of the narrow part of the boundary to the field if (31) is not fulfilled, is a decrease in the energy spread which drives the system even farther from satisfying (31). Essentially this is a feedback mechanism and if (31) is not true, it may be expected that the beam will always be pinched off.

It is natural to wonder if a useful result obtains from a similar calculation at a value φ where W_B is a maximum. There W_B'' is negative and a potentially unstable situation exists if maximum $\frac{W_B}{r\sigma} \leq 2$. There is no feedback mechanism here, and the criterion does not seem to be of such general importance as (31). Thus, equation (31) determines whether or not beam bunching will occur, while the latter result gives only a little information as to how the bunching will occur when it does.

If immediate bunching does not occur, the perturbation travels along the boundary. Because the system is periodic, the disturbance returns to a given azimuth repeatedly, and after doing this a number of

times, could conceivably interact with itself strongly enough to yield a potentially unstable situation. However, this motion is too complex to follow with any of the digital calculations made, and analytical studies have not given any information concerning such an instability.

Given sufficient energy spread, the perturbation will cause little change in the distribution. This will be made more exact in the section on the computer results.

The requirement (31) has been obtained for a very special case corresponding to some digital calculations made. Very similar results are obtained when $\partial^2\rho/\partial t^2$ is analyzed for other perturbations of the uniform beam state. Thus if

$$\Psi^\circ = \sigma(1 - \delta\cos\eta\varphi)\cdot f(w),$$

the beam will tend to pinch off unless

$$\langle w^2\rangle \geq \tfrac{1}{2}(N r/2\pi),$$

where

$$\langle w^2\rangle = \int w^2 f(w)\,dw \Big/ \int f(w)\,dw.$$

If $f(w)$ is one when $|w| \leq \bar{w}$, and zero elsewhere, the result may be stated as: The minimum of $W/r\sigma$ must be greater than three for stability. The result for uniform phase density with boundary perturbations is the same except that the number is two rather than three.

An interesting restatement of these calculations is that unless the "temperature" $\frac{1}{2}\langle w^2\rangle$ is greater than a multiple of order one of the potential energy $r\rho$ at all points within the one-dimensional "gas",

a "condensation" or beam bunching will occur. The multiple depends upon the detailed nature of the distribution and the perturbation, but dimensional analysis fixes the form of the critical energy spread to that given.

Resume of Physical Experiments

The experiments of Barton and Nielsen[1] at the Cosmotron yielded the following behavior: 1. In a coasting beam with low energy spread, high frequency modulations develop rapidly. 2. These decay or coalesce after their initial growth, to yield lower frequency modulations. 3. Similar space charge bunching can occur when the RF accelerating fields are on. 4. These space charge bunches are highly stable in the coasting beam but may not be completely stable when the RF is on. 5. The bunches give characteristic triangular peaks in the azimuthal density, and contain appreciable amounts of charge. 6. Frequently, the stationary final state toward which a coasting beam tends, gives a uniform azimuthal density with triangular notches in it.

Recently, instabilities below transition energy have been noted in the MURA 50 Mev electron FFAG synchrotron.[6] Recalling that a unimodal energy distribution cannot give such instabilities, and noting that the injection devices were previously thought to give such a distribution, we include this as another phenomenon needing understanding. Similar phenomena have been noted in other machines.[14,15,16]

II. COMPUTER EXPERIMENTS

An IBM 704 digital computer was used to test which of the results of the physical experiments could be attributed to the longitudinal reaction of the particle beam to its own Coulomb forces.

In a broad sense, three numerical techniques have been used to seek solutions to the Vlasov equation (12) which satisfy given initial conditions. The nonpropagating field approximation is usually made. The first method described here was not used in the present study; it is however, the most straightforward approach and a brief discussion of it seems worthwhile.

Mesh Solution of the Vlasov Equation

The numerical integration of (12) by replacing the derivatives of the distribution function by difference operations on the values of it given on a mesh in the (W, φ) plane has been investigated by Sessler,[17] by Nielsen and Sessler,[18] and by Christian.[19] At the risk of oversimplification, it may be said that these results have not been too successful. Because the equation involves two independent variables W and φ as well as time, care must be taken to assure that in the limit of arbitrarily fine mesh, the solutions to the difference equation used converge to solutions of the differential equation. This convergence does not

appear automatically and highly sophisticated differencing schemes have been used to obtain it. These processes cause the calculation to require large amounts of computer time because the solutions exhibit such complex behavior that convergence becomes very slow at just those times where the system is most interesting.

An explicit differencing scheme computes the value of the distribution function at time $t+\Delta t$ for a given mesh point, from the values at nearby mesh points at time t. As a function of the time step Δt and the size of the mesh, the solution generated by an explicit scheme converges to a solution of the differential equation only if the limits $\Delta t \rightarrow 0$ and mesh size $\rightarrow 0$ are taken properly. This places a requirement on the relative values of these parameters, and this is often too restrictive to make the method useful. There are however, numerical algorithms which do not have such restrictions.[20]

Among the unrestricted schemes is the implicit solution of the difference systems wherein the values of Ψ at the mesh points at time increased by one step are written implicitly, that is as a function of one another and of the previous values, and the resultant matrix inverted. Another is an iterated explicit scheme. From $\Psi|_t$ on the mesh, a simple estimate of the change $\Delta\Psi = \Psi|_{t+\Delta t} - \Psi|_t$ is computed. An approximation to $\Psi|_{t+\Delta t}$ is now known. From it may be calculated a different estimate of $\Delta\Psi$. The average of the old and new estimates will now give a better approximation to $\Psi|_{t+\Delta t}$. The re-

computation of the estimates is continued until the desired accuracy in $\Psi|_{t+\Delta t}$ is obtained. The iteration scheme is reversible in time to within any accuracy asked. Since such a reversible calculation generally yields a spurious periodic behavior during very long calculations because of the discrete representation of the distribution function and because this periodic nature is unphysical, various schemes have been used to introduce an irreversible mixing of the phase space.

An interesting difficulty arises in that a distribution function on a mesh is necessarily of finite extent in the W direction, and must then be zero outside a given region. Numerical derivatives calculated near the boundary of the region then tend to extend farther than the boundary and as a result, after one time step, the distribution function is surrounded by a thin region in which the value is negative and unphysical. The more accurate the difference system used, the smaller and farther away does this region become but it appears impossible to eliminate it completely without some arbitrary procedure such as throwing away negative values of Ψ and thus causing charge conservation to fail. A somewhat related problem is that the W spread of a distribution increases by at least one mesh width on each time step. This is a sort of conduction process, the distribution attempting to smooth itself out at each step. The difficulty lies in the finite storage space available in a computer. Once again, a cutoff procedure must be introduced.

The following two sections discuss methods which were used to try to avoid the difficulties mentioned.

Following the Motion of Particles

An integration of the equations of motion was performed numerically (see Appendix II) for each of a large number of particles. The interaction field was calculated before each time step.

The actual procedure was to calculate the field $\mathcal{E}_m^\ell = \mathcal{E}(m\Delta\varphi, \ell\Delta t)$, and integrate the equations (4):

$$\begin{aligned} \dot{\varphi}_j^\ell &= \frac{d}{dt}\varphi_j \Big|_{t=\ell\Delta t} = \mp W_j^\ell, \\ \dot{W}_j^\ell &= \frac{d}{dt} W_j \Big|_{t=\ell\Delta t} = \mathcal{E}(\varphi_j^\ell, \ell\Delta t), \end{aligned} \tag{32}$$

where subscript j indexes the particles, superscript ℓ the number of discrete time steps performed so far, and subscript m indexes the field values at equidistant points in φ. The values φ_j^ℓ and W_j^ℓ give the position of the jth particle in the synchrotron phase space after the ℓth step.

The first attempt used the simplest possible method of calculation, that of finding a histogram representing the density $\rho(\varphi, t)$ as $\rho_m^\ell = \rho(m\Delta\varphi, \ell\Delta t)$, on a sufficiently fine mesh to allow the field to be calculated accurately. The immediate result was that the number of particles required was prohibitively large.

If an insufficient number of particles was used, the statistical variations in the density were large. These occurred at a wavelength of the order of the width $\Delta\phi$ of the histogram channels, and because

the growth rate of instabilities at least in the linear region goes roughly as $h/\sqrt{\alpha^2+h^2}$, where h is the harmonic number and α is relatively large, the growth of the statistical fluctuations is much faster than that of low harmonics which were to be studied, and the development of the latter was quickly obscured.

However, regarding each of the (φ_j, W_j) not as the position of a particle, but as the center of a macroparticle or distribution of particles whose shape is not allowed to change, allows the kernel to be smoothed out from the exponential form given in equation (11) to a form such as shown in Fig. 4. This has the immediate effect of reducing the fields caused by disturbances whose wavelength is less than the kernel width.

The growth of the short wavelength statistical fluctuations may thus be reduced by having a kernel whose half width is several times the channel width $\Delta\phi$. Structure of the distribution with wavelength shorter than this is washed out in the calculation of the field and is not well represented in the macroparticle interpretation, so that the macroparticle can be given a fixed azimuthal spread equal to $\Delta\phi$. Contribution to the jth density channel, i.e., to the value ρ_j, by a macroparticle is now made in proportion to the amount of its azimuthal width which lies between the edges of the channel. The channels now contain nonintegral "counts", so that the coarse nature of the discrete representation is reduced. The statistical fluctuations at high harmonic

Fig. 4. Typical kernel $K(\varphi)$ obtained by convoluting the exponential field kernel with a Gaussian particle distribution of similar range.

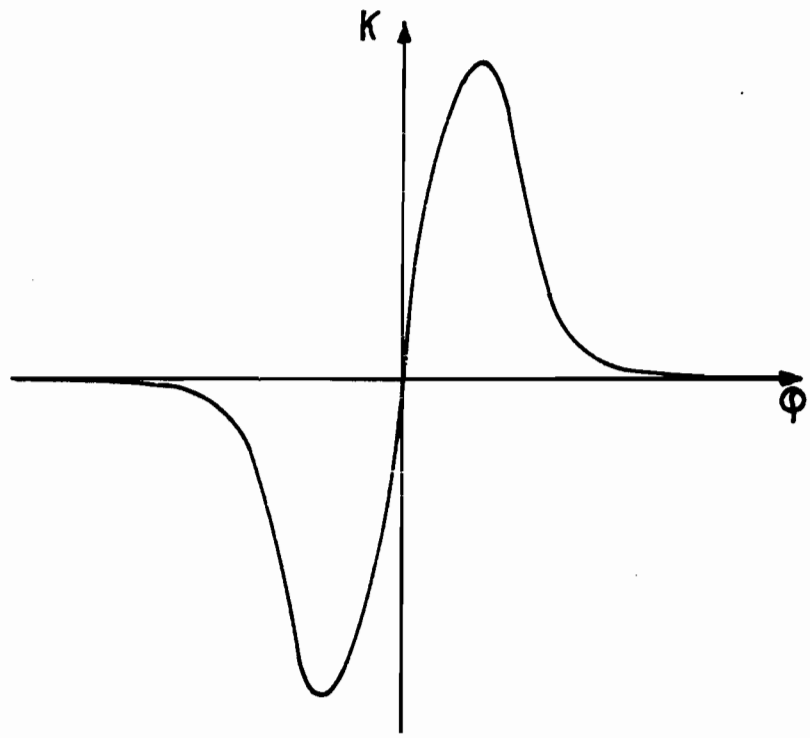

Figure 4

are then further suppressed, without substantial change in the fields at low harmonic, and the latter may be studied without being obscured by the former.

In reasonable amounts of computer time it was found possible to follow of order 2000-5000 macroparticles (hereafter called just particles) using a representation allowing 128 channels to provide the field throughout the range $-\pi \leq \varphi \leq \pi$. With linear interpolation for finding the field between the tabulated values, the field calculation allows harmonics from the first to about the twentieth to be well represented. A potential kernel with a half width at half maximum of about seven times the channel width allows an adequate representation of the kernel shape and provides good suppression of harmonics higher than about the thirtieth. With such a kernel and field, the statistical fluctuations in the density values were small enough given roughly 2000 particles, to allow the first through twentieth harmonics to be studied with relatively little interference. The threshold for growth of statistical "hash" was never too far away and lack of care in choosing the initial distribution was observed to push the system across the threshold. Thus interference from the hash occurred if for example, the initial distribution was a series of horizontal rows of particles at different values W, and the particle spacings in φ of the various rows were in phase. This distribution is quite unrealistic and quick growth of the hash resulted.

The first integration scheme used to step the particles through time was the straightforward linear algorithm

$$\begin{aligned} \varphi_j^{\ell+1} &= \varphi_j^{\ell} \mp W_j^{\ell} \cdot \Delta t \\ W_j^{\ell+1} &= W_j^{\ell} + \mathcal{E}(\varphi_j^{\ell+1}, \ell\Delta t) \cdot \Delta t. \end{aligned} \tag{33}$$

This has the interesting property that the stepping of φ_j from $t = \ell\Delta t$ to $t = (\ell+1)\Delta t$, followed by the stepping of W_j using the new value of φ_j, may be regarded as a canonical transformation since the generating functions

$$\begin{aligned} T_1^{\ell} &= \sum_j W_j^{\ell} \varphi_j^{\ell} \mp (W_j^{\ell})^2 \Delta t, \\ T_2^{\ell} &= \sum_j W_j^{\ell+1} \varphi_j^{\ell+1} - U(\varphi_j^{\ell+1}, \ell\Delta t)\Delta t, \end{aligned} \tag{34}$$

in turn yield the transformations

$$\begin{aligned} &\varphi_j^{\ell} \rightarrow \varphi_j^{\ell+1} \quad \text{and} \quad W_j^{\ell} \rightarrow W_j^{\ell}, \\ &\varphi_j^{\ell+1} \rightarrow \varphi_j^{\ell+1} \quad \text{and} \quad W_j^{\ell} \rightarrow W_j^{\ell+1}, \end{aligned} \tag{35}$$

and therefore this approximation has in common with the true solution of the differential equations (32), the property of preserving local densities in phase space. The coarseness of the representation however, does not allow this property to be ascertained from the computer runs.

A pragmatic approach to the question of required fineness of the time step Δt was used, starting with a value clearly too large and halving it until doing so had no observable effect on the nature of the motion. A similar process was used to ascertain the effectiveness of using only 128 channels to represent the field and of using of the order of 2000 particles.

A comprehensive testing of the growth rates and critical energy spreads predicted by the linear theory was carried out. For this purpose, initially pure harmonic perturbations were made on a uniform beam. For example, a phase density of the form $\frac{N}{2\pi}\left[1+\epsilon\cos(h\varphi)\right]\delta(W)$ was used as an initial distribution for a monoenergetic $(\Delta E = \Delta W = 0)$ beam. The values of the azimuthal density at $\varphi = 0$ were then tabulated as a function of time, and the hyperbolic cosines C^{l} of the ratios of these values to the initial value $\frac{N}{2\pi}(1+\epsilon)$ were computed. The linear theory[2] predicts the initial growth of such a system to have the form $A\exp(\Gamma_0 t) + B\exp(-\Gamma_0 t)$. The initial distribution used here requires the initially stationary linear combination to be taken because the continuity equation (27) shows that for states symmetric in W, the value $\partial\rho/\partial t$ is zero when $\omega(W)$ is taken as $\mp W$. The hyperbolic cosine of $\rho(\varphi,t)/\rho(\varphi,0)$ should vary as $t\Gamma(t)$ where $\Gamma(t)$ is Γ_0 in the limit of very small perturbation. Because even small perturbations grow exponentially, the region of nonlinear motion is entered quickly. However, the extrapolation of the derivative of $t\Gamma(t)$ to zero time does give Γ_0. Since equal times elapsed between the observations of the C^{l}, the first differences $C^{l+1} - C^{l}$ are a good representation of the derivative if Δt is sufficiently small. On extrapolation of the differences to zero time, the value Γ_0 is obtained.

In order to provide comparison with the theory it was necessary to know the Fourier amplitudes of the kernel used. The field $\mathcal{E}^{l}_{m}$ at

azimuth $m\Delta\phi$ was obtained from the density ρ_m^l at time $l\Delta t$ by the prescription

$$\mathcal{E}_m^l = \sum_{m'} \rho_{m+m'}^l \cdot K_{m'}, \tag{36}$$

where the values K_m are $\Delta\phi \cdot K(m\Delta\phi)$, a tabulation of the values of the field kernel. In view of the linear interpolation used to find the field between the mesh points and the spreading described, of the effects of one particle over one channel, the kernel used may be considered to be that piecewise linear function connecting the tabulated values K_m. Its Fourier amplitude at harmonic n then is

$$K_F = -in\, K_{UF} = -in \frac{\Delta\phi}{2\pi n}\left[\frac{2}{n\Delta\phi}\sin\left(\frac{n\Delta\phi}{2}\right)\right] \sum_{m'} K_{m'} \sin(nm'\Delta\phi), \tag{37}$$

which is so written to indicate that the spreading of a particle is equivalent to the process of "sigma-smoothing" often introduced in applications of Fourier transformations to reduce fluctuations caused by cutting off the series after a finite set of terms.[21] The factor in brackets is the smoothing factor.

This series was evaluated for representative kernels and for various harmonics in the usable range $0 \le h \le 20$ and the numbers were put into (20) after making the reduction $\omega_1 = S = 0$ and $\omega_2 = 0$, $\sigma = \infty$, with $\omega_2\sigma$ held fixed at $N/4\pi$. The resulting expression is the growth rate

$$\mathrm{Im}\,(h\Omega) = \mathrm{Im}\left\{h\left[\omega_2^2 + 4\pi e R K_{UF} N\right]^{\frac{1}{2}}\right\}. \tag{38}$$

These results and the growth rate measurements were found to be in accord to within about 5%, both in absolute magnitude and in dependence upon the harmonic number. The harmonics tested were the first, second, fourth, eighth, and sixteenth. The discrepancy 5% was in accord with the estimated accuracy of the extrapolation of $\Gamma(t)$ to zero time, which was done graphically.

Further comparisons were made by varying the size ϵ of the perturbation from 0.01 to 0.25. Again to within the accuracy of the extrapolation, the results were the same, and were in accord with theory.

Since it is difficult to provide a smooth density variation in a monoenergetic string of a finite and small number of particles, the initial modulation was provided by varying the interparticle spacing.

Figure 5 shows the field kernel used for the greater part of the calculations made, and its Fourier amplitude as calculated from equation (37). Checks were made to assure that the computer program gave the proper field for a density varying as $\sin n\varphi$. The field in this case is proportional to the nth Fourier amplitude of the kernel. The results differed negligibly for n less than 16 and by less than 10% for harmonics up to the thirty-second. The discrepancy was in the form of reduction of the high harmonic fields.

Figures 6 and 7 show representative behavior of a monoenergetic beam used in growth rate comparisons, and the corresponding curve $\Gamma(t)$.

calculated as described. The last extends in time past the time at which the wave in the string breaks over on itself. It is this breaking time at which an analogous computation using a mesh approach has difficulty in converging.

A limited exploration of other field kernels was made, again with results in accord with theory. Thus, kernels with different shapes but the same width and kernels of similar but smoother appearance and doubled and quadrupled width were used. Because the analytical growth rates and stability limits are always expressed here in terms of the Fourier coefficients of the kernel, its actual form is not important, and the one shown in Fig. 5 was used throughout most of the exploratory calculations.

There are of course limitations on the states which may be analyzed with this type of calculation. The most important use is for the analysis of beams with small energy spread. Attempting to represent a large energy spread or structured energy spectrum is not possible under the conditions cited because as we have seen, an adequate representation of the field (that is, of the φ dependence of the distribution) requires of order of 128 values to be given. Now the general result of an instability is a twisting in the phase space of the distribution so that if a detailed W dependence is desired in the initial beam, it must be represented to the same accuracy as the φ dependence. A calculation using good statistics then would require more time and more computer

Fig. 5. (a) Typical kernel $K(\varphi)$ used in digital computations. The density histogram channel width is $\Delta\phi$. (b) Relative Fourier coefficients K_n of K.

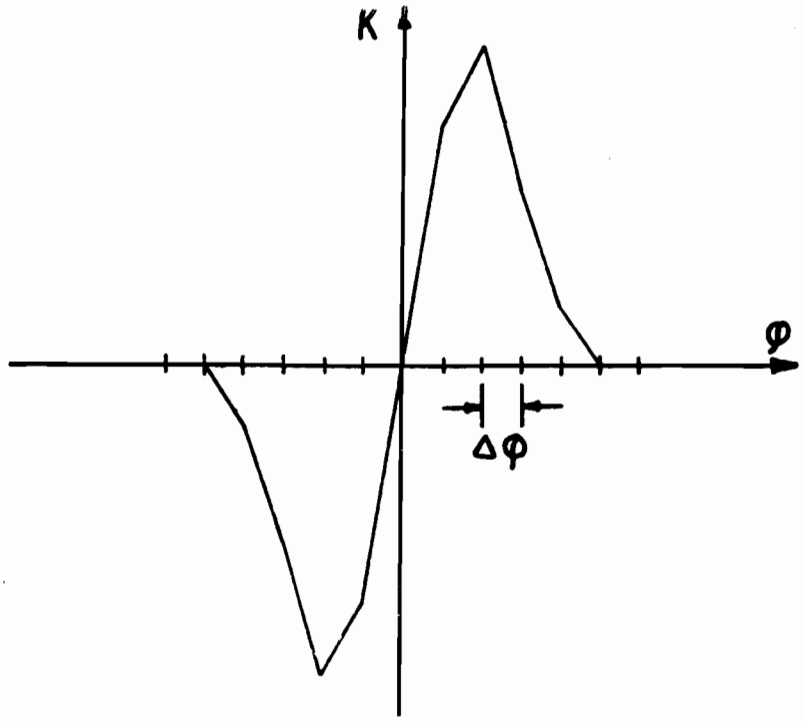

(a)

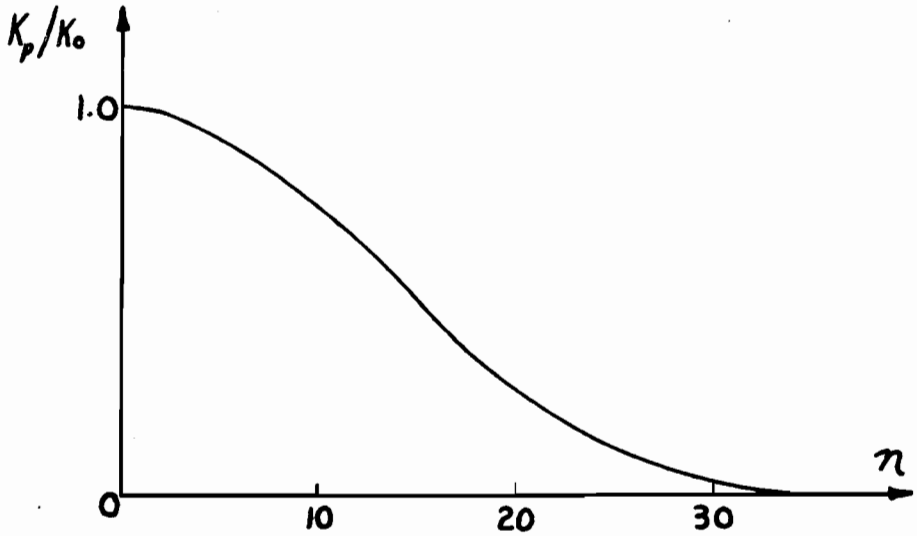

(b)

Figure 5

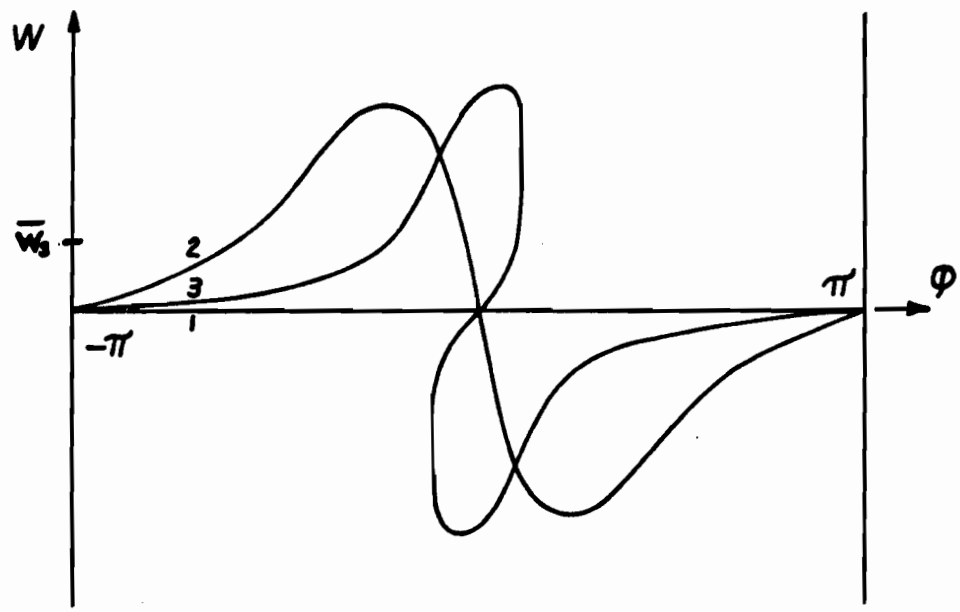

Figure 6

Fig. 7. Nonlinear growth of a sinusoidal perturbation of a mono-energetic beam above transition. The values $C^{\ell} = t\Gamma(t)|_{\ell\Delta t}$ and the first differences or $\frac{d}{dt}[t\Gamma(t)]_{\ell\Delta t}$ are graphed as functions of $t = \ell\Delta t$. The system was given an initial 25% perturbation $(\epsilon = 0.25)$ at the first harmonic.

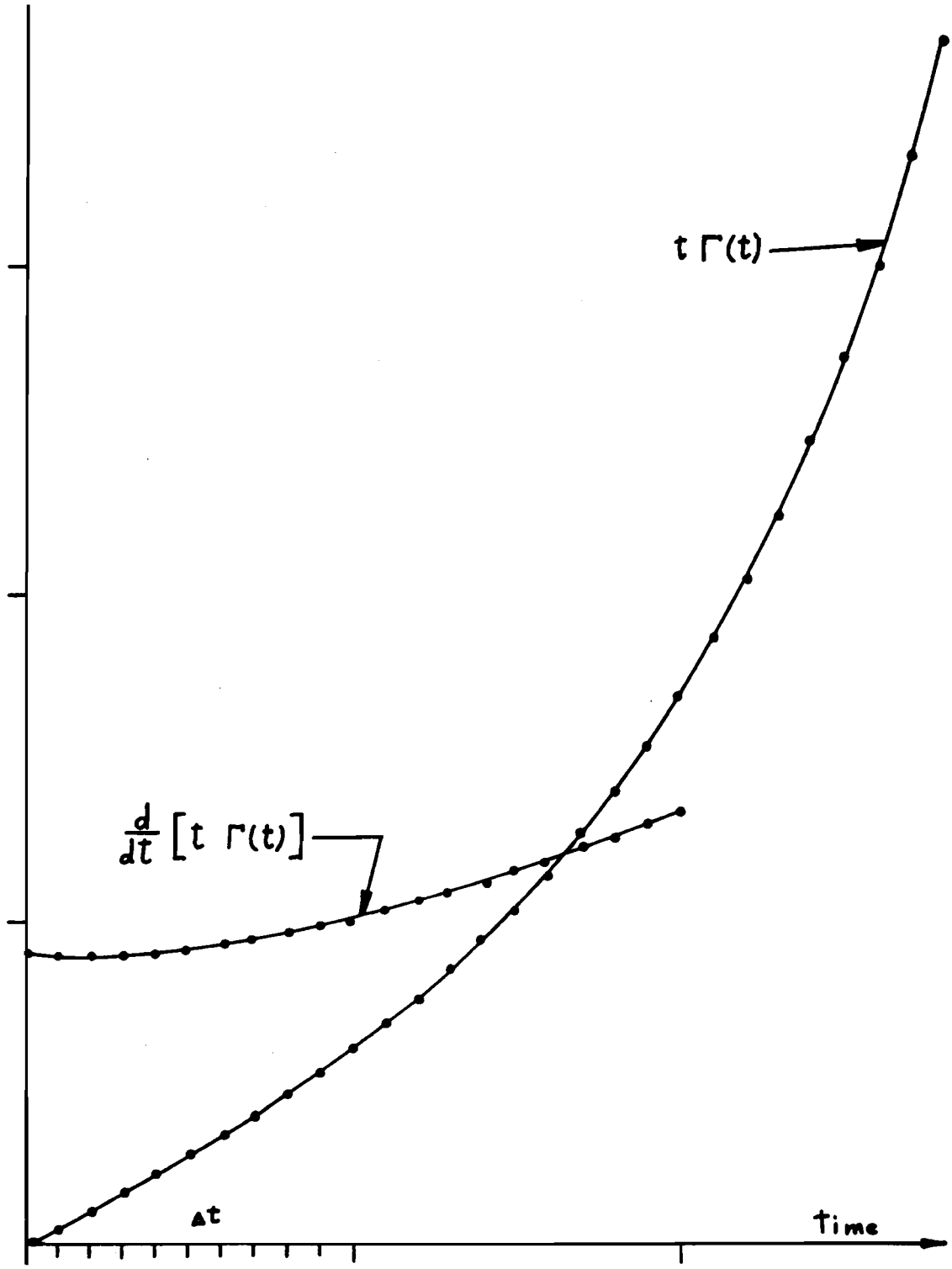

Figure 7

space than was available. The conclusion then is that the particle following approach is most applicable to stable distributions, or to unstable ones having an unstructured energy dependence. For other states a different type of calculation is required. One such is described in the latter half of this section.

Stability of Clusters above Transition Energy. An extensive search was made for evidence that the statistical fluctuations in the calculated field or interaction of the clusters among themselves could cause destabilization of particle clusters.

For this purpose, an energy spread was simulated by using an initial distribution having rows of particles on each of 15 equidistant lines at constant values W. In each row, the particle spacing varied smoothly in φ so that the initial azimuthal density was

$$\rho(\varphi) = \frac{N}{2\pi}\left[1 + \epsilon_1 \cos\varphi + \epsilon_2 \cos h_2 \varphi\right].$$

The modulation ϵ_1 was usually taken as 25%. This served to allow several different clusters to be observed at once because it caused the height, width, and separation of the density peaks to be different among the h_2 peaks formed when the energy width failed to stabilize the system against the field of the perturbation at harmonic h_2.

The actual values h_2 which were used were 5 and 10, while ϵ_2 was varied so that the high harmonic field ranged from much less than to much greater than that at the first harmonic. The energy spread used was always sufficient to ensure strong instability of the first har-

monic if left alone, but was varied from much less than, to just greater than that required to stabilize the higher harmonics. The ratios of stabilizing energy spreads of first to fifth and tenth harmonic perturbations for the usual kernel are

$$W_5(5)/W_5(1) = 0.96 \qquad \text{and} \qquad W_5(10)/W_5(1) = 0.86 .$$

The result in all cases, except when the energy spread washed out the high harmonic growth and only the first harmonic grew, was that the higher harmonic grew quickly until a saturation value of energy spread was reached, and remained there for as long as the system was watched. Figure 8 shows a sample azimuthal density histogram from a run where the value h_t was five. The behavior is similar to the results for all the variations tried. It is seen that the beam has formed five major clusters at the azimuthal positions of the maxima of the initial perturbation. A sixth maximum may be seen near the azimuth $\varphi = \pm\pi$. This has a rather strange history: The initial growth of the fifth harmonic was sufficiently quick to deplete the number of particles in the azimuthal vicinity of the five growing bunches. This depleted region extends one kernel width on either side of the bunches. Since the centers of the bunches were azimuthally separated by three to five times this width, this left small auxiliary peaks in the density between the five large peaks. These are also unstable and they grew to saturation energy spread. The result of the fifth harmonic was a smaller amount of the tenth. Of the five small humps, four were absorbed

Fig. 8. Sample histogram obtained for the azimuthal density. This shows the bunching which occurs in the particle-following numerical calculations when the energy spread is too small to stabilize the initially uniform distribution. The perturbation was 1% at the fifth harmonic.

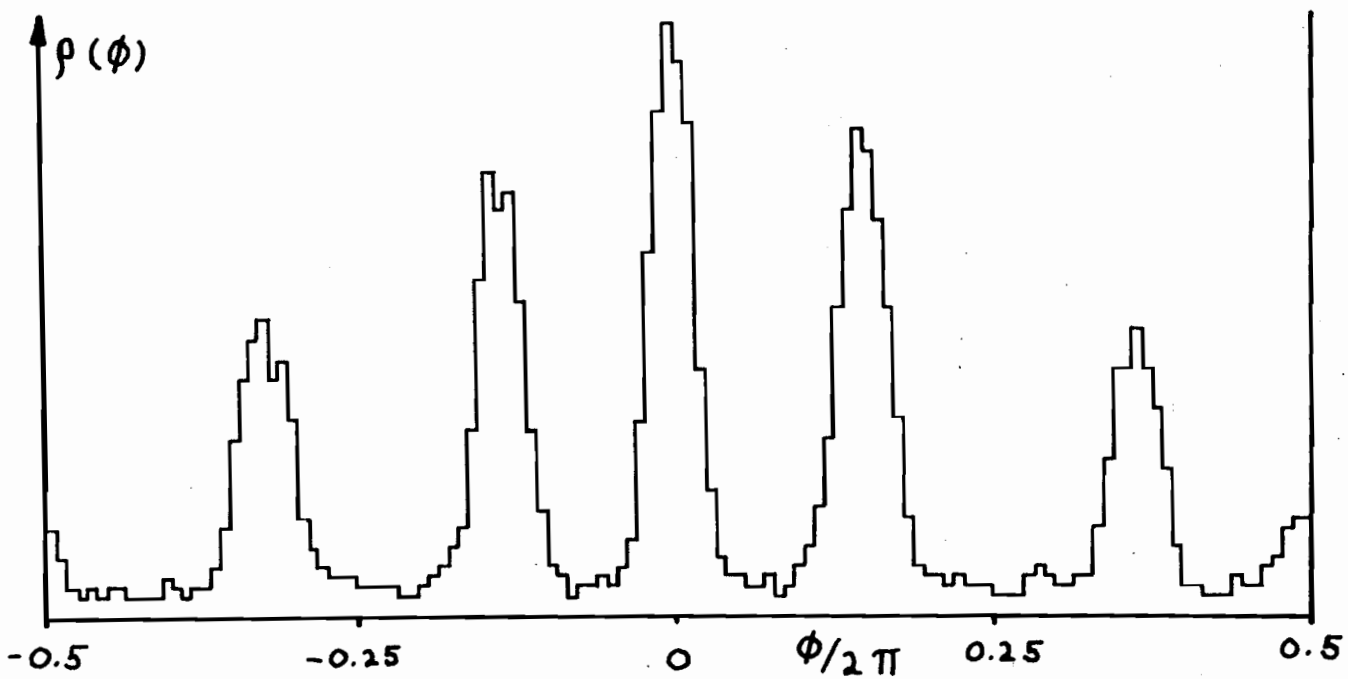

Figure 8

eventually by the large peaks nearby, but the fifth was sufficiently far from the peaks to be able to exist independently. This behavior was observed to a degree in all the runs attempted at $h_2 > 1$, including one where the phase of the first harmonic perturbation was shifted by π to be sure that no spurious effect was generated by an incorrect method of making the system periodic in φ. In the last case, the sixth hump appeared at 0 rather than $\pm\pi$. The absorption of the small humps by the larger clusters is reminiscent of the coalescing of bunches observed at the Cosmotron.[1]

In several of these calculations where the energy spread was initially small and the resulting clusters tightly bound, it was observed that an auxiliary cluster could revolve around a main one as a distinct object, rather than just being absorbed. In no such case did a small cluster make more than two such revolutions before losing its identity. Such behavior was also observed in the experiments.

A run at twice the energy spread used in Fig. 8 was stable toward the fifth harmonic perturbation. With all other parameters unchanged, the result was that the first harmonic grew and formed a very definitely bunched beam in just one-eighth of the time at which Fig. 8 was observed. Because the configuration displayed in Fig. 8 had endured for over 70% of the time elapsed without detectably organized variation, further computation was regarded as uninformative, and it was discontinued. At this time, approximately ten million particle

steps had been made, at the expense of about sixteen hours of computer time. The similar runs with variations of energy spread and relative excitation of the perturbations showed this same reluctance to change once the bunching had taken place and were also discontinued.

The shape of the density peaks which obtained in this series of calculation are at least consistent with the experimental triangles, but are not sufficiently well determined to allow a flat statement that the triangles have been shown to be the result of the azimuthal motion alone. The analogous calculation for lower harmonics would yield more definite information on this point, but a sufficiently fine representation of the energy dependence of the distribution function was not possible with the limited storage available in the ordinary digital computer. A rough estimate indicates that approximately fifty thousand particles would be required to obtain reasonably good statistics.

Limiting Energy Spreads. Because the final energy spreads resulting from the space charge instability can be a determining factor for the amount of current captured in an acceleration bucket, it is important to have some idea how great the growth is in the event of instability.

A search through all the calculations made showed that in no case did the final energy spread attained in an unstable configuration exceed three times the stabilizing value given by (23). The worst case of course was that where the initial energy spread was zero. The re-

sulting state for zero energy spread is a sharply bunched beam, with the bunch width equal to the kernel width.

Instabilities in the presence of appreciable initial energy spread cause final energy spreads to be more nearly just that required for stabilizing the system; an initial energy spread of half the stable value yields a final spread of roughly twice stable, and an initial 90% of stable energy spread gave a final value of 130%. It appears that the product of the initial and final energy spreads $\bar{W}_0$ and $\bar{W}_f$ in case of purely sinusoidal perturbations gives the square of the stable energy spread $\bar{W}_c$ for the given current density, to an accuracy of about 25%, if the initial value is not too far from stabilizing. Figure 9 shows a graph of $\bar{W}_0 \bar{W}_f / \bar{W}_c^2$ as a function of $\bar{W}_0 / \bar{W}_c$.

<u>Space Charge Clusters in RF Buckets.</u> We have quoted the result that the radio-frequency accelerating fields in an accelerator are well represented by adding the term

$$-\dot{W}_s + V \sin \varphi$$

to the field in the motion equation

$$dW/dt = 2\pi e R \, \mathcal{E}(\varphi, t).$$

Two methods often discussed for turning on the RF field are the "adiabatic" (slow) and the "sudden" turn-on programs. Adiabatic has been found to mean that the change from $V=0$ to the full value V_A should take at least one-half the synchrotron oscillation period (period of oscillation of a particle around the synchronous point when it is very

Fig. 9. Relation of initial ($\overline{W}_0$) and final ($\overline{W}_F$) energy spreads to the critical energy spread ($\overline{W}_c$) for a uniform beam. The final value gives the maximum energy spread of the bunches which result from instabilities when $\overline{W}_0 < \overline{W}_c$.

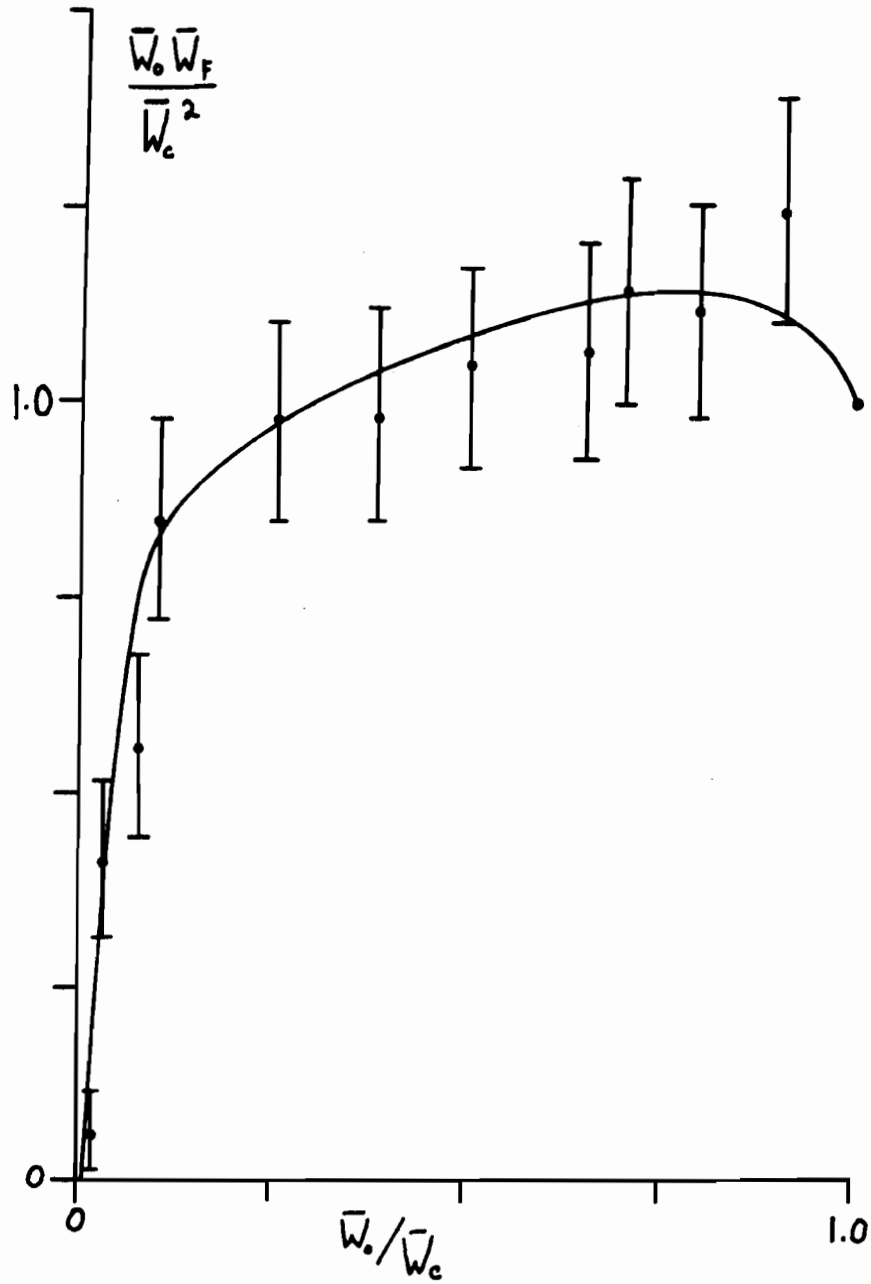

Figure 9

close to synchronous).

Several runs were made for beams above transition, using the sudden turn-on. When the energy spread was so adjusted to make the phase area occupied by the beam about a tenth the area of the bucket and enough particles were injected to make the beam unstable toward a relatively high harmonic perturbation (fifth or tenth) the result was that immediate formation of the stable space charge clusters occurred, and that these stable bunches revolved on phase orbits in the RF bucket roughly as single particles did. The bunches appeared to have a tendency to be destabilized by the coherent action of the RF term, so that the particles "leaked" out of the bunches and tended to spread out throughout the bucket.

This behavior is quite similar in nature to that observed in the absorption of small clusters by large ones. The value $\dot{W}_s$ used was too small to allow any loss of the particles from the bucket because of the space charge field to be observed.

The effect of a more adiabatic time program for turning on the RF field was obtained by giving the voltage V a linear time dependence with $V=0$ at zero time, and V taking the same value as in the previous run after a time equal to one synchrotron oscillation period at the full voltage. The voltage was then held constant.

With the slow turn-on, the instabilities had more time to develop before the question of capture into the bucket arose. In general the

increased energy spread caused by the instability reduced the total number of particles captured. The existence of circulating space charge bunches in the bucket was found in this case also.

Following the Motion of Boundaries

Nielsen and Sessler[2] suggest that most contemplated injection schemes cause a distribution in the phase space which is nearly constant inside a bounded region, and zero elsewhere. From this assumption, the linear calculation of perturbations on the uniform state yields the stability criterion (23) for a beam above transition. Even in the linear approximation however, following the motion of a perturbed system is difficult because the equations for the boundaries can usually be written only in parametric form. Thus in the limit of no interaction at all the boundary whose initial form is $W_B = \bar{W}\,[1 - \epsilon \cos(h\varphi)]$ takes the form $W_B = \bar{W}\,[1 - \epsilon \cos(h\varphi - W_B t)]$ for later times. This gives W_B only implicitly, while an explicit form must be known to calculate a density. Turning on the interaction does not help the situation, but Fourier methods allow solution in series form, in the linear approximation. In the nonlinear limit, the Fourier series do not provide a convenient solution.

Numerical solutions however may be obtained easily, although these are limited to following the motion only for a short time.

The essence of the calculation is that if the motion of the region boundary is found, then that of the system as a whole is uniquely deter-

mined. Movement of particles inside the boundary is unimportant here because the Vlasov equation says the phase density will remain constant wherever its gradients $\partial\Phi/\partial\varphi$ and $\partial\Phi/\partial W$ are zero and no explicit time dependence exists. For this system, the only gradients occur at the boundary. Computing the azimuthal density then becomes trivial, being simply the calculation of an area.

A computer program (see Appendix III) was written to follow the system. The phase boundary was represented by giving a large number of points on it and following their phase motion. The azimuthal density and field were represented as before, by 128 channel histograms. The motion of the boundary point (φ_j, W_j) is then determined by equations (32), which were integrated using algorithm (33).

Two topologically distinct types of filled regions (beams) in the phase space were studied. These are shown in Fig. 10. The upper region represents a perturbed uniform beam, the middle one a bunched beam, and the lower one a hybrid case with topological properties of the middle one.

In the program used, the boundary was assumed to be rectilinear between the points representing it. If the initial state is an unperturbed uniform beam, the motion is represented exactly for all time except for round-off error which should cause no trouble until a relatively large time. Any other state was approximated. Difficulties arise from this because the boundaries were stretched and distorted by

Fig. 10. The topology of phase boundaries in synchrotron phase space. The upper region is periodic in φ. The lower ones differ topologically from the upper one, and need not be periodic. The periodic nature of the space is accentuated by drawing it on a cylinder.

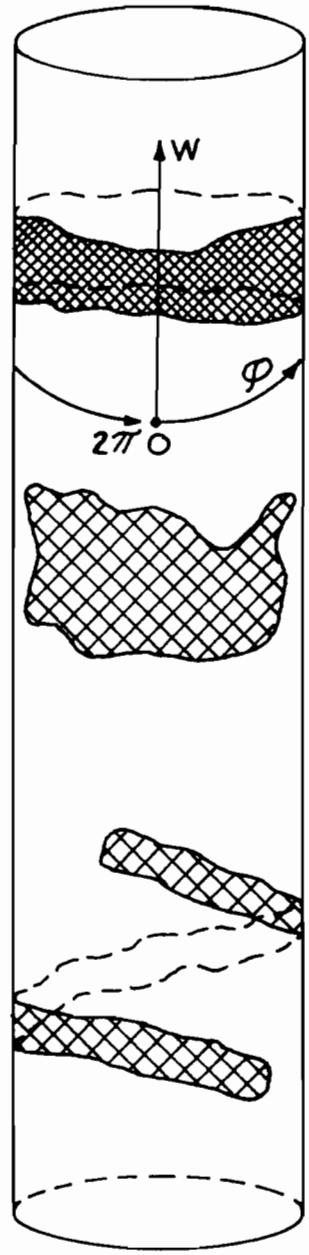

Figure 10

the motion of the system. For a finite number of points representing the boundary, a very definite upper limit was then placed on the time for which the calculation is valid. After this time the points on the boundary were so far apart that a straight line is not a good approximation to the boundary, and as it happened, the polygon connecting the points usually became multiply connected. This was easy to detect because its result was that one of the regions then contributed a density twice too large, or the right magnitude but wrong sign. Figure 11 shows just such a breakdown.

The azimuthal density was calculated using the polygonal formula

$$A = \frac{1}{2} \sum_j (X_{j+1} - X_j) \cdot (Y_{j+1} + Y_j)$$

for finding the area enclosed by the simply connected polygon whose vertices are (X_j, Y_j). The sum requires the points to be taken in turn as they are passed in circumnavigating the polygon in the clockwise direction in the (X, Y) plane. The area within the phase boundary and within the semi-infinite strip $(m - 1/2)\Delta\varphi \leq \varphi \leq (m + 1/2)\Delta\varphi$ was multiplied by the particle density σ and taken as the azimuthal density ρ_m in the same region of φ.

We note that one advantage of the boundary solution over the particle solution is loosely that the proximity of initially adjacent point pairs (W_j, φ_j) and (W_{j+1}, φ_{j+1}) is used in the calculation, so that more information is carried by the two numbers. Because the numbers φ_j

Fig. 11. A sample of one difficulty inherent with calculating boundary motion numerically by following the motion of points on it. The region in the center should have remained simply connected.

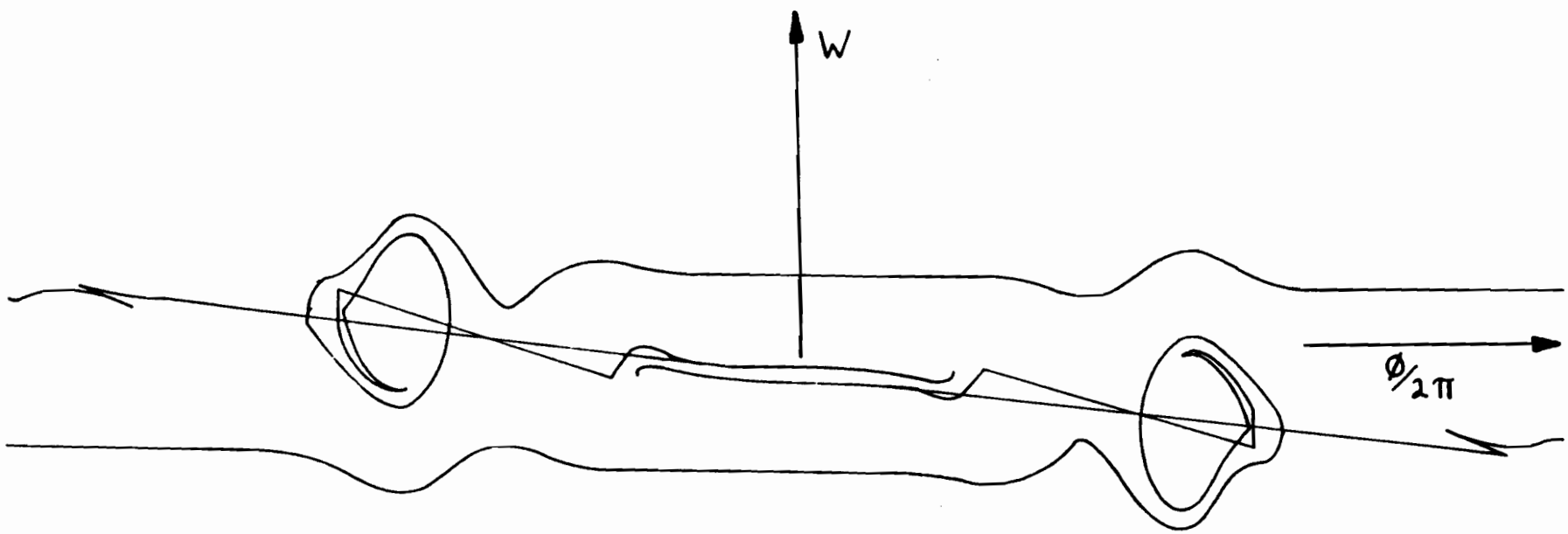

Figure 11

and W_j are kept in consecutive locations in the core storage of the computer, the subscript value j is implied by the locations of the numbers, and need not be stored separately. The major advantage however is that the representation has a continuous nature and no problems arise from poor statistics. The disadvantage is that already mentioned: In general, a boundary becomes arbitrarily complicated in infinite time, and an infinite number of points must be used to represent it. This difficulty could be alleviated by a more elaborate scheme for the area calculation, but would not be completely solved. This failure at long times was accepted and the method used to investigate behavior on a smaller scale.

The normalization was checked as before by analyzing growth rates of perturbations on a uniform beam. With a finite energy spread (average) of $2\bar{W}$ and a perturbation of harmonic h, these are given by equation (38). The same analysis scheme was used as in testing the particle program, viz. extrapolation to zero time. The results were accurate, again to within the error estimated for the extrapolation, roughly 5%.

The type of perturbation available in this calculation is necessarily limited to variation of the form of the boundary. The dividing line between stability and instability under a perturbation of a boundary is not at all well defined.

Figure 12 shows the configuration in the (W,φ) space taken by the boundaries initially given by $W_{\pm}(\varphi) = \pm \bar{W}(1-\epsilon\cos\varphi)$, after the elapse of time approximately $1/\bar{W}\epsilon$. The five pairs of lines represent a boundary at five successive times in this neighborhood. The upper wave front is moving toward the left. For this run, no interaction at all was included. It is seen that the distribution, just by its streaming motion, becomes radically different from the original one in the region $\bar{W}(1-\epsilon) \leq |W| \leq \bar{W}(1+\epsilon)$. The three diagonal straight lines are spurious, and represent failure by oversight to raise the pen on the digital plotter. The points connected by these lines are those which were initially at $\varphi = 0$.

<u>Beams above Transition Energy.</u> Turning on a small interaction yields behavior similar to the zero field case, except that the region of "included air," the thin streams of unfilled phase space going into the filled region, penetrates farther toward the center of the band. There appears to be some limiting case where the streamer crosses the $W=0$ line. In this symmetrical initial load, the upper and lower streamers will then eventually wind around one another. If a bunching of the beam can occur because of this, it cannot be seen before the approximation breaks down. Figures 13 and 14 show a weak field run and a run which has the streamers crossing the axis. In the latter case, the field strength was within 10% of the critical value for immediate bunching given by equation (31). In the former it was roughly 50% of

Fig. 12. Boundary motion when no fields are present. The initial boundaries were $W(\varphi) = \pm \bar{W}(1 + \epsilon \cos \varphi)$. The phase diagram shows them after 5, 6, 7, 8, and 9 equal time intervals. The wave front on the upper set of curves is moving to the left; that on the lower, to the right.

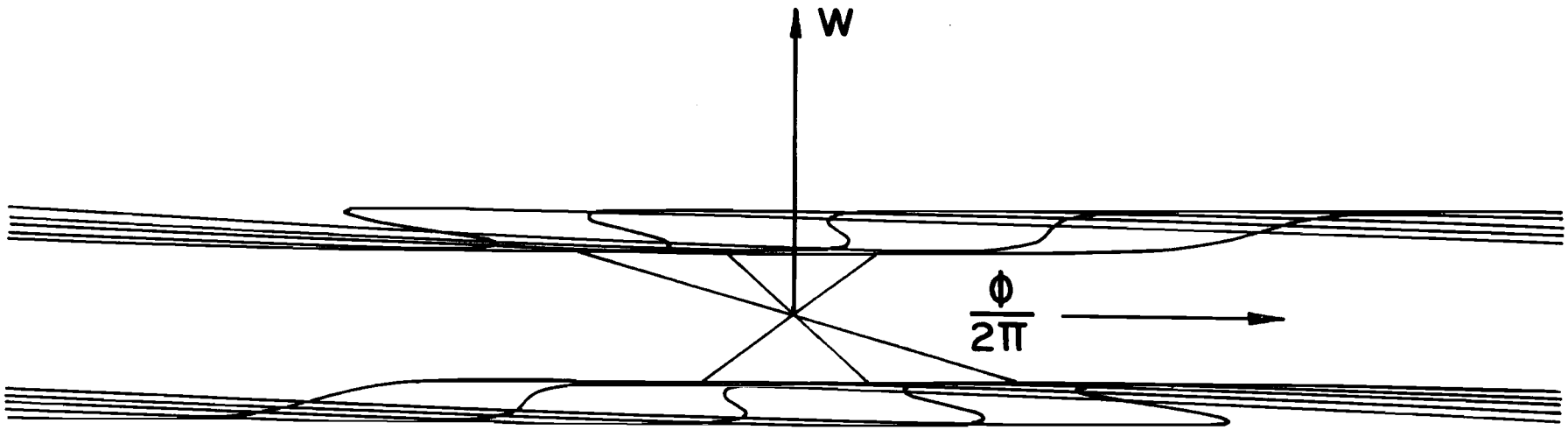

Figure 12

Fig. 13. Boundary motion, as in Fig. 12 except that a very small interaction is present. The interaction is that of a beam above transition energy. The time intervals here are smaller than those in Fig. 12, but the elapsed time is comparable.

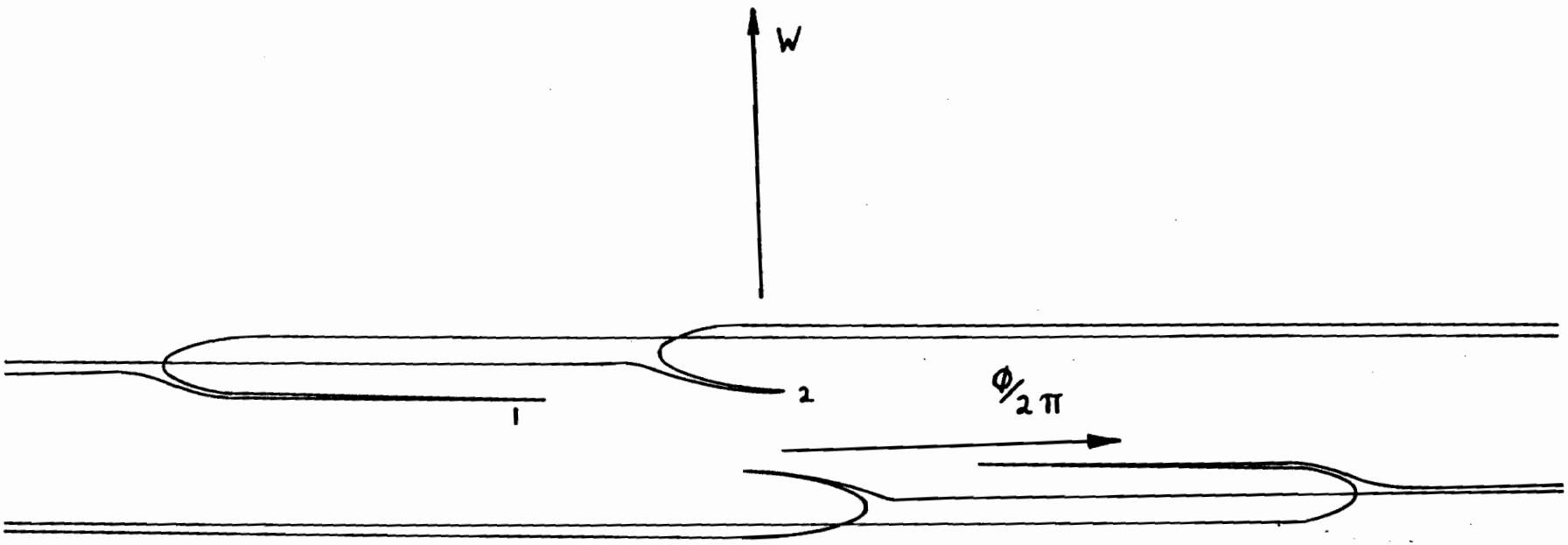

Figure 13

Fig. 14. Boundary motion, as in Fig. 12 and Fig. 13, except that the interaction is larger. The system is above transition energy. The field here is nearly large enough to cause immediate bunching of the beam. The elapsed time is comparable to that in the previous two figures.

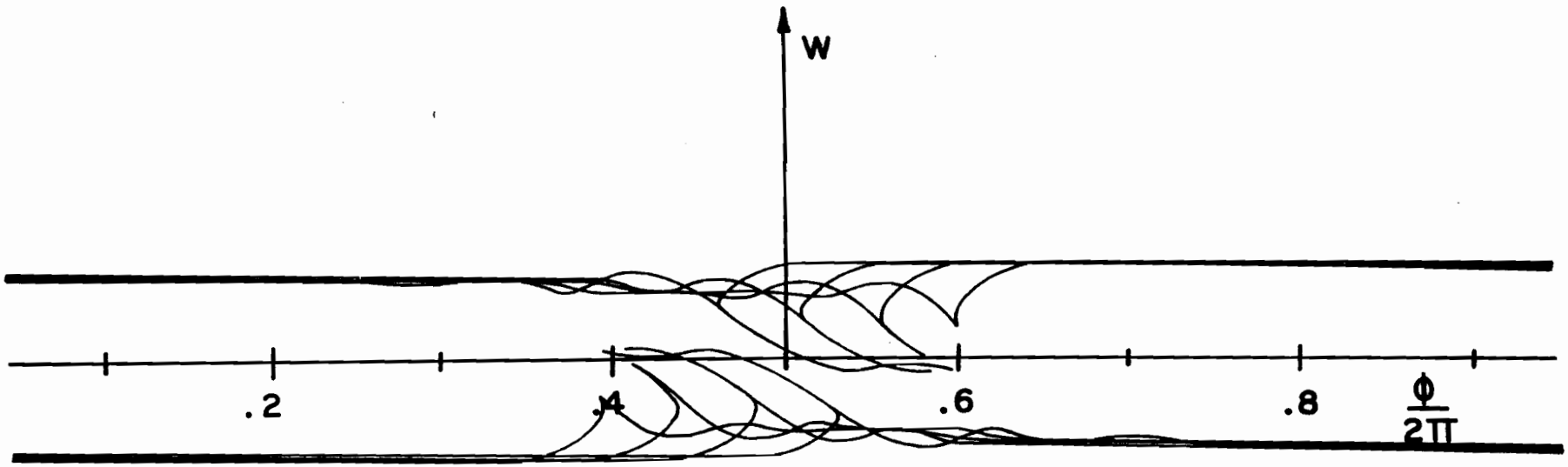

Figure 14

this value.

In the following sections on the uniform beam, the value $\bar{W}$ was taken as 1.0, while $2\pi eRN$ was $64/\pi^2$ and the parameter K_0 was varied to change the field. This number is a multiplicative factor for the entire kernel whose functional form was fixed throughout this section at the form shown in Fig. 4. Since the entire problem scales, the value $\bar{W}/\sigma$ and the value K_0 suffice to determine all the parameters of the system when it is known that the critical value of K_0 is given by

$$K_0^c = 0.189\ (1-\epsilon),$$

where $\epsilon\bar{W} = \epsilon$ is the amplitude of the perturbation. The perturbations used were 25% variations, that is, $\epsilon = 0.25$ for which $K_0^c = 0.145$. The values K_0 used for the runs in Fig. 13 and 14 were 0.0625 and 0.125.

A run which shows the behavior under the bunching phenomenon is shown in Fig. 15. The value K_0 here was 0.1875.

It was from observation of these pictures that the criterion for immediate beam bunching was noted. Another run, using $K_0 = 0.25$ is shown in Fig. 16.

Because the resultant states in Fig. 15 and 16 seemed reminiscent of the square-hump state described except that ends were rounded off in an azimuthal distance of approximately the half width of the kernel, some test runs having the nature of a perturbed and rounded square distribution were tried. The Casini Oval

$$[y(x)]^2 = (\alpha^4 + 4x^2)^{1/2} - 1 - x^2$$

Fig. 15. Boundary motion above transition, in the presence of interaction large enough to cause beam bunching. All parameters are identical to those of Fig. 12-14, except that a multiplicative factor in the interaction is larger.

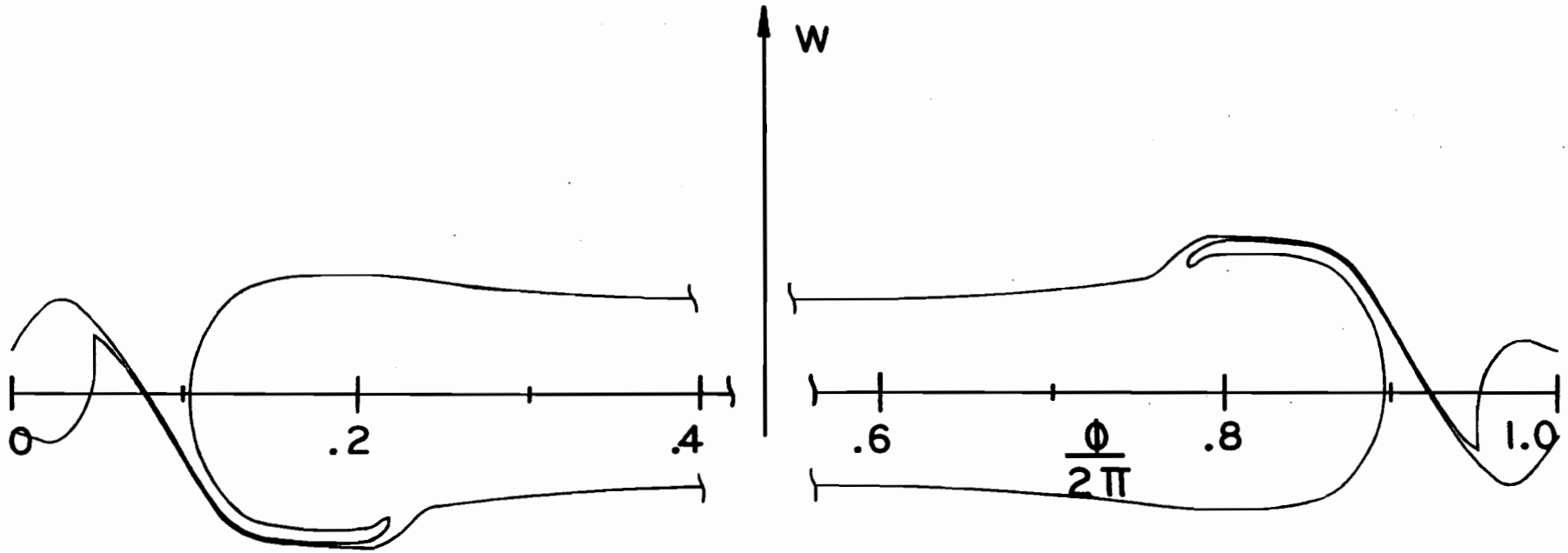

Figure 15

Fig. 16. Boundary motion as in Fig. 15, except that the interaction is stronger. Three boundaries are shown, indicating the motion during equal time intervals.

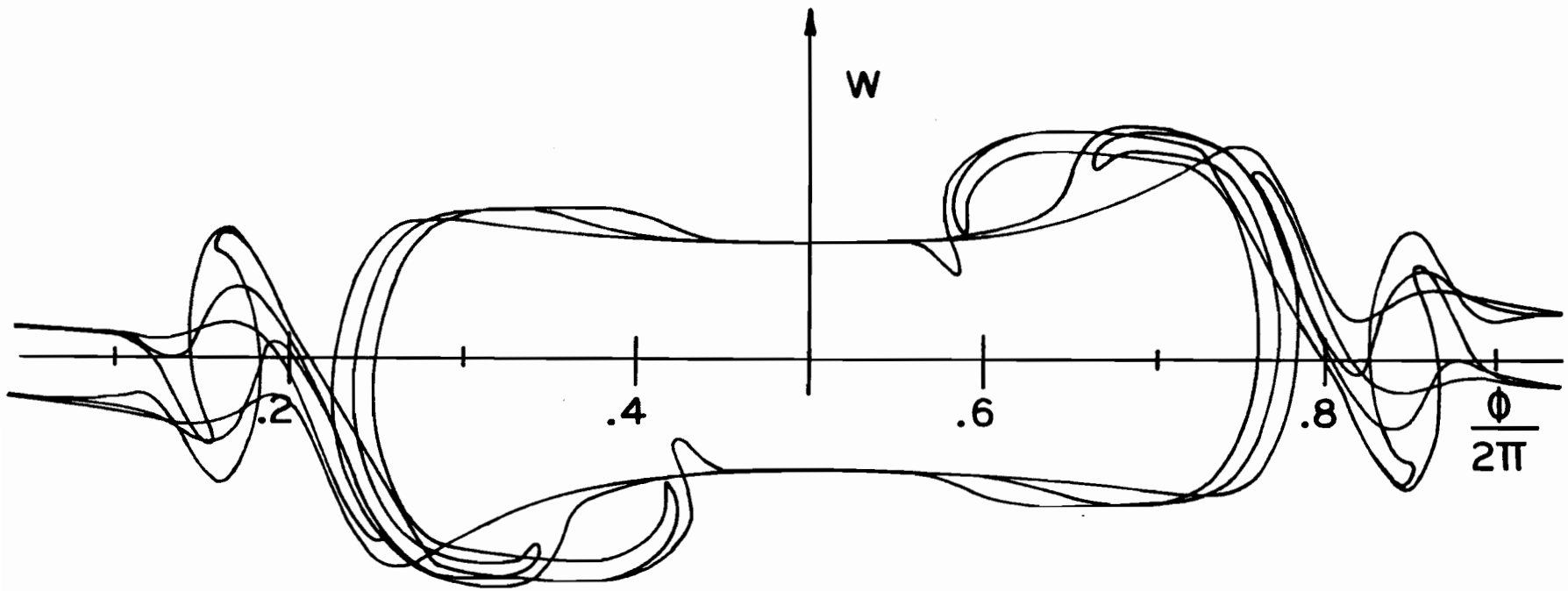

Figure 16

was chosen as a tractable if vague approximation to these final state bunches. The rounded corners of this oval do not have the correct functional dependence for the stationary state, and this constitutes an additional perturbation. Figures 17 and 18 show such a run. In these, graphs of the field are superimposed on the plots of the boundary. The field increases with time and perturbations travel counterclockwise around the boundary. The second figure shows three successive configurations of the system at a time much later than that of the first. Later pictures were not judged presentable because of pen troubles on the digital plotter, but showed that the perturbation travels around the end of the distribution with no ill effects. That is, it does not become any larger, nor does any other part of the boundary become substantially different. The strong nonisochronism of this state caused the small cusp discernible in these pictures to spoil the approximation shortly after the latter picture and long time behavior could not be studied. An analogous computation with the particle following program gave the same results for a much longer time. The perturbations travel around the boundary with little discernible decay and no apparent tendency to eject particles from the bunches.

Beams below Transition. One of the more interesting results of the boundary program obtained when a mispunched input card changed the sign of the field kernel. This is equivalent to calculating the motion

Fig. 17. Boundary motion approximating further evolution of the large cluster formed in Fig. 16. Curve 1 is the initial form, and 2 and 3 follow at equal time intervals. The interaction field at the corresponding times is superimposed. The field increases with time.

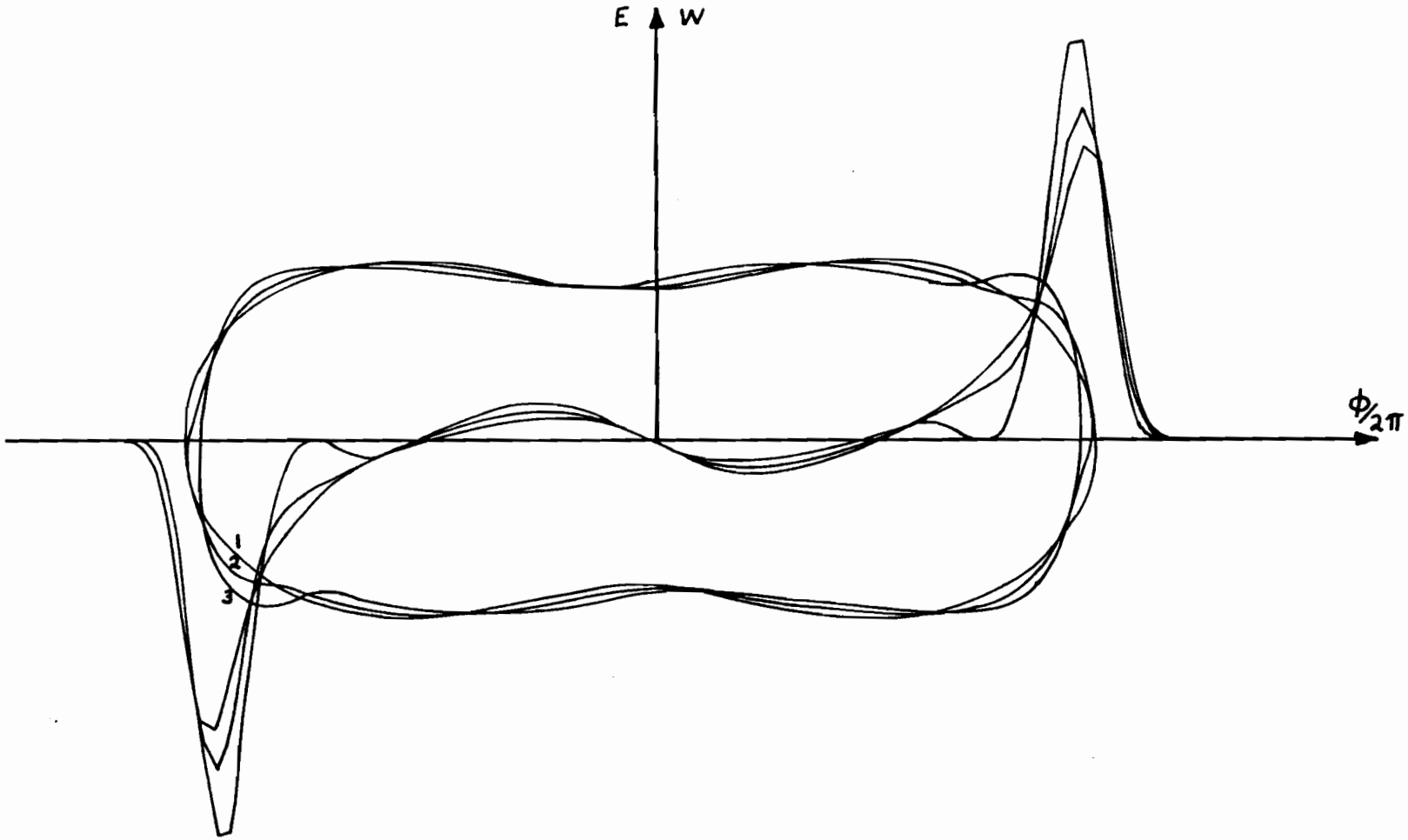

Figure 17

Fig. 18. Continuation of Fig. 17, showing the boundary after 11, 12, and 13 time intervals. The lines are broken to aid distinguishing them.

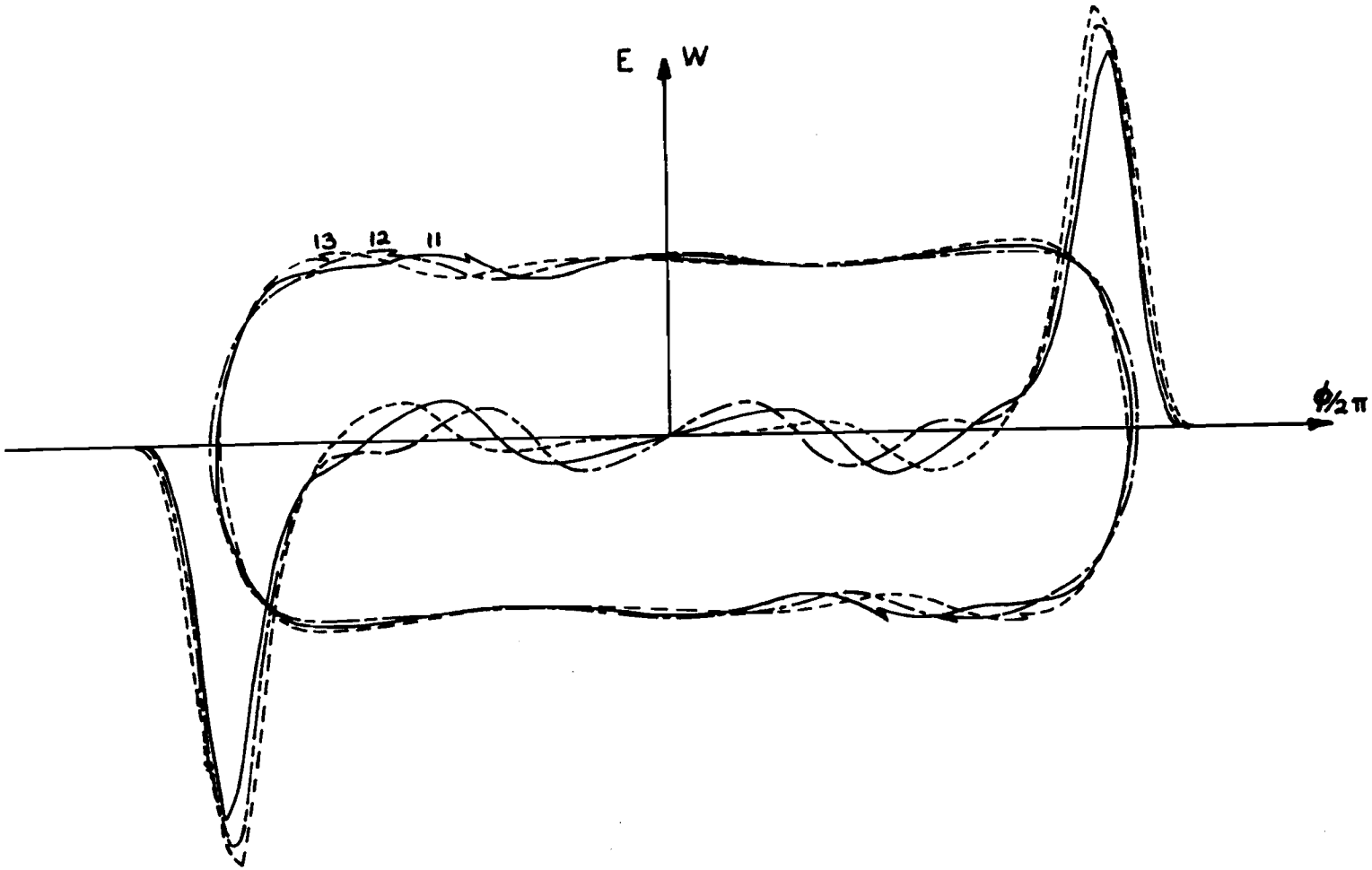

Figure 18

of a beam below transition, in view of equations (32). The distribution proved to be unstable in a certain sense. Shortly after this, beam bunching phenomena below the transition energy were observed in the MURA 50 Mev electron test model, and similarity to results in other machines was noticed.[6] Some further investigations therefore were made on the computer.

Rowe[6] has noted that the two-stream instability (cf. equation (20)) might cause this type of instability. As we have seen here, such an instability can occur with only a very small depression on the velocity distribution and analysis is complicated by an overabundance of mechanisms. As we have seen, a perturbation in the boundary of a distribution streams around, in the absence of interaction, until a two-stream distribution obtains. After the wave crest in Fig. 12 has overtaken the slower portions of the boundary, a two-stream situation exists. Sufficiently here means by the width of the field kernel, which is very small as we have seen.

We may generalize this result and say that with no interaction, the streaming motion acting on a boundary of the form $w = \bar{w}(1 + \epsilon \cos\varphi)$, first causes the boundary to attain a vertical tangency at time $1/\bar{w}\epsilon$, and that thereafter a two-stream mode exists. At this time, a particle at $\bar{w}$ has traveled an azimuthal distance $1/\epsilon$. Thus a perturbation of 16% yields a two-stream mode after the wave crest moves by $\Delta\varphi = 2\pi$ in the rotating coordinate system. Using the numbers

this same effect increases the width of the gap which will develop to form the two streams, so that the instability is less likely or will take longer to develop.

However, another mechanism for instability exists, as may be seen in Fig. 20 and 21. It is seen that for a strong perturbation (ϵ is 25% here) the interaction of a boundary perturbation with itself tends to increase the energy spread as should be clear, but also causes a very definite wave to appear on the boundary. It is noted that this occurs before the beam can be claimed to be in a bimodal configuration. The time at which these waves have definitely appeared is just that time taken by the fastest particle to lap one with the average energy, and this is the same as the time calculated in the previous paragraph, and therefore for the 25% modulation this nonlinear instability can also occur after roughly the observed interval. The perturbation required for this seems to be larger than that thought to exist, but we repeat that there are few experimental observations upon which to base any firm conclusions.

To assure that this wave development is not dependent upon some approximation in the numerical computation, various parameters were changed. It is recalled that the field kernel of Fig. 4 was used for most of the calculations and that this shape was taken to account for the width of the macroparticles in the particle program. Since most of the present results do not depend upon the shape but upon the Fourier ampli-

Fig. 20. Boundary motion with interaction as in a beam below transition, showing nonlinear effects and development of a wave. The upper boundary was initially $W(\varphi) = \bar{W}(1+0.25\cos\varphi)$, and the lower was $W(\varphi) = -\bar{W}$.

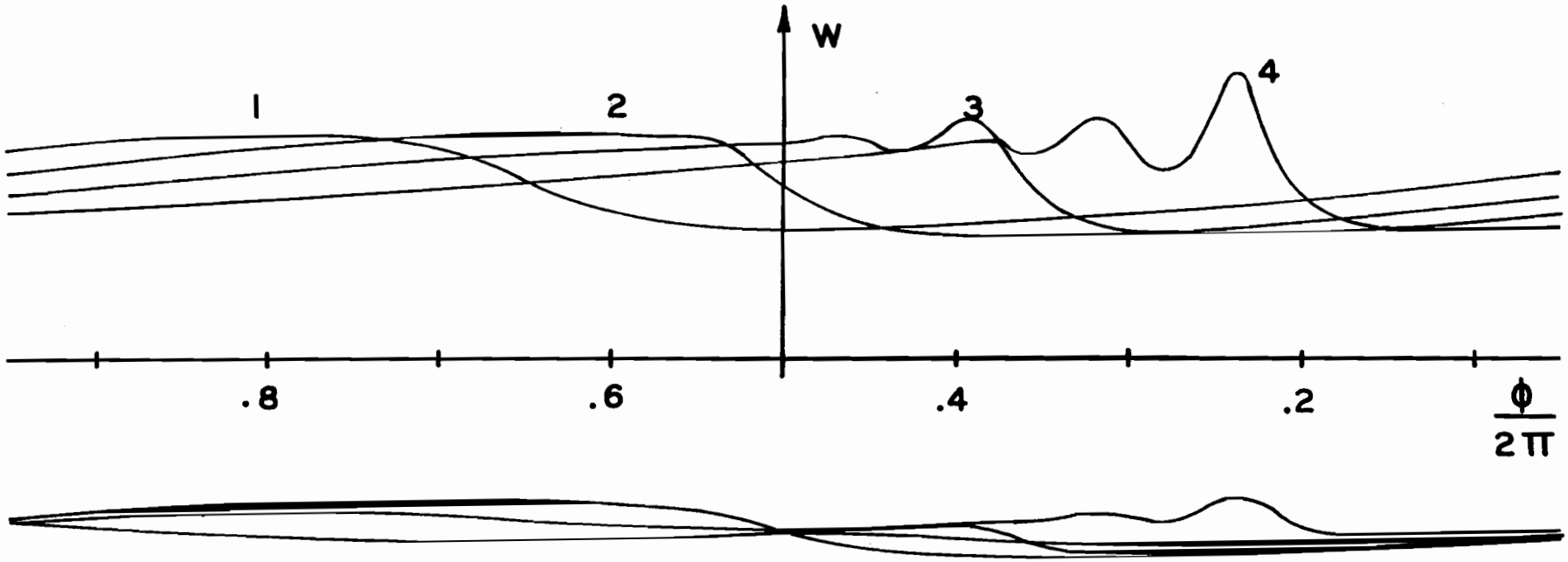

Figure 20

Fig. 22. Development of the wave structure below transition when the lower boundary is moved far enough away to have negligible reaction to the modulation on the upper one. The boundaries here were initially at $W = \bar{W}(1+0.25\cos\varphi)$, and at $W = -5\bar{W}$.

quoted by Rowe,[6] viz., $\delta\omega_s/\omega_s = 4.0\cdot 10^{-4}$ and $\omega_s = 2.0\cdot 10^{7}$ cps, for the frequency spread $\delta\omega_s$ and frequency (stationary frame) ω_s, as being reasonable estimates for the injection process used in the MURA 50 Mev electron accelerator, we obtain the result that in the time required by the fastest particle (angular frequency $\omega_s + \delta\omega_s$ to circle the machine twenty times, the two-stream mode appears, given a modulation of only 8% of the total energy spread of the beam. According to Rowe,[22] this is a fairly reasonable number of circuits, and instabilities have been observed 20 to 200 particle circuits after injection begins. It is thought that a reasonable picture of the injection process used gives a phase density roughly constant in the shaded region shown in Fig. 19 and zero elsewhere. The scheme is multiturn injection with betatron acceleration giving an average energy gain per turn of order 100 ev. This energy should correspond to the height of the steps in the diagram. After 20 turns the step is roughly 5% of the total energy width and we see that all the numbers are roughly consistent. We have a mechanism for obtaining a two-stream mode in roughly the time for which experiment yields an instability. The calculation here has really been to zeroth order in the field strength, but we can argue heuristically that the first-order effects cancel. Thus, under the influence of space charge this step in the boundary being a nonuniformity, will tend to have its height increased, and therefore will tend to stream faster, and the two-stream mode will appear sooner. On the other hand,

Fig. 19. Conjectured phase distribution at injection in the MURA 50 Mev electron accelerator. The particle density is regarded as uniform within the shaded region, and zero elsewhere.

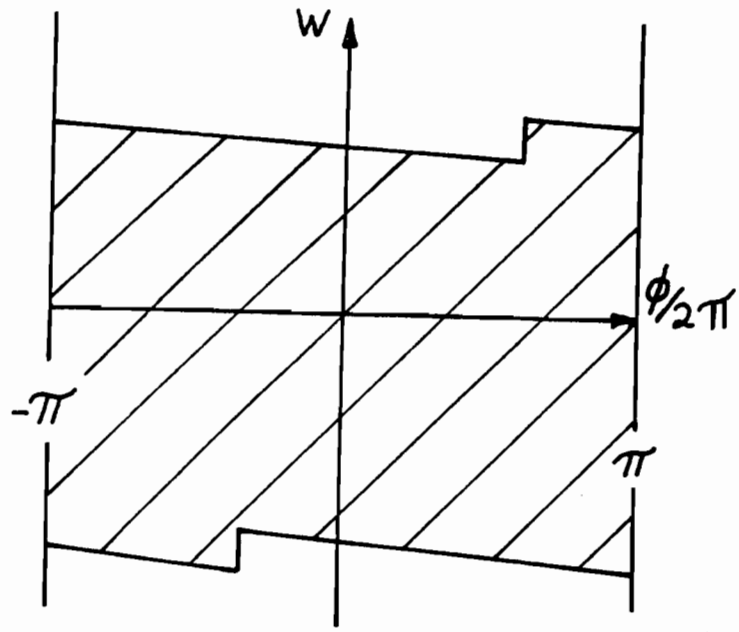

Figure 19

this same effect increases the width of the gap which will develop to form the two streams, so that the instability is less likely or will take longer to develop.

However, another mechanism for instability exists, as may be seen in Fig. 20 and 21. It is seen that for a strong perturbation (ϵ is 25% here) the interaction of a boundary perturbation with itself tends to increase the energy spread as should be clear, but also causes a very definite wave to appear on the boundary. It is noted that this occurs before the beam can be claimed to be in a bimodal configuration. The time at which these waves have definitely appeared is just that time taken by the fastest particle to lap one with the average energy, and this is the same as the time calculated in the previous paragraph, and therefore for the 25% modulation this nonlinear instability can also occur after roughly the observed interval. The perturbation required for this seems to be larger than that thought to exist, but we repeat that there are few experimental observations upon which to base any firm conclusions.

To assure that this wave development is not dependent upon some approximation in the numerical computation, various parameters were changed. It is recalled that the field kernel of Fig. 4 was used for most of the calculations and that this shape was taken to account for the width of the macroparticles in the particle program. Since most of the present results do not depend upon the shape but upon the Fourier ampli-

Fig. 20. Boundary motion with interaction as in a beam below transition, showing nonlinear effects and development of a wave. The upper boundary was initially $W(\varphi) = \bar{W}(1+0.25\cos\varphi)$, and the lower was $W(\varphi) = -\bar{W}$.

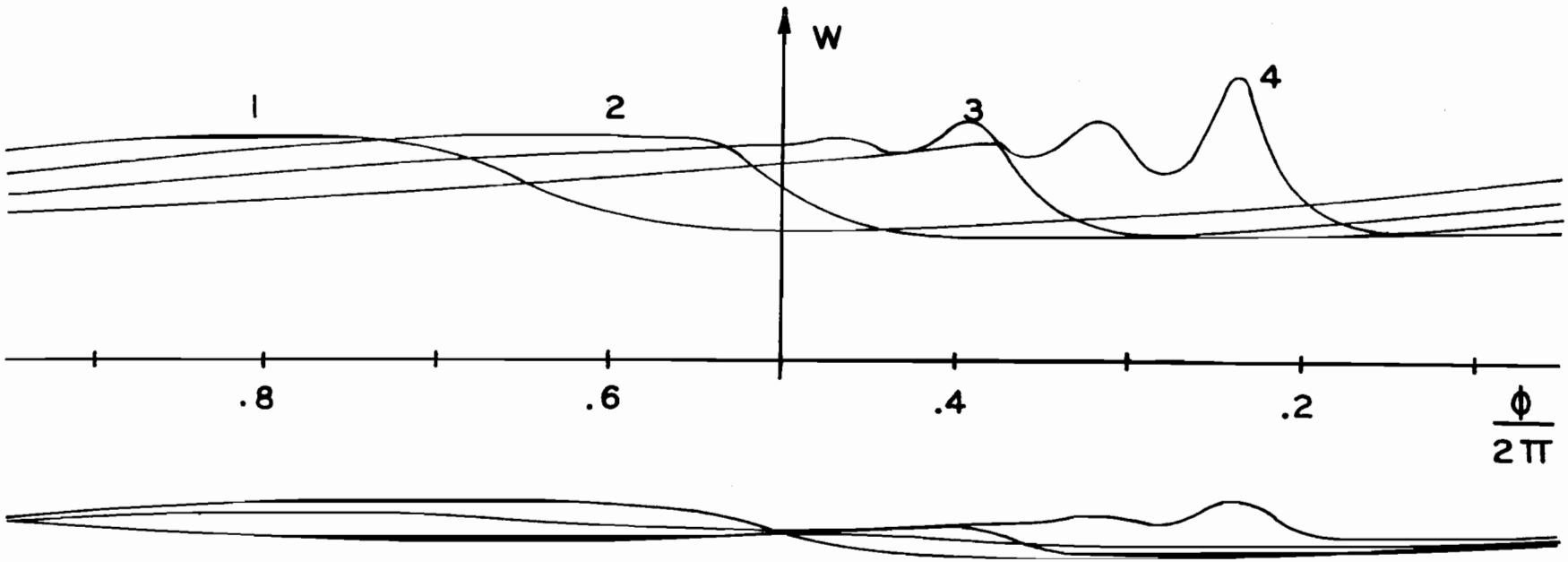

Figure 20

Fig. 21. Further development of the system in Fig. 20. The curve labeled 1 is double, showing the motion during 1/16 the time interval between curves 1 and 2.

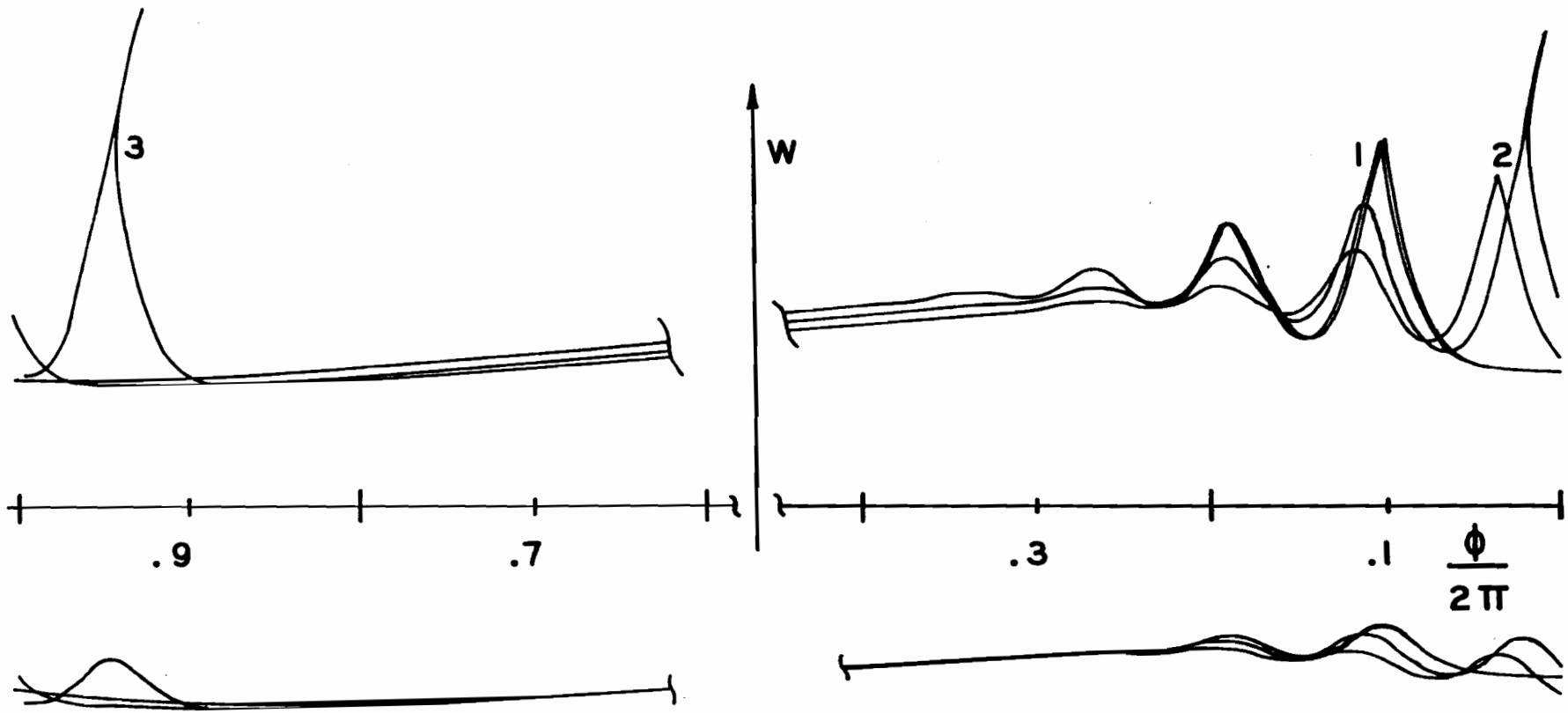

Figure 21

tudes of the kernel, the shape is normally not critical. Using the more proper exponential kernel by taking K_m proportional to 2^{-m}, except cut-off after the seventh term, gives a kernel with the same range as the usual one, but higher harmonics contribute proportionately more. The results were similar, and growth occurred again, with the same wavelength to within 10%, the accuracy of the measurement. A run doubling the kernel width appeared to double the wavelength of the waves, again to within the 10% measurement accuracy. The wavelength is roughly equal to the kernel width. The measurements suggest that the wavelength increases somewhat with amplitude, for large values. However, the change was less than the error quoted. It was found that the same waves develop when the lower boundary is not excited initially, when it is made farther away by increasing the energy spread by a factor five, and when it is not allowed to react to fields caused by the waves on the upper boundary. (Charge is not conserved in the last.) It is thought that this instability is a proper behavior of the mathematical model in the nonlinear region below transition.

The term instability as used here, is subject to the objection of being vague. It is not clear that a growth rate can be defined for it. The growth occurs sufficiently close to the "saturation" point where streaming tends to eliminate further growth (see Fig. 22) so that exponential behavior is a poor fit to the form of the growth.

Fig. 22. Development of the wave structure below transition when the lower boundary is moved far enough away to have negligible reaction to the modulation on the upper one. The boundaries here were initially at $W = \bar{W}(1+0.25\cos\varphi)$, and at $W = -5\bar{W}$.

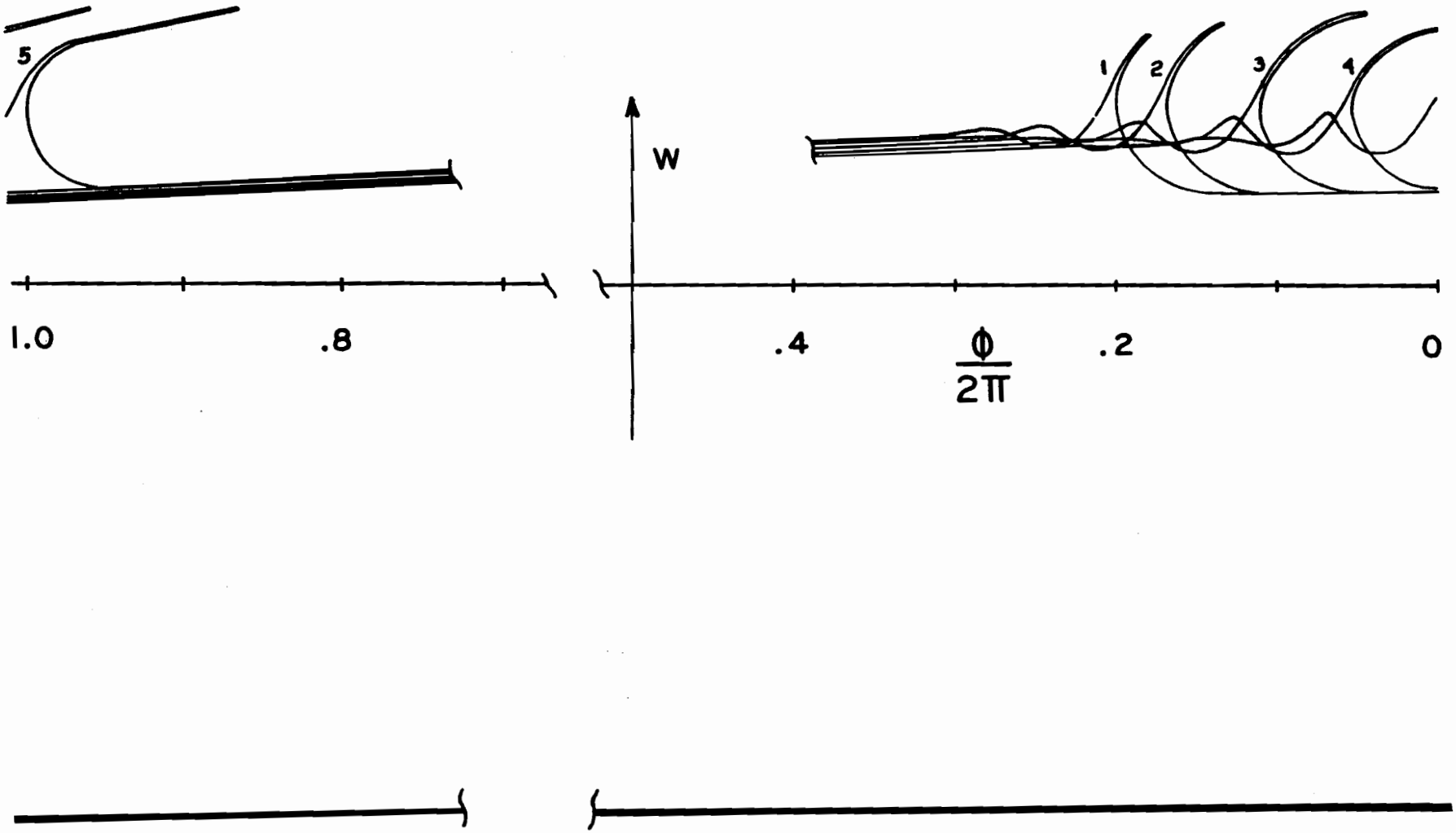

Figure 22

We have then two mechanisms by which an instability can occur below transition, using only the longitudinal interaction of the beam. There are many others possible for obtaining a multimodal distribution and especially in view of the instability of the distribution with a very narrow depression, it is not surprising that beam modulations develop below transition.

Attempts to differentiate or further understand the two mechanisms mentioned by using the computer programs available have proved unsuccessful because of the inherent limitation of the programs: One cannot follow a system for long times, and the other cannot represent fine grained structure in the distribution function.

The simplest two-stream system for which the computations were attempted was one in which an initially chopped-off beam with a reasonable energy spread was allowed to shear by streaming until many streams were formed. Figures 23 and 24 show such a system initially and after two revolutions in the moving coordinate system. The result of the interaction is that the bands tend to remain well separated despite the shearing, and no evidence of any exponential growth is seen. The elapsed time at the second picture is roughly twice that calculated for two-stream instability to occur by assuming no interaction until the instability is ready to begin. Restated, the bands of filled phase space remain separated about twice as far as they should under the streaming motion alone and this is sufficient to stabilize the distribution for some

Fig. 23. Phase space boundary enclosing a region filled with particles. This is the initial distribution used in seeking two-stream effects below transition.

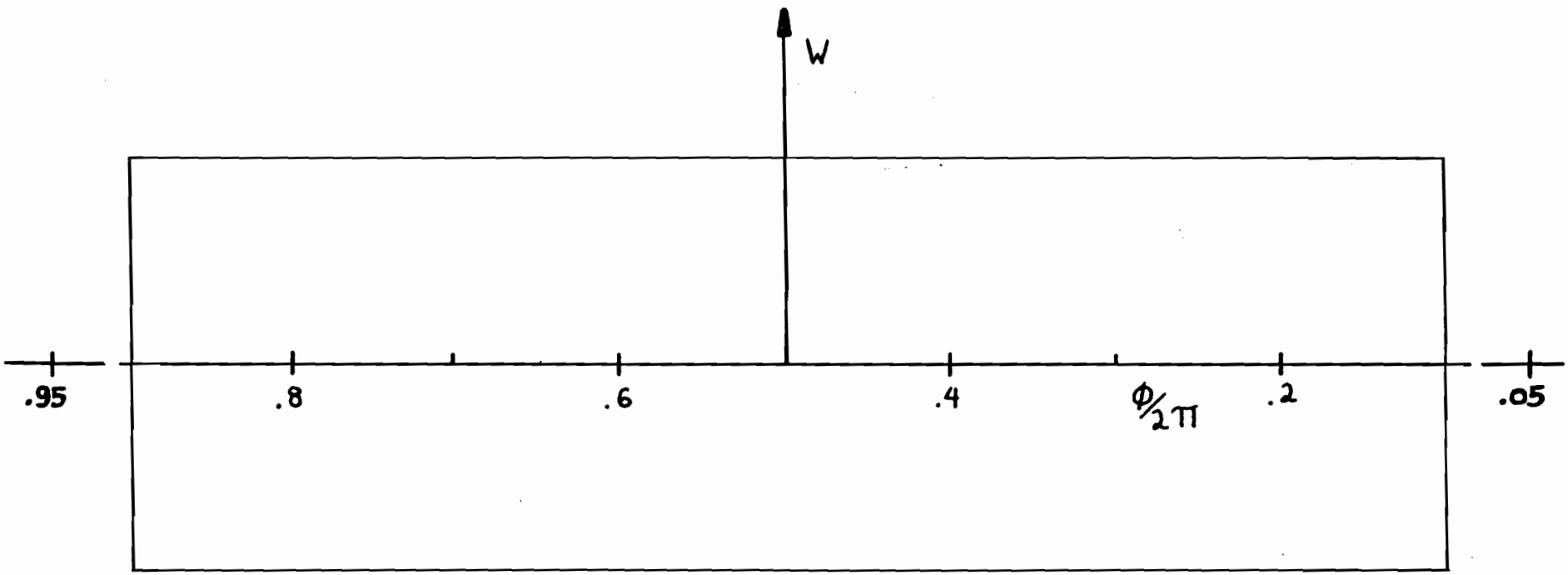

Figure 23

Fig. 24. Evolved form of the boundary in Fig. 23. The interaction has increased the energy spread enough to stabilize the system toward two-stream instability.

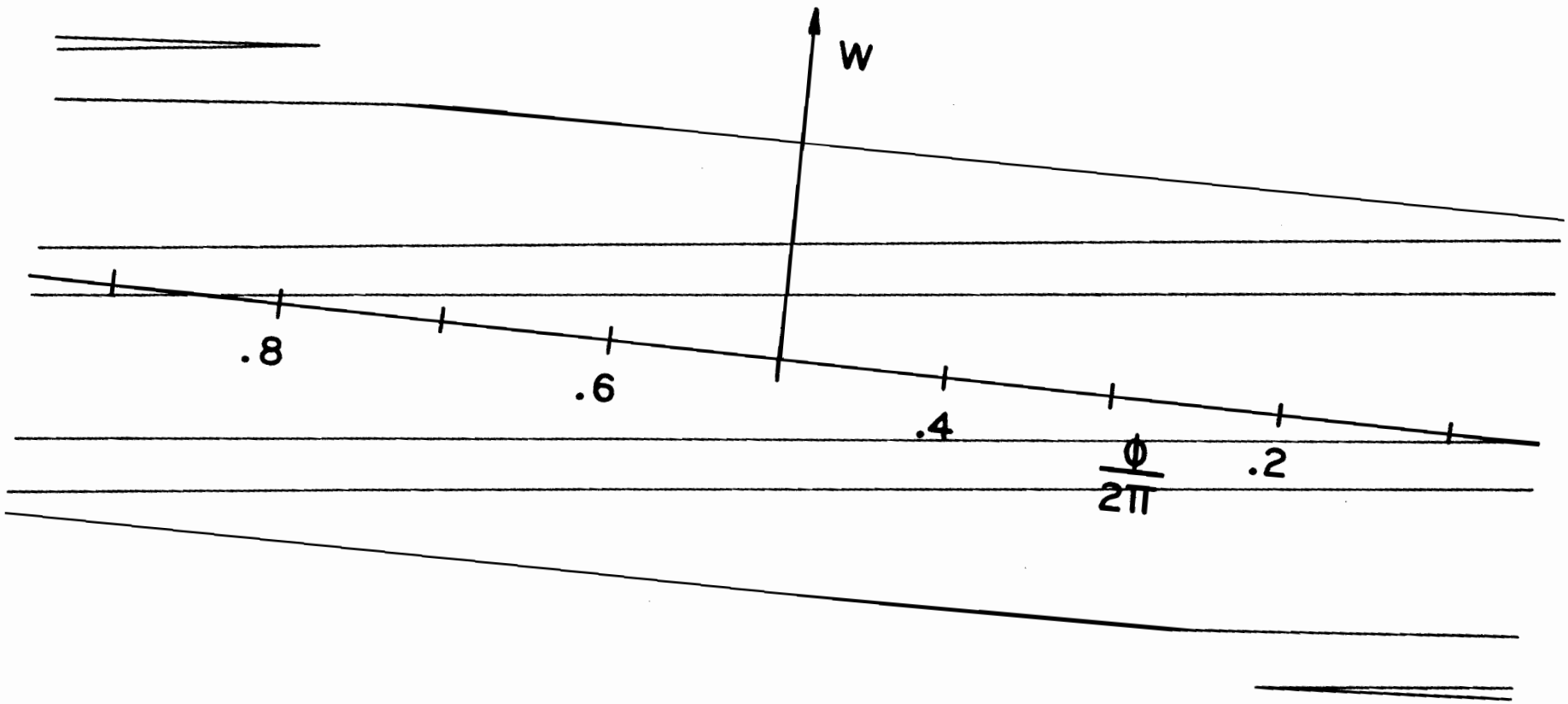

Figure 24

time. Again the approximation began to fail after the last picture, and the run was not continued. Similar runs were carried out with greater and smaller field strengths (by factors two) with the same result. In each case, the separation of the streams remained greater than the critical value, and roughly twice that given by a calculation assuming no interaction. It is possible that this type of initial system is always self-stabilizing and that two-stream instabilities cannot occur as a result of the shearing of bunched beam, unless the gap in the azimuthal spread is very small.

CONCLUSIONS

Computer studies have indicated that azimuthal modulations of the current densities in the Cosmotron and the MURA 50 Mev electron accelerator may be understood qualitatively. The theory given by Nielsen, Sessler, and Symon[2] appears to provide phenomena corresponding to most of the gross features of the experimental observations. The theory predicts these phenomena, despite failure to include details of the transverse motion of the beam or to do a more careful analysis of the fields. The extension to the nonlinear region appears to be the only modification required to obtain such results.

The phenomena noted both in the computer experiments and those on the accelerators include the tendency of a uniform beam above transition energy to assume a stably bunched configuration when the energy spread is too small to stabilize the uniform state. Also found are interactions of such clusters as entities, both with one another, and with the RF accelerating fields. Both types of experiments indicate that insufficiently tightly bound clusters may coalesce to form larger clusters in which the original ones lose their identities.

More detailed correspondence between the two types of experiments was not obtained because of time limitations on the amount of

detail which could be analyzed numerically. Thus, the shapes of the stable bunches were consistent with those seen in the accelerator experiments, but to claim them to be the same would be unjustifiable.

The bunching of uniform beams below transition has been observed to occur through at least two mechanisms, the two-stream instability and the growth of large perturbations. The accelerator experiments have not yet been made in sufficient detail to obtain an accurate picture of the beam profile (say $\rho(\varphi)$ vs. φ), and determination of which, if either, of the two mechanisms is responsible for the modulations is not yet possible.

A symmetry principle has been demonstrated showing that particle clusters above transition energy, and particle deficiencies below behave in the same fashion.

In private communication, C. E. Nielsen has suggested that this result can be combined with the nonlinear behavior noted here, of a small energy spread beam above transition. This shows the configuration taken after long times, when a two-stream instability occurs below transition. The modulations observed at the MURA 50 Mev electron accelerator could be regarded as the result of the formation of a stable hole in an otherwise uniform distribution in the synchrotron space. The experiments also show that the density modulations are themselves amplitude modulated at a very low frequency; that is, a

beating phenomenon occurs. Two stable holes in an otherwise uniform distribution would exhibit just such behavior if they were centered at slightly different energies.

It has been seen that the motion of a one-dimensional many-body system may be studied with the current digital computers when analytical approaches prove to be too difficult.

ACKNOWLEDGEMENTS

The study made here has been supported by the United States Atomic Energy Commission Contract No. AT(11-1)-384 through Midwestern Universities Research Association, Madison, Wisconsin. Personal support for two years by the Wisconsin Alumni Research Foundation, Madison, Wisconsin, in the form of a fellowship, coincided with part of this work.

The author wishes to thank Professor K. R. Symon for suggesting and supervising this research. Conversations with C. E. Nielsen, R. S. Christian, and D. C. Morin, Jr. were extremely fruitful. The entire computer staff at MURA was very helpful when the computer programs were written. An especial debt is acknowledged to Miss Jean Luniak for deciphering the manuscript and assisting with the proofreading.

APPENDIX I. AN APPROXIMATION TO THE RELATIVISTIC FIELD

We proceed with a solution to equation (5) in the approximation that we are discussing situations where the azimuthal dependence of the field is at a harmonic sufficiently high to allow the dependence of K_j' upon n to be neglected.

The periodicity requirement in φ proves to be an unnecessary complication here, so we will synthesize a periodic solution from solutions to

$$\left(\frac{\partial^2}{\partial x^2} - K^2 - \frac{1}{c^2}\frac{\partial^2}{\partial t^2}\right) g(x,t) \equiv \underline{O}\, g(x,t) = -4\pi f(x,t), \tag{A1}$$

where a particular transverse mode is chosen with $K_j/R^2 = K^2$, and $-\infty < x < \infty$. The boundary condition is now that the solution $g(x,t)$ should be bounded for large x. This is the equation governing propagation of the electric field in a rectangular waveguide excited in a transverse electric mode.

The Green's function $G(x,t)$ for the system is given by the well-known formal expression[23]

$$G(x,t) = 4\pi \sum_{\lambda} \psi_\lambda^*(x,t)\, \psi_\lambda(0,0)\, \omega_\lambda^{-1}, \tag{A2}$$

where ψ_λ and ω_λ are the eigenfunctions and eigenvalues of the operator $\underline{O}$:

$$\underline{O}\,\psi_\lambda = \omega_\lambda \psi_\lambda . \tag{A3}$$

Suitably normalized forms for these are

$$\psi_\lambda(x,t) = (2\pi)^{-1} \exp(ikx - i\omega t), \quad \text{and} \quad \omega_\lambda = \omega^2 c^{-2} - K^2 - k^2. \tag{A4}$$

Then

$$G(x,t) = \frac{1}{\pi}\int_{-\infty}^{\infty} d\omega\, e^{-i\omega t} \int_{-\infty}^{\infty} dk\, e^{ikx} [\omega^2 c^{-2} - K^2 - k^2]^{-1}. \tag{A5}$$

A contour in the k plane which passes between the two poles at

$$k = \pm k_0 = \pm\sqrt{\omega^2 c^2 - K^2},$$

results on making the replacement

$$(k_0 - k)(k_0 + k) \longrightarrow (k_0 + i\epsilon - k)(k_0 + i\epsilon + k). \tag{A6}$$

if ϵ is real and positive. This contour yields a Green's function symmetric in x, the appropriate symmetry here. The result of the integration is then

$$G(x,t) = -2\pi i\, e^{-\epsilon|x|} \frac{1}{2\pi i}\int_{-i\infty}^{i\infty} d\rho\, e^{\rho t} [i\epsilon + ic^{-1}\sqrt{\rho^2 + c^2K^2}]^{-1} e^{-\epsilon\sqrt{\rho^2+c^2K^2}}, \tag{A7}$$

where ρ is $-i\omega$. Taking a contour to the right of all singularities in the ω plane in order to obtain a Green's function which satisfies the principle of causality, this integral becomes a Laplace transformation inversion, which is found in the more comprehensive tables.[24] The result, using the unit step function $\Theta(x)$, which is zero for negative argument and unity for positive argument is:

$$G(x,t) = 2\pi c\, \Theta(t)\, \Theta(ct - |x|)\, J_0(K\sqrt{c^2t^2 - x^2})\, e^{-\epsilon c t}. \tag{A8}$$

Here J_0 is the first-order Bessel function of the first kind, and ϵ may

now be set equal to zero.

For a complete solution we must add to this a general solution to the homogeneous equation where $f(x,t)$ is taken to be identically zero. Fourier and Laplace transformations yield the complementary solution

$$C(x,t) = \frac{1}{2}\Big\{ g(x-ct,0) + g(x+ct,0) + \\ + \int_{-ct}^{ct} dx' c^{-1} \frac{\partial}{\partial t''} g(x'',t'')\Big|_{\substack{x''=x-x' \\ t''=0}} \cdot J_0\left(K\sqrt{c^2t^2-x'^2}\right) + \\ + Kct\int_{-ct}^{ct} dx' g(x-x',0)\cdot J_1\left(K\sqrt{c^2t^2-x'^2}\right)\Big/\sqrt{c^2t^2-x'^2}\Big\}\,\Theta(ct-|x|). \tag{A9}$$

The complete solution then is

$$g(x,t) = C(x,t) + 2\pi\int_0^t c\,dt' \int_{-ct'}^{ct'} dx' f(x-x',t-t')\, J_0\left(K\sqrt{c^2t'^2-x'^2}\right). \tag{A10}$$

One interesting consequence of the term in K in the equation is shown by taking the simple case

$$g(x,0) = \delta(x) \quad \text{and} \quad \frac{\partial}{\partial t} g(x,t)\Big|_{t=0} \equiv f(x,t) \equiv 0, \tag{A11}$$

where $\delta(x)$ is the Dirac delta function. The solution becomes

$$g(x,t) = \frac{1}{2}\Theta(ct-|x|)\Big\{\delta(x+ct)+\delta(x-ct)+Kct\, J_1\left(K\sqrt{c^2t^2-x^2}\right)\Big/\sqrt{c^2t^2-x^2}\Big\}. \tag{A12}$$

The first two terms are propagation of the initial disturbance as in the ordinary one-dimensional wave equation, while the third may be regarded as a wake following the disturbance.

Solution to the periodic problem may be obtained by replacing x by $(\varphi + 2m\pi)R_0$ and summing over m, in equation (A10). It

is to be understood that each term is to be included only when the square roots in it are real and only if $(\varphi + 2m\pi)R \leq ct$. The mth term represents the effects of a disturbance at $\varphi = 0$ and $t = 0$ on the field at φ and t , after the disturbance has traveled $|m|$ times around the toroid. If m is positive, the direction of travel is the φ direction, if negative, the $-\varphi$ direction. The display of the result does not seem warranted here.

The modes found by Neil[35] in which K_j is negative, do not satisfy the conditions under which (A1) is a good representation of the wave equation. These modes have transverse field dependences which make invalid the assumption that the eigenvalues K_j are independent of wave number k . The integration yielding (A7) is then incorrect.

APPENDIX II. THE PARTICLE FOLLOWING PROGRAM (MU F51)

The philosophy of this calculation was described in the body of this paper. A few of the details are mentioned here and the actual code is included.

A listing of the program is attached. It is in the form of one main control program and numerous subroutines. These subprograms are written in Fortran[25] language or in the SAP[26] language for the IBM-704. There is some slight mixing of SAP instructions and literals into the Fortran parts where this saved a reasonable amount of indirection in accomplishing what was required.

The most often repeated part of the program, subroutine OPUS 3 was written for Fortran until it was noticed that using the SAP language (essentially the actual machine language) allowed a reduction in operating time of roughly 20%. This is the part of the program which is repeated for each particle at each integration step. The reductions consisted primarily of omission of superfluous operations included by the Fortran assembler. An estimated 10% further reduction in time could be made by revising some of the conventions used throughout the program, e.g., carrying the azimuth in units such that width of a density channel is unity would allow some multiplications to be left out.

The system admits up to 10,000 particles but less than half this number were used normally. To carry 2500 particles through one time step requires roughly 15 seconds on an IBM 704 with add time of 24 μs and multiply time of 204 μs. The time required for writing the output data on a tape is roughly 45 seconds for each complete set.

Extra subroutines required for operation as written are MURCD2, MUSAVE, MUSIN4/COS4, MUPLOT, and MURAN6.[27] All but the last are described in Appendix III. MURAN6 computes a digital computer-type psuedo-random integer modulo 2 to some power using the argument given it as the modulus.

Two types of particles are admitted: normal particles and test particles, of which the latter does not contribute to the fields. The motions of the two types of particles are computed in the same fashion, and the test particles serve only to allow a small sample to be looked at in detail. Their coordinates can be included with the output at specifiable intervals.

The main program initializes the memory, determines the form of the input and calls various subroutines. The two input forms are card input using subroutines BEGIN and INPT3, and tape input using subroutine TAPES.

Subroutine BEGIN reads input card data, computes useful numbers for the rest of the program, and provides output which includes listing of the input parameters.

Subroutine INPT3 allows the initial distribution to be specified with just a few control parameters. Two types of input are possible. The first computes a function $f(W,\phi)$ and depending on the value of f decides how many particles to place in a ΔW by $\Delta\phi$ rectangle centered at (W,ϕ). The second enters the particles along a line

$$W = \langle W \rangle + (A_0 + A_1 \langle W \rangle) \cos(h_1\phi + \phi_1),$$

with azimuthal spacing

$$\Delta\phi = \{ \langle \Delta\phi \rangle^{-1} + A_2 \sin(h_2\phi + \phi_2) + A_3 \sin(h_3\phi + \phi_3) \}^{-1}.$$

Using the second form, the distributions can approximate those used in the boundary program.

Subroutine WORPRO controls the output sequence and contains sense switch options which allow some indication of the progress of a run to be printed on the on-line printer, allow discontinuing of a run, or allow the subroutine SAVE to store the status of the machine on a tape for continuing later. The output options here are the printing or plotting of the azimuthal density, printing of the field, printing of test particle coordinates, or calling of the subroutines TPPR, PLRXY, or TAPES.

Subroutine TPPR is an attempt to allow study of the phase space orbits of the test particles. It creates an image of a blank output page, and thereafter when called, enters letters into this image, regarding the page as a part of the (W,ϕ) plane and putting the letters in the positions corresponding to the locations of test particles. Each of 44

test particles may be given a distinct symbol A, B, C, ··· , Z, 1, 2, 3, ··· , 9, -,), (, =, ' , $, . , 1, or +. The symbol * is reserved for indicating that at different times, different particles entered the same region. The idea was that by connecting all the A's on the page, the trajectory of particle A could be seen, with similar possibilities for the other 43 particles. In practice it became difficult to control the scales and not too much information was obtained from these pictures. One of the better examples is included here as Fig. 25.

Subroutine PLRXY proved more useful. This treats an output page as the (W, φ) plane between W_{min} and W_{max}. The banks of particle coordinates are scanned and a two-dimensional histogram is formed giving the number of particles in the δW by $\delta\varphi$ region centered at (W, φ). When these numbers are printed in the proper order, the page may be regarded as a "plot" of the distribution function. An example of this is reproduced in Fig. 26. Where no numbers occur, no particles were found. The resolution is limited to a 60 by 40 channel histogram. The scale factor is automatically adjusted if any points fall outside the nominal range (W_{min}, W_{max}) given.

Subroutine PRINT provides diagnostic print out for the computer operator if any difficulties occur during the manipulation of tapes in subroutine TAPES.

Subroutine INFELD calculates the fields present, in preparation for the first integration. Thereafter they are calculated by subroutine

Fig. 25. Sample phase trajectories of test particles, calculated with the particle-following program. The motion is in the counterclockwise direction, and represents the motion under the influence of a fixed frequency RF field.

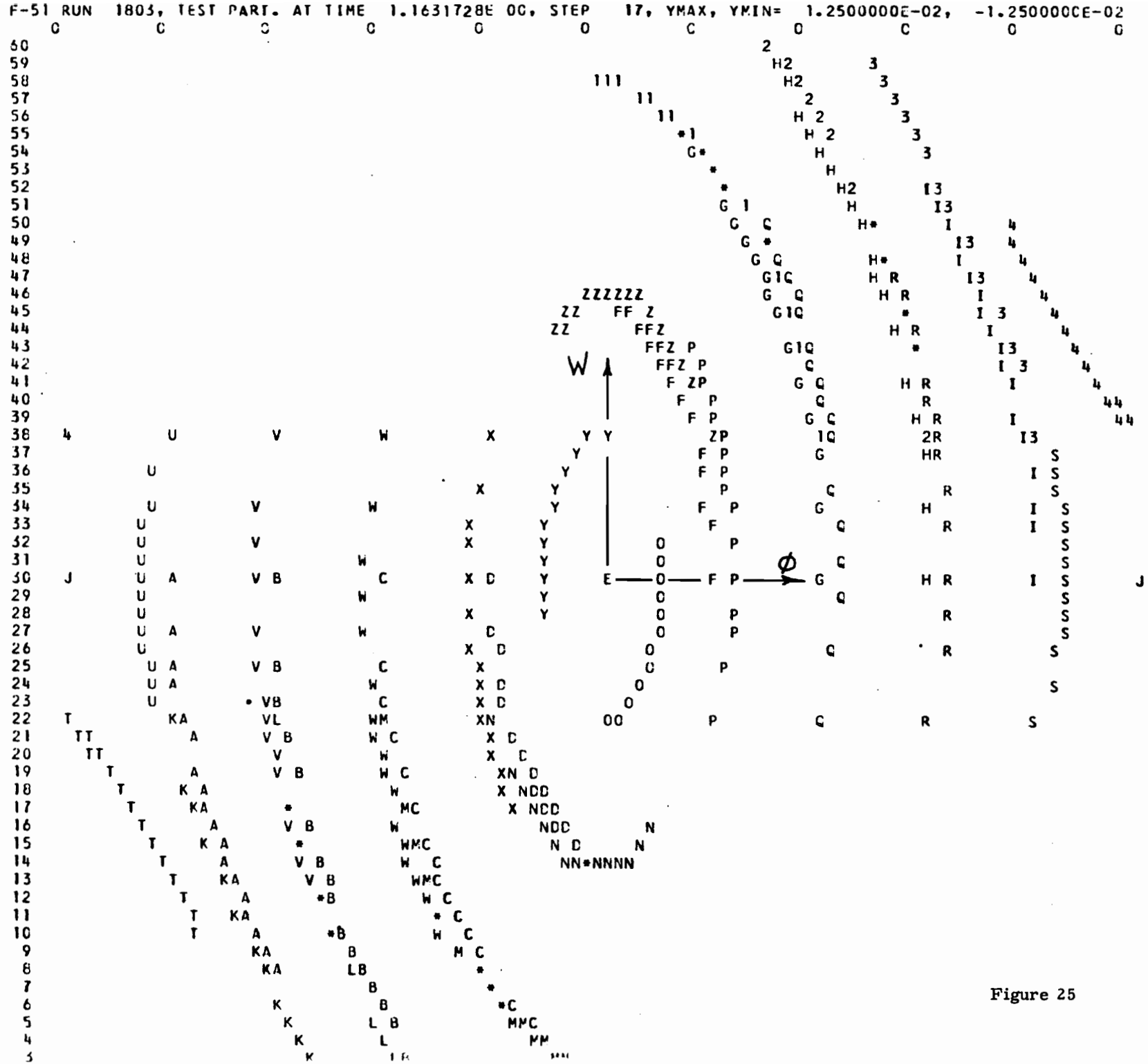
F-51 RUN 1803, TEST PART. AT TIME 1.1631728E 00, STEP 17, YMAX, YMIN= 1.2500000E-02, -1.250000CE-02
W
Φ

Figure 25

OPUS 3, of which INFELD is a copy with the integration steps omitted. It is here that a potential user would first have trouble with the normalization. During the evolution of the program, it was noted that a multiplication per particle per time step could be saved (multiplication and division are usually the determining factors for the operating speed of a program) if the size Δt, of the time step was incorporated into the unit system. Thus (33) may be written

$$X_j^{\ell+1} = X_j^{\ell} \mp Y_j^{\ell},$$

$$Y_j^{\ell+1} = Y_j^{\ell} + \mathcal{E}(2\pi X_j^{\ell+1}, \ell\Delta t)\cdot(\Delta t)^2/2\pi,$$

where X_j is $\varphi_j/2\pi$ and Y_j is $W_j\Delta t/2\pi$. Another multiplication was saved by taking $(\Delta t)^2/2\pi$ to be an integral power of 2. This caused no trouble until it was found that the time step had to be adjusted occasionally to keep the integration accurate. To save rewriting the entire program this adjustment was made by doubling or halving all the values Y_j when necessary. Because the Y_j rather than the W_j are the numbers listed in the output, this expanding and contracting coordinate system is somewhat inconvenient, but since adequate notice is provided when the scale changes, it can be tolerated. The output graphs are so adjusted that the points plotted will be in the same position on the page, whatever the current scale factor.

Subroutine OPUS 3 does the actual integration of the motion equations for all the particles, and recomputes the fields after each such step. It also tests and corrects the scale factor to assure accurate

integration.

Included in the listing is some patching required for the IBM 704 Fortran input-output subroutine (IOH).[25] This is required by subroutine PLRXY to prevent the distribution function plots from being filled out with zeros, which make them harder to interpret. With this patch, no zero integers are ever printed, the proper space being left blank instead.

Subroutine SWITCH tests all six sense switches on the operating console and informs the calling program of the configuration in them. This simplifies testing of the switch settings.

Subroutine TAPES provides for storing on tape just enough of the data used in a run to allow the run to be continued from that point at a later time. It also allows such a tape to be interpreted properly and this rerunning to be carried out, with revised control parameters, if desired. A fairly complicated format is used to be sure the proper tape is used for this.

The program is sufficiently general to make definition of all the parameters a lengthy process. This will be done in the form of a MURA report, and only a few important ones mentioned here to allow the code to be decipherable.

For the most part, integer-type parameters are stored as members of an array IG(I) where $1 \leq I \leq 128$. Floating point parameters are stored in the array Z(I) for $1 \leq I \leq 1024$. These are common to all the subprograms. The numbers x_n and y_n are called X(N) and Y(N).

Fig. 26. Sample phase density of particles, calculated with the particle-following program. The single integers represent the number of particles found in the corresponding region in the (W, φ) phase space. The run shows one stage of the evolution of a band of particles initially spread uniformly in a region $-\overline{W}_0 \leq W \leq \overline{W}_0$ and $-\pi \leq \varphi \leq \pi$, under the influence of a fixed frequency RF field.

F-51, RUN 1803 RHO(X,Y) AT TIME 7.2005935E-01. NO. PARTICLES= 2526 STEP= 9
YMAX, YMIN= 1.2500000E-02, -1.2500000E-02, NO. ABOVE, BELOW= 0, 0

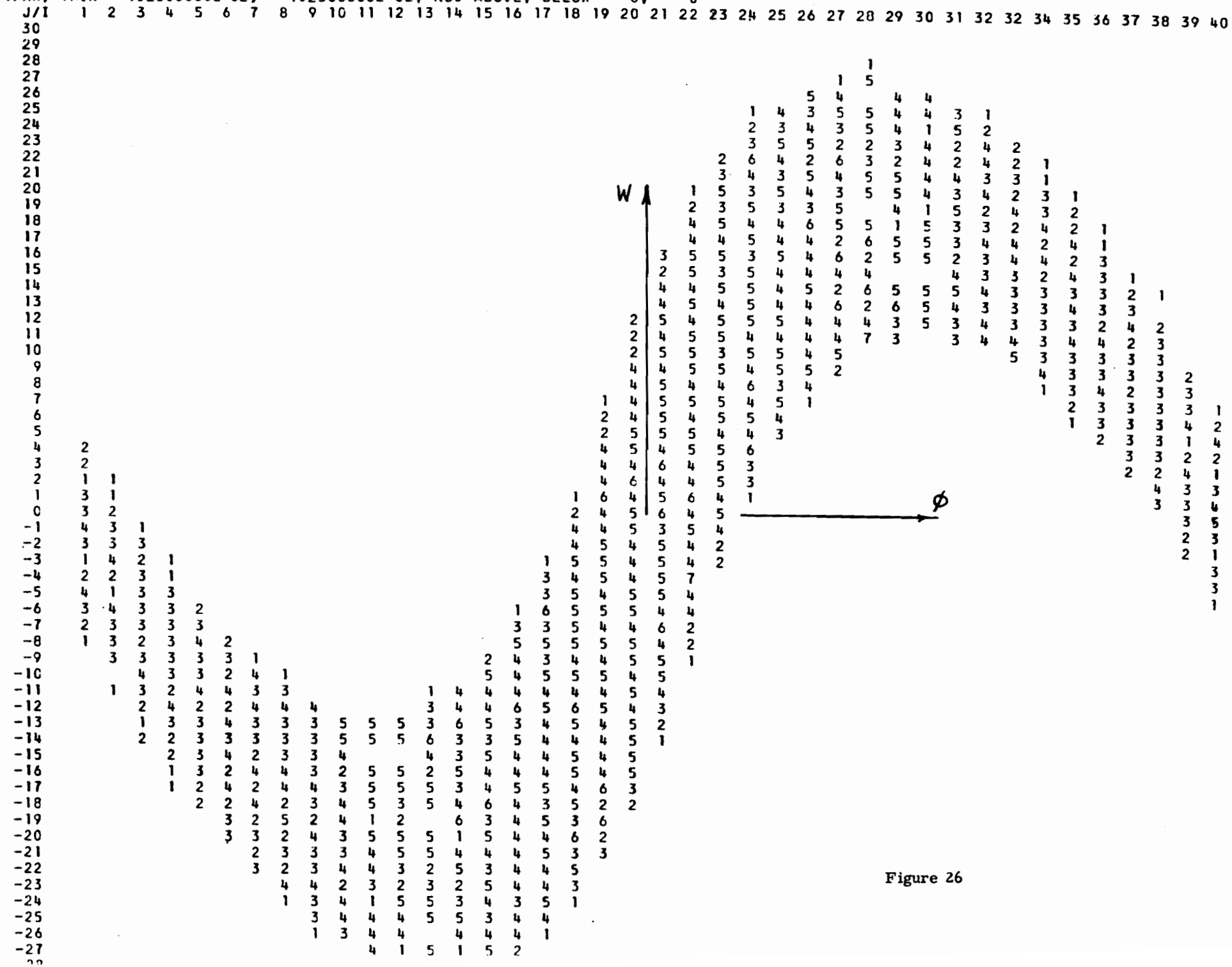

Figure 26

The field and density are named mnemonically. The arrays IP and BANK are the locations of the printer page images used in the subroutines PLRXY and TPPR.

The equivalence statement of subroutine WORPRO provides a good dictionary of mnemonical variable names. For clarification, INDX is the total number of particles and NBOX is the number of channels in the field and density histograms. (This is an integral power of 2.) The field kernel is stored in locations Z(101) through Z(132).

For further details, the MURA report* must be consulted.

*MURA reports are available upon request from the Office of Technical Services, U. S. Department of Commerce, Washington 25, D. C.

```
C       F 51  MAIN IV
         COMMCN IG,Z,FIELC,BBB,RHO,X,Y,CCC,IP,BANK
        CIMENSIONIG(128),Z(1024),FIELD(1024),RHO(1024),X(10000),Y(10000)
        CIMENSICN BANK(1C2C), IP(6CC), G(1)
        EQUIVALENCE (IG(2),INCX),(IG(21),NBOX),(G(1),Z(801))

        SENSE LIGHT C
        Z (79) = 0.
        Z(6) = 1.
        Z(25) = 1.
        Z(27) = 1.
        Z(9C) = 1.
 1      IF (SENSE SWITCH 3) 4C,101
 101    CALL MURCD2(G)
        IG(1) = G(1)
        IG (2) = G(2)
        NEWCT = G(3)
        CALL TAPES (+1)
 9      SENSE LIGHT 3
        SENSE LIGHT 4
        REWINC 3
        IF (NEWCT) 901, 811, 9C1
 901    IG(31) = NEWCT * 512
        NRE  =NEWCT-IG(32)
        IG(32)=NEWCT
        Z(82)=SCRTF(6.2831853*(2.0**(-IG(32))))
        B=SQRTF(2.0**(-NRE  ))
        CC 1C I=1,INCX
 10     Y(I)=Y(I)*B
        CC 12 I=1,5
 12     Z(I+139)=Z(I+139)*B
 811    IG(69) = NEWCT
        CC 82 I=1,128
 82     G(I)=IG(I)
 40     CALL BEGIN
        CALL WCRPRO
        GC TC 1
        END(C,1,1,1,0)


C       F-51 BEGIN   IV
        SUBRCUTINE BEGIN
         COMMCN IG,Z,FIELC,BBB,RHO,X,Y,CCC,IP,BANK
        CIMENSIONIG(128),Z(1024),FIELD(1024),RHO(1024),X(10000),Y(10000)
        CIMENSION BANK(1020),IP(600), G(1), RF(1)
        EQUIVALENCE (LN2NBX, IG(3C)), (CT, Z(82)), (ENBOX, Z(81)), (LNTAU,
       1IG(31)),(LNBXD2, IG(32)), (GAMMA, Z(80)), (IG(1), ID), (IG(2), INC
       2X), (Z(10), TIME), (IG(33), NKERN), (Z(801),G(1)), (IG(21),NBCX)
       3 ,(Z(851),RF)
 500    FCRMAT(A1, 9HF 51  RUN I6,2H  2A6,15H BANK AT TIME = 1PE15.7)
 501    FCRMAT(I6,4E15.7)
 502    FCRMAT(13HOSPACE CHARGE,A6)
 503    FCRMAT(12I6)
 504    FCRMAT(16HORACIC FREQUENCY,A6)
 505    FCRMAT(I6,11F6.0)
 506    FCRMAT(A6,11H TRANSITION)
```

```
 509   FCRMAT (9H1F 51 RUNI6)
 510   FORMAT (1H2)
SCN    ALF     ON
SCFF   ALF     OFF
SBOVE  ALF    OABOVE
SBLCW  ALF    OBELOW
SBLNK  ALF
SBBBI  ALF          I
SNTGR  ALF    NTEGER
SCATT  ALF      CATA
SCNE   ALF    1

 17    CALL MURCD2 (G)
       CALL MURCD2 (Z)
 18    CO20I=1,128
 20    IG(I)=G(I)*1.000001
       PRINT 509, IC
       PRINT 510
       IF(SENSE LIGHT 3) 62,50
 50    IG(2) = 0
       SENSE LIGHT 3
       Z(81)=2.0**IG(30)
       IG(21)=Z(81)+B
       Z(82)=SQRTF(6.2831853*(2.0**(-IG(32))))
       CALL INPT3
       IG (4) = 0
       TIME = 0.
       IG(38) = 0
       IG(31)=IG(32)
       IG(30) = IG(30) * 512
       IG(31) = IG(31) *512
       CO 51 I=1,NBOX
 51    RF(I)=0.
       IF(IG(34))  54,52,52
 52    CO 53 I = 1, NBOX
 53    RF(I) = GAMMA + SIN4F(FLOATF(I-1) /ENBOX)
 54    CALL INFELD
 62    NZ=IG(19)
       BBB=INCX
       IF(SENSE LIGHT 3) 60,55
 55    IF (IG(15)) 60, 63, 60
 60    CO 61I = 1, 1020
 61    BANK (I) = BLNK
 63    WRITE OUTPUT TAPE 9, 500,  ONE,ID,BBBI,NTGR,TIME
       WRITE OUTPUT TAPE 9,
      1503,(K,IG(K),IG(K+1),IG(K+2),IG(K+3),IG(K+4),IG(K+5),IG(K+6),IG(K+
      27),IG(K+8),IG(K+9),IG(K+10),K=1,77,11)
       WORD = ON
       IF (IG(23)) 66,67,67
 66    WORD = OFF
 67    WRITE OUTPUT TAPE 9, 502, WORD
       WORD = OFF
       IF (IG(34)) 69, 68, 68
 68    WORD = ON
 69    WRITE OUTPUT TAPE 9, 504, WORD
       WORD = BOVE
```

```
      IF(Z(84)) 70,80,8C
 70   WORD = BLOW
 70   WORD = BLOW
 80   WRITE OUTPUT TAPE 9, 5C6, WORD
      CALL NAME
      WRITE OUTPUT TAPE 9,500,BOVE,ID,BLNK,DATT,TIME
      WRITE OUTPUT TAPE 9,
     1501,(K,Z(K),Z(K+1),Z(K+2),Z(K+3),K=1,NZ,4)
      RETURN
      END (0,1,1,1,0)


C     F-51 INPT3 IV
      SUBROUTINE INPT3
       COMMCN IG,Z,FIELC,BBB,RHO,X,Y,CCC,IP
      DIMENSIONIG(128),Z(1024),FIELD(1024),RHO(1024),X(10000),Y(10000)
      EQUIVALENCE (IG(2),INDX), (Z(24),Y30 ), (Z(23),DY3), (Z(45),TOTAL)
     1, (Z(46),ODULTN), (IG(3),NTEST), (IG(4),III), (IG(5),JJJ), (IG(6),
     2NVAL), (Z(47),PHASE), (Z(48),HARMON), (Z(7),TRIGF)
      NTEST=Z(150)+H
      YE=Y30-DY3
      IND=INCX+1
      ISWTC=Z(5)+H
      IF (Z(6)-1.0) 1,2,2
 1    Z(6)=1.0
      Z(6) = Z(6) + .01
B     Z(6) = Z(6) * 3774COCOCOCC
      LRANC=Z(6)+H
 15   IF (NTEST) 30,30,19
 19   IM=INC+NTEST-1
      CC 20 I=INC,IM
      X(I)=Z(2*I+149)
 20   Y(I)=Z(2*I+150)
      INC=IM+1
 30   IF(TRIGF) 300,31,3CO
 31   CX3=1./Z(21)
      NVAL=Z(29)+H
      J3X=Z(21)+H
      K3Y=Z(22)+H
      B=Z(26)+0.5*Z(25)/Z(21)
      C=Z(28)+0.5*Z(27)*Z(23)
      CRANX=CX3/Z(6)
      CRANY=Z(23)/Z(6)
      A=0.5*CX3
      C=0.5*CY3
      CC 70 K=1,K3Y
      YE=YE+CY3
      WY=Z(27)*YE+C
      WY2=WY*WY
      XS=-CX3
 40   CC 70 J=1,J3X
      XS=XS+CX3
      EX=Z(25)*XS+B
      EX2=EX*EX
 50   F=Z(30) + Z(31)*EX + Z(32)*EX2 + Z(33)*COS4F(Z(35)* EX + Z(36)) +
```

```
     1Z(41)* WY + Z(42)*WY2 + Z(43)*WY*WY2 + Z(44)* WY2*WY2
      IF(Z(8)) 55,60,60
55    NO=F
      GO TO 64
60    DO 63 I=1,NVAL
      IF (F-Z(3*I+298))63,61,61
61    IF (F-Z(3*I+300))62,62,63
62    NC=Z(3*I+299)+H
      GO TO 64
63    CONTINUE
      GO TO 70
64    IF(NC) 70,70,6401
6401  IF(Z(9))65,66,66
65    DDX3=DX3/FLOATF(NC)
      XN=-.5-DDX3+XS
      GO TO 6601
66    XN=A+XS-.5
6601  NC=NC+INC-1
      YN=YE+C
      DO 69 I=IND,NO
      IF(ISWTO) 6701,67,67
67    XN=DRANX*FLOATF(XRANF(LRANO))+XS-.5
      YN=DRANY*FLOATF(XRANF(LRANO))+YE
6701  IF(Z(9)) 6702,68,68
6702  XN=XN+DDX3
68    X(I)=XN
      Y(I)=YN
69    IND=INC+1
70    CONTINUE
      GO TO 1000
300   J3X=TOTAL+H
      K3Y=Z(22)+H
      DX=0.0
      DO 600K=1,K3Y
      YE=YE+DY3
      XS=0.0
400   DO 600J=1,J3X
410   DENOM=TOTAL+ODULTN*SIN4F(HARMON*XS+PHASE)
     1+Z(50)*SIN4F(Z(52)*XS+Z(51))
      IF (DENOM) 500,460,500
460   PAUSE 77777
      GO TO 410
500   XS=XS+1./DENOM
      IF (ISWTO) 520,560,560
520   DX=-FLOATF(XRANF(LRANO))/(Z(6)*DENOM)
560   X(IND)=XS+DX
      Y(IND)=YE-(Z(37)+YE*Z(38))*COS4F(Z(39)*X(IND)+Z(40))
      IF(ABSF(Y(IND))-Z(30)+Z(31)*COS4F(Z(32)*X(IND)+Z(33))) 570,570,600
570   IND=IND+1
600   CONTINUE
1000  INDX=IND-1
      RETURN
      END (0,1,1,1,0)


C     F-51 WORPRO  IV
```

```
      SUBROUTINE WORPRO
       COMMON IG,Z,FIELD,BBB,RHO,X,Y,CCC,IP,BANK
      DIMENSIONIG(128),Z(1024),FIELD(1024),RHO(1024),X(10000),Y(10000)
      DIMENSION BANK(1020), IP(600)
      EQUIVALENCE (IG(1),ID), (IG(2),INDX),(IG(16),NO), (IG(4),III), (IG
     1(5),JJJ), (IG(16),ISWT16), (IG(20),NPLRXY), (IG(21),NBOX), (IG(25)
     2,NPRR), (IG(26),NPLR), (IG(27),NPLXY), (IG(28),NPRXY), (IG(29),NTC
     3TAL),(IG(35),NTODC),(IG(58),NFIRS),  (IG(38),NNN), (IG(39),MMM), (
     4Z(10),TIME), (Z(81),ENBOX), (IG(41),NP1),(IG(43),NP3),(S(1),Z(76))
     5,(IG(44),NP4),(IG(45),NP5),(IG(57),NLAS),(IG(46),NP6),(IG(50),NDUM
     6P),(IG(42),NP2),(IG(52),NBM1),(IG(53),NRHO1),(IG(54),NRHO)
     7,(IG(55),NFEELD),(IG(56),NFELD1)
      DIMENSION S(1)
 500  FORMA
     1     T(A1,9HF 51  RUNI6,2H  ,2A6,15H BANK AT TIME =1PE15.7,21H   NO
     2. OF PARTICLES =0PF6.0,6H AFTERI7,8H   STEPS)
 501  FORMAT(I6,F13.8,E15.7,F13.8,E15.7,F13.8,E15.7,F13.8,E15.7)
 503  FORMAT(I6,8E15.7)
 505   FORMAT(I6,10F12.6)
 507  FORMAT(10H*F 51  RUNI6,13H RHO(X) AT T=1PE15.7,16H HOR, VER SCALE=
     10P4F11.5,6H AFTERI7,8H   STEPS)
 508  FORMAT (71H SWITCH 6 IS UP.  TO  ABANDON  RUN RAISE THE OTHER FIVE
     1 AND PUSH START.   )
 509  FORMAT(27HORUN ABANDONED VIA SWITCH 6)
 512  FORMAT(17HOTAPE DUMP   ID =I8, 9H   STEP =I8,13H   F 51 TAPE A6)
 513  FORMAT(24HOSAVE CALLED BEFORE STEPI5,22HMOUNT ERASABLE TAPE 1./52H
     1 REMOVE ANY F 51 TAPES. PROCESS TAPE 9. SAVE TAPE 1./67H TO RESTOR
     2E REPLACE ALL TAPES SET SWITCHES (1 DOWN) CLEAR LOAD TAPE)
 514  FORMAT (9H1F 51 RUNI8,31H RESUMED FROM SAVE TAPE AT STEPI8)
 515  FORMAT (1H2)
SONE  ALF    1
SBLNK ALF
SESTP ALF        PA
SRTCL ALF    RTICLE
SROW  ALF       RHO
SFLD  ALF     FIELD
SF51T ALF    F51TAP

      ZER = 0
      Z(145)=Z(140)
      Z(146)=Z(141)
      Z(147)=Z(143)
      Z(148)=Z(144)
      NRHO=((NBOX-1)/10)*10
      NRHO1=NRHO+1
      NFEELD=((NBOX-1)/8)*8
      NFELD1= NFEELD+1
      S(1)=ENBOX+2.0
      S(2)=1.
      IF (SENSE LIGHT 4) 5,10
 5    NO=NNN
      BBB=INDX
      GO TO 15
 10   DO 11 I=1,5
 11   IG(I+40) = 32760
```

```
      NP6 = 0
      NO=0
15    CO89NNN=NO,NTOTAL,NTOCO
      CC 16 I=1,6
16    IG(I+40)=IG(I+40)+1
      IF (NCUMP) 7000, 18, 7000
7000  IF (NDUMP-NP6) 7001, 7001, 18
7001  NP6 = 0
      CALL TAPES(-1)
      CALL TAPES (0)
7003  WRITE CUTPUT TAPE 9, 512, IG(1), NNN,IG(17)
18    IF (NPLR) 1800, 2101, 1800
1800  IF(NPLR-NP2) 1801, 1801, 2101
1801  NP2 = 0
      S (3) = AMAX(RHO, NBOX)
      S (3) = MAX1F(S(3), Z(87))
2001  CC 21 I=1,NBCX
      AYE=I
21    CALL PLCT (9, AYE, RHO(I), S, 1, 0)
      CALLPLCT(9,ZER,ZER,S,1,1)
      WRITE CUTPUT TAPE 9, 507, ID, TIME,       (S(I), I=1,4),NNN
2101  IF (NPRR) 2102, 3C, 21C2
2102  IF(NPRR-NP1) 2103, 2103, 30
2103  NP1 = 0
      WRITE CUTPUT TAPE 9,500,ONE,IC,      BLNK,ROW,TIME,BBB,NNN
      IF (NRHC) 23, 25, 23
23    WRITE CUTPUT TAPE 9, 505, (K,RHO(K), RHO(K+1),  RHO(K+2), RHO(K+3)
     1, RHO(K+4), RHO(K+5), RHO(K+6), RHO(K+7), RHO(K+8), RHO(K+9),
     2                    K=1,NRHO,10)
25    WRITE CUTPUT TAPE9,5C5,NRHO1,(RHO(K),K=NRHO1,NBOX)
      IF(IG(23)) 30, 26, 26
26    WRITE CUTPUT TAPE 9,500,ZER,ID,      BLNK,FLD,TIME,BBB,NNN
      IF (NFEELD) 2601, 27, 2601
2601  WRITE CUTPUT TAPE9,5C3,(K,FIELD(K),FIELD(K+1),FIELD(K+2),FIELD(K+3
     1),FIELC(K+4),FIELC(K+5),FIELD(K+6),FIELD(K+7),K=1,NFEELD,8)
27    WRITECUTPUTTAPE9,5C3,NFELD1,(FIELD(K),K=NFELD1,NBOX)
30    IF (NPLRXY) 31, 4C, 31
31    IF (NPLRXY-NP3) 32, 32, 40
32    NP3 = 0
      WRITECUTPUTTAPE9,5CO,ZER,IC,     ESTP,RTCL,TIME,BBB,NNN
      WRITE CUTPUT TAPE 9, 501, (K, X(K), Y(K), X(K+1), Y(K+1), X(K+2),Y
     1(K+2), X(K+3), Y(K+3), K=NFIRS,NLAS,4)
40    IF (NPLXY) 41, 50, 41
41    IF (NPLXY-NP4) 42, 42, 50
42    NP4 = 0
      CALL TPPR (TIME, NNN, NP4)
50    IF(NPLRXY) 51, 60, 51
51    IF (NPLRXT - NP5) 52, 52, 60
52    NP5 = 0
      CALL PLRXY (TIME, NNN)
60    IF (SENSE SWITCH 1) 61,6001
6001  CALL BELL
      REWINC 2
      SENSE LIGHT 0
      PRINT 513,NNN
      PRINT 515
```

```
      WRITE CUTPUT TAPE 9,513
      CALL SAVE
      WRITE CUTPUT TAPE 9,514,ID,NNN
      PRINT 514,ID,NNN
      PRINT 515
 61   IF(SENSE SWITCH 4) 6102,6101
 6101 PRINT 500,ZER,ID,BLNK,BLNK,TIME,BBB,NNN
 6102 IF (SENSE SWITCH 6) 70,62
 62   PRINT 508
      CALL BELL
      PRINT 515
      CALL SWITCH (NUTS)
      IF (NUTS) 70, 65, 70
 65   PRINT 509
      PRINT 515
      WRITE CUTPUTTAPE9,509
      GC TC 90
 70   IF(NNN-NTOTAL) 80,89,89
 80   CALL CPUS 3
 89   CCNTINUE
 90   IF (NPLXY) 100, 1CC, 91
 91   CALL TPPR(TIME,NNN,NTOCO)
 100  Z(140)=Z(145)
      Z(141)=Z(146)
      Z(143)=Z(147)
      Z(144)=Z(148)
 11C  RETURN
      END (0,1,1,1,0)
      PRINT 515


C     F-51  TPPR  II                                                  DORY
      SUBRCUTINE TPPR (T, N, ISW TCH)
       CCMMCN IG,Z,FIELC,BBB,RHO,X,Y,CCC,IP
     1,BANK
      CIMENSIONIG(128),Z(1024),FIELD(1024),RHO(1024),X(10000),Y(10000)
      CIMENSION BANK (17,60), M(1), A(1)
     1,IP(10,60)
      ECUIVALENCE (IG(4),III),(IG(5),JJJ),(Z(143),YMAX),(Z(144),YMIN)
     1,(IG(1),ID)
SPLUS ALF   ++++++
SSLSH ALF   //////
SPERC ALF   ......
SDOLR ALF   $$$$$$
SCOMA ALF   ,,,,,,
SEQUL ALF   ======
SLPRN ALF   ((((((
SRPRN ALF   ))))))
SMINS ALF   ------
SNINE ALF   999999
SEIGT ALF   888888
SSEVN ALF   777777
SSIX  ALF   666666
SFIVE ALF   555555
SFOUR ALF   444444
```

```
STHRE ALF    333333
STWC  ALF    222222
SCNE  ALF    111111
SZZ   ALF    ZZZZZZ
SYY   ALF    YYYYYY
SXX   ALF    XXXXXX
SWW   ALF    WWWWWW
SVV   ALF    VVVVVV
SUU   ALF    UUUUUU
STT   ALF    TTTTTT
SSS   ALF    SSSSSS
SRR   ALF    RRRRRR
SCQ   ALF    CCCCCC
SPP   ALF    PPPPPP
SCO   ALF    COCOOO
SNN   ALF    NNNNNN
SMM   ALF    MMMMMM
SLL   ALF    LLLLLL
SKK   ALF    KKKKKK
SJJ   ALF    JJJJJJ
SII   ALF    IIIIII
SHH   ALF    HHHHHH
SGG   ALF    GGGGGG
SFF   ALF    FFFFFF
SEE   ALF    EEEEEE
SCD   ALF    CDCDDD
SCC   ALF    CCCCCC
SBB   ALF    BBBBBB
SA    ALF    AAAAAA
SBLNK ALF
SSTAR ALF    ******
SMARK ALF    C
SM6   OCT 000000000077
SM5   OCT 000000007700
SM4   OCT 000000770000
SM3   OCT 000077000000
SM2   OCT 007700000000
SM    OCT 770000000000
 500  FORMAT (9H3F-51 RUNI6,20H, TEST PART. AT TIMEIPE15.7,6H, STEPI5,13
     1H, YMAX, YMIN=E15.7,2H, E15.7/22A5)
 501  FORMAT (1H*,I2,3H   17A6)

      T1=YMAX-YMIN
      IF(T1) 30,150,30
 30   FACTOR=59.0/T1
      BIAS=1.-FACTOR*YMIN
      IF (JJJ-44) 35,35,34
 34   IX=44
      GO TO 50
 35   IX=JJJ
 50   DO 90 I=III,IX
      IY=Y(I)*FACTOR+BIAS
      IF (IY-60) 52,52,51
 51   NOV=NOV+1
      GO TO 90
 52   IF (IY) 53,53,54
```

```
 53     NUN=NUN+1
        GO TC 90
 54     IX6=(X(I)+1.)*102.
        IX=IX6/6+1
        IDX=IX6+7-IX*6
        IF (IX-17) 56,56,55
 55     IX=IX-17
 56     K=IX+17*IY-17
S       CAL M(IDX)
S       SLW T1
S       SLW T5
S       COM
S       SLW T4
S       CAL BLNK
S       ANS T5
S       CAL A(I)
S       ANS T1
S70     CAL BANK(K)
S       ANS T4
S       ANA M(IDX)
S       TZE*82
S       SLW T2
S       CLA T2
S       CAS T5
S       TRA*76
S       TRA*82
S76     CAS T1
S       TRA*79
S       TRA*90
S79     CAL STAR
S       ANA M(ICX)
S       TRA*84
S82     CAL T1
S84     CRA T4
S       SLW BANK(K)
S       DED,(K)
S       CEC,(ICX)
 90     CCNTINUE
        IF(ISW TCH) 100,15C,100
 100    IF(SENSE SWITCH 5)110, 120
 11C    WRITE CUTPUT TAPE 9,
       1500,IC,T,N,YMAX,YMIN,(BLNK,MARK,L=1,11)
        DO111 I=1,60
        K=61-I
 111    WRITE CUTPUT TAPE9,
       1501,K,(BANK(J,K),J=1,17)
        GC TC 150
 120    PRINT
       1500,ID,T,N,YMAX,YMIN,(BLNK,MARK,L=1,11)
        DO121 I=1,60
        K=61-I
 121    PRINT
       15C1,K,(BANK(J,K),J=1,17)
 150    RETURN
        END (0,1,1,1,0)
```

```
C       F-51  PLRXY III                                                  DOR'
        SUBROUTINE PLRXY (T,N)
         COMMON IG,Z,FIELC,BBB,RHO,X,Y,CCC,IP
        DIMENSIONIG(128),Z(1024),FIELD(1024),RHO(1024),X(10000),Y(10000)
 500    FORMAT (10H3F-51, RUNI6, 17H RHO(X,Y) AT TIME 1PE15.7, 16H. NO. P/
       1RTICLES=I6,10H      STEP=I6/ 12H YMAX, YMIN=1PE15.7,2H, E15.7,
       219H, NO. ABOVE, BELOW=I4,2H, I4/127H   J/I   1  2  3  4  5  6  7
       38  9 10 11 12 13 14 15 16 17 18 19 20 21 22 23 24 25 26 27 28 29 3
       40 31 32 33 34 35 36 37 38 39 40  )
        CIMENSION IP(10,60), IU(1),RM(1), IM(1)
        EQUIVALENCE(IG(2),INDX)
 503    FORMAT (1H*,I4,I5,39I3)
SI600   CCT 001130000000
SIU4    CCT 000000000001
SIU3    OCT 000000001000
SIU2    OCT 000001000000
SIU     CCT 001000000000
SM4     CCT 000000000777
SM3     CCT 000000777000
SM2     CCT 000777000000
SRM     CCT 777000000000
SIM4    CCT 777777777000
SIM3    CCT 777777000777
SIM2    CCT 777000777777
SIM     CCT 000777777777

        YMAX=Z(140)
        YMIN=Z(141)
        IF (Z(142)) 9, 5, 9
 5      YMAX = AMAX(Y, INCX)
        YMIN = AMIN (Y, INDX)
        IF (YMAX-Z (140)) 7, 7, 6
 6      YMAX = Z(140)
 7      IF (YMIN - Z(141)) 8, 9, 9
 8      YMIN = Z(141)
 9      TEMP1=YMAX-YMIN
        IF(TEMP1) 10,71,10
 10     FACTOR=59.0/TEMP1
        BIAS=1.-FACTOR*YMIN
        DO 20 I = 1, 600
 20     IP (I) = 0
        NOV = 0
        NUN = 0
        DC 50 K=1,INDX
 24     J=Y(K)*FACTOR+BIAS
        IF (J) 25,25,26
 25     NUN=NUN+1
        GC TC 50
 26     IF (J-60) 28,28,27
 27     NOV=NOV+1
        GC TC 50
 28     IT4=(X(K)+1.)*40.
        I=1+IT4/4
        L=IT4-4*I+5
```

```
      IF(I-11) 30,29,29
 29   I=I-10
 30   M=10*J+I-10
S35   CAL IP(M)
S     SLW TEMP1
S     ACL IU(L)
S     ANA RM(L)
S     SLW IP(M)
S40   CAL TEMP1
S     ANA IM(L)
S     ORS IP(M)
S     DED,(M)
S     DED,(L)
 50   CONTINUE
      WRITEOUTPUTTAPE9, 500, IG(1), T, INDX, N, YMAX,   YMIN,   NOV, NUN
      DO 70 K=1,60
      L=61-K
      DO 60 M=1,10
S     CAL IP(M,L)
S     SLW TEMP1
S     ANA RM(1)
S     ARS 9
S     SLW IG(4*M+77)
S     CAL TEMP1
S     ANA RM(2)
S     SLW IG(4*M+78)
S     CAL TEMP1
S     ANA RM(3)
S     ALS 9
S     SLW IG(4*M+79)
S     CAL TEMP1
S     ANA RM(4)
S     ALS 18
S60   SLW IG(4*M+80)
      I=L-30
 70   WRITE OUTPUT TAPE 9, 503, I, (IG(J), J=81,120)
 71   RETURN
      END (0,1,1,1,0)


C     F 51 PRINT                                                    DORY
      SUBROUTINE PRINT (NTAPE,N)
SREAD ALF   READIN
SWRIT ALF   WRITIN

      NT = NTAPE
      M = N
      GO TO (100, 200, 300, 400, 500, 600) , M
 100  PRINT 102, NT
      GO TO 1000
 102  FORMAT (5H TAPEI3,59H  IS NOT A CANONICAL F 51 TAPE.  REPLACE IT A
     1ND PUSH START.)
 200  WORD = READ
 201  PRINT 202, WORD, NT
      GO TO 1000
```

```
 202  FORMAT (18H TAPE ERROR WHILE A4,6HG TAPEI3,23H  .PUSH START TO RE
     2RY.)
 300  WORD = WRIT
      GO TO 201
 400  PRINT 402, NT
      GO TO 1000
 402  FORMAT (22H THE F 51 TAPE ON UNITI3,44H IS FULL.  MOUNT AN ERASABI
     4E AND PUSH START.)
 500  PRINT 502, NT
      GO TO 1000
 502  FORMAT (79H THE RUN REQUESTED IS NOT ON THE INPUT TAPE.  YOU MIGHT
     5 TRY ANOTHER INPUT TAPE.)
 600  PRINT 602
      GO TO 1000
 602  FORMAT (65H YOU DID NOT REPLACE THE TAPE AS REQUESTED.  DO SO AND
     6PUSH START)
 1000 PRINT 1002
 1002 FORMAT (1H2)
      PAUSE 70707
      RETURN
      END (0, 1, 1, 1, 0)


       REM  F 51 INFELD S     (SAP ASSEMBLER LANGUAGE)
       FUL  PROGRAM CARD
       MZE 0,0,4
       CCT                    CHECK SUM
       PZE LAST+1,,S
       PZE 0
       BCD 1INFELD
       PZE START
       REM
       REL  PROGRAM
       REM
       ORG 0
(FIL)  BCD 1(FIL)
(STH)  BCD 1(STH)
(IOH)O BCD 1(IOH)O
(LEV)  BCD 1(LEV)
S      HTR 0
       HTR 0
       HTR 0
START  SXD S,1
       SXD S+1,2
       SXD S+2,4
20A    CLA IG-2
21A    STO 51A
       CLA NBOX
       STO 49B
       STO 71B
       STO 75B
       LXD NBOX,2
25A    STZ RHO+1,2
       TIX 25A,2,1
26A    LXD INDX,2
27A    CLA X+1,2
```

```
        UFA 6)
        FAD 6)
        CHS
        FAD X+1,2
        STO X+1,2
28A     TPL 32A
29A     TZE 32A
30A     FAD ONE
31A     STO X+1,2
32A     LDQ X+1,2
        FMP ENBOX
        FAD ONE
        STO FNO
        UFA 6)
        STO TEMP
        FAD 6)
        CHS
        FAD FNO
        STO DEL
        CLA TEMP
        ANA 7)
        ALS 18
        PDX 0,4
47A     ADD 2)
        PDX 0,1
49B     TIX *+1,1,**
51A     TXL 63B2,2,**
52A     CLA RHO+1,4
        FSB DEL
        FAD ONE
        STO RHO+1,4
53A     CLA RHO+1,1
        FAD DEL
        STO RHO+1,1
63B2    TIX 27A,2,1
        REM
67A     LXD NBOX,1
67B     SXD I,1
 68A    CLA RF+1,1
        STO FIELD+1,1
        LXD 32530,2          NKERN
70B     SXD J,2
70A     CLA I
        ADD J
        PDX 0,4
71B     TIX *+1,4,**
73A     CLA I
        SUB J
        ADD NBOX
74B     PDX 5,1
75B     TIX *+1,1,**
78A     CLA RHO+1,4
        FSB RHO+1,1
        STO TEMP
        LDQ Z-99,2
```

```
        FMP TEMP
        LXD I,1
        FAD FIELD+1,1
        STO FIELD+1,1
        TIX 70B,2,1
        TIX 67B,1,1
        REM
80B     LXD INDX,7
        CLA 32345              YLIMIT
        SSP
81B     LDQ Y+1,2
        LRS 0
        TLQ *+2
        TRA 90A
        TIX 81B,2,1
        TRA 103A
90A     CLA Y+1,1
        FDH TWO
        STQ Y+1,1
        TIX 90A,1,1
91B     LXA 74B,1
92A     CLA Z-138,1
        FDH TWO
        STQ Z-138,1
        TIX 92A,1,1
93A     CLA LNTAU
94A     SSP
95A     ADD FNAG
96A     STO LNTAU
97A     CLA DT
        FDH TWO
        STQ DT
98A     CLA 2)
        ADD IG-13
        STO IG-13
99A     CAL *
        XIT (LEV)
        ETM
        CAL (IOH)0
        SLW 1
        CAL (STH)
99D1    NTR 8)FK,0,9
100A    ETM
        NTR IG-37
        NTR IG-13
        LTM
101A    CAL *
        XIT (FIL)
        TRA 80B
        REM
103A    LXD S,1
        LXD S+1,2
        LXD S+2,4
        TRA 1,4
2)      OCT +000001000000
FNAG    OCT +002000000000
```

```
CNE     OCT +201400000000
TWO     OCT +202400000000
6)      OCT +233000000000
7)      OCT +000000077777
        BCD 7I8)   NUMBER8, 7H  STEPINGE ATEP CHAIME ST
 8)FK   BCD 1(25HOT          FORMAT (READ UP)
I       BSS 1
J       BSS 1
CEL     BSS 1
FNO     BSS 1
LAST    BSS 1
TEMP    SYN LAST
     IG EQU 32562
   INCX EQU 32561
   NBCX EQU 32542
  LNTAU EQU 32532
      Z EQU 32434
  ENBCX EQU 32354
     CT EQU 32353
  FIELD EQU 31410
    RHO EQU 30385
      X EQU 29361
      Y EQU 19361
 RF     SYN Z-850
XIT     OPC 002100000000
NTR     OPC 100000000000
        END 0


        REM  F 51 OPUS IV      (SAP ASSEMBLER LANGUAGE)
        FUL  PROGRAM CARD
        MZE ,,6
        OCT                    CHECK SUM
        PZE LAST,,S
        PZE 0
        BCD 1OPUS3
        PZE START
        BCD 1NAME
        PZE NAME
        REM
        REL
        ORG 0
        DEF DATA,13
        REM
        REM  F 51 OPUS IV
        REM
(FIL)   BCD 1(FIL)
(STH)   BCD 1(STH)
(IOH)O  BCD 1(IOH)O
(LEV)   BCD 1(LEV)
S       HTR 0
        HTR 0
        HTR 0
START   SXD S,1
        SXD S+1,2
```

```
        SXD S+2,4
        NOP
        NOP
        TOV *+1
10A     CLA 5)
        STC LCC4
11A     CLA 5)+1
        STO LCC3
12A     CLA IFIELD
 12A1   TZE 18A
        TPL 18A
13A     CLA 5)+2
        STO LCC4
14A     CLA 5)+3
        STC LCC3
18A     STZ TEMP
19A     STZ FEILD
20A     CLA IG-2
21A     STC 51A
        CLA NBOX
        STD 49B
        STD 71B
        STD 75B
        LXD NTOOC,1
22B     SXD C)200,1
23A     CLA TIME
        FAD DT
        STO TIME
        LXD NBOX,2
25A     STZ RHO+1,2
        TIX 25A,2,1
26A     LXD INDX,2
        REM
27A     CLA X+1,2
        FSB Y+1,2
        STO 1)+1
        UFA 6)
        FAD 6)
        CHS
        FAD 1)+1
        STC X+1,2
 28A    TPL 44A
 29A    TZE 44A
30A     FAD ONE
31A     STC X+1,2
44A     LDQ X+1,2
        FMP ENBOX
        FAD 3)+1
        STC FNO
        UFA 6)
        STO FNOO
        FAD 6)
        CHS
        FAD FNO
        STO DEL
        CLA FNOO
```

```
        ANA 6)+1
        ALS 18
        PDX 0,4
47A     ADD I1
        PDX 0,1
49B     TIX *+1,1,**
51A     TXL 54A,2,**
52A     CLA RHO+1,4
        FSB DEL
        FAD 3)+1
        STO RHO+1,4
53A     CLA RHO+1,1
        FAD DEL
        STO RHO+1,1
54A     TRA LOC4
55A     CLA FIELD+1,4
        FSB FIELD+1,1
        STO 1)+1
        LDQ 1)+1
        FMP DEL
        CHS
        FAD FIELD+1,4
        STO FEILD
56A     CLA FEILD
        FAD GAMMA
        FSB TEMP
        LRS 0
57A     SSP
58A     SUB LNTAU
60A     LLS 0
61A     FAD Y+1,2
62A     STO Y+1,2
        REM
63B2    TIX 27A,2,1
66A     TRA LOC3
67A     LXD NBOX,1
        REM
67B     SXD I,1
 68A    CLA RF+1,1
        STO FIELD+1,1
        LXD NKERN,2
70B     SXD J,2
70A     CLA I
        ADD J
        PDX 0,4
71B     TIX *+1,4,**
73A     CLA I
        SUB J
        ADD NBOX
74B     PDX 5,1
75B     TIX *+1,1,**
78A     CLA RHO+1,4
        FSB RHO+1,1
        STO 1)+1
        LDQ Z-99,2
```

```
        FMP 1)+1
        LXC I,1
        FAD FIELD+1,1
        STO FIELD+1,1
        TIX 70B,2,1
        REM
        TIX 67B,1,1
79A     LXC C)200,1
        TIX 22B,1,1
        REM
80B     LXC INDX,7
        CLA YLIMIT
        SSP
81B     LDC Y+1,2
        LRS 0
        TLQ *+2
        TRA 90A
        TIX 81B,2,1
        TRA 103A
90A     CLA Y+1,1
        FDP 3)+2
        STQ Y+1,1
        TIX 90A,1,1
91B     LXA 74B,1
92A     CLA Z-138,1
        FDP 3)+2
        STQ Z-138,1
        TIX 92A,1,1
93A     CLA LNTAU
94A     SSP
95A     ADD FNAG
96A     STO LNTAU
97A     CLA DT
        FDP 3)+2
        STQ DT
98A     CLA 2)
        ADD IG-13
        STO IG-13
        CLA IG-37
        ADD I1
        STO TEMP
99A     CAL *
        XIT (LEV)
        ETM
        CAL (IGH)0
        SLW 1
        CAL (STH)
99D1    NTR 8)FK,0,9
100A    ETM
        NTR TEMP
        NTR IG-13
        NTR 32353           DELTAT
        NTR 32532           LNTAU
        NTR 32532           ..
        LTM
101A    CAL *
```

```
        XIT (FIL)
        TRA 80B
103A    LXD S,1
        LXD S+1,2
        LXD S+2,4
        TRA 1,4
        REM
NAME    CAL *                   PRINT SUBROUTINE NAME + DATE
        XIT (LEV)
        ETM
        CAL (ICH)0
        SLW 1
        CAL (STH)
        NTR 8)FL,0,9
        ETM
        NTR ANAME
        NTR ADATE
        LTM
        CAL *
        XIT (FIL)
        TRA 1,4
        REM
5)      TRA 55A
        TRA 67A
        TRA 56A
        TRA 79A
        TRA 33A
        TRA 44A
2)      OCT +00000100000C
        OCT +00200000000C
3)      OCT +20040000000C
        OCT +20140000000C
        OCT +20240000000C
6)      OCT +23300000000C
        OCT +000000077777
        OCT +00000000000C
        OCT +00000100000C
        OCT +00000000000C
        BCD 9I6)   4H OR  =013, LNTAU5.7,8HDT =E1I4,5H H NC. EPI4,5
        BCD 4TER STVED AFCT HAL******
 8)FK   BCD 1(28H**             FORMAT (READ UP)
        BCD 4A6)   4H OF US A6,SES OP
8)FL    BCD 1(11HOU            FORMAT (READ UP)
ANAME   BCD 1IV S              ASSEMBLY NAME
 ADATE  BCD 1052862
1)      BSS 10
DATA    PZE 0
IHF     SYN 3)
CNE     SYN 3)+1
I1      SYN 2)
FNAG    SYN 2)+1
     IX EQU 29361
    IRF EQU 32529
   INDX EQU 32561
     IG EQU 32562
```

```
IFIELD EQU 32540
 GAMMA EQU 32355
 FIELD EQU 31410
 ENBCX EQU 32354
    DT EQU 32353
   BBB EQU 30386
LN2NBX EQU 32533
 LNTAU EQU 32532
  NBCX EQU 32542
 NKERN EQU 32530
 NTCDC EQU 32528
   RHO EQU 30385
  TIME EQU 32425
     X EQU 29361
YLIMIT EQU 32345
     Y EQU 19361
     Z EQU 32434
 RF    SYN Z-850
XIT    OPC 002100000000
NTR    OPC 100000000000
LAST   SYN DATA+30
       END 0


       REM PATCH                (SAP ASSEMBLER LANGUAGE)                DCRY
       REM PATCH FOR IOH FOR USE WITH F 51 SUBROUTINE =PLRXY=
       REL PRECLUDES USE OF OCTAL INPUT FEATURE OF IOH)I
       ORG 609                CAUSES ZERO INTEGER TO PRINT AS BLANK
       HPR 3,3                STOP BECAUSE OCTAL INPUT CALLED
       TRA **+800             PUSH START TO IGNORE DATA
       ARS 18                 PATCH TO TEST INTEGER FOR ZERO
       TNZ **+769             NOT ZERO  CONTINUE
       TXI **+782,4,-2        ZERO--FOOL FORTRAN
       REM
       ORG 768
       TRA **+609             GO TO PATCH
       END 0


       REM INTERROGATE SENSE SWITCHES--FORTRAN SUBROUTINE
       REM ALLOWS SIMPLIFIED USE OF THE FULL 64
       REM POSSIBLE SETTINGS. CALLING SEQUENCE IS
       REM        CALL SWITCH (INTGER)
       REM INTGER IS REPLACED BY AN INTEGER AS FOLLOWS
       REM       INTGER(DEC) (OCT)   SWITCH SETTINGS
       REM                 0     0        UUUUUU
       REM                 1     1        UUUUUD
       REM                 2     2        UUUUDU
       REM                 3     3        UUUUDD
       REM                 8    10        UUDUUU
       REM                32    40        DUUUUU
       REM                63    77        DDDDDD
       FUL                      PROGRAM CARD
       MZE ,,4
       PZE 0
       PZE SWIT+16
```

```
        PZE 0
        BCD 1SWITCH
        PZE SWIT
        REM
        REL
        REM
        ORG 0                    PROGRAM
SWIT    SXD SWIT+15,1
        LXA SWIT+15,1
        CLA 1,4
        STA SWIT+5
        STA SWIT+9
        STZ **
        CLA SWIT+14
        PSE 119,1
        TRA SWIT+10
H       ORS ES
        ARS E
        TIX SWIT+7,1,1
        LXD SWIT+15,1
        TRA 2,4
        PZE ,,32
        PZE 6,,**
E       EQU 1
ES      SYN **
        END SWIT


        REM F51 TAPE HANDLING (SAP LANGUAGE)                          DORY
        FUL PROGRAM CARD
        MZE ,,6
        PZE
        PZE LAST,,FIRST
        PZE
        BCD 1TAPES
        PZE FIRST
        BCD 1BELL
        PZE BELL
        REL
        REM
        ORG 0
PRINT   BCD PRINT
FIRST   SXD X1,1
        SXD X2,2
        SXD X4,4
        CLA 1,4
        STA *+1
        CLA **
        TZE TAPOUT
        TPL TAPIN
TAPOS   CLA IG-49
        TZE BACK
        TMI BACK
        SLT 1
        TRA A2
```

```
        SLN 1
        TRA 2,4
A0      SLT 1
X1      TXI A2,0,**          OFF
        SLN 1                ON
        BST 2
        BST 2
A1      RTB 2
        CPY LIMBC
        TRA *-1
        TRA A4
        ETT
        TRA A5
X2      TXI A1,,**
A2      REW 2
        SLN 1
        RTB 2
        CPY LIMBC
X4      TXI *+3,0,**
        TRA A3
        TRA A3
        CLA LIMBC
        SUB CODEWD
        TNZ A3
        CPY LIMBC
        TRA A3
        TRA *+2
        TRA A3
        RTB 2
        CPY IG-16
        TRA A1
A3      REW 2
        TSX BELL,4
        TSX PRINT,4
        PZE ,,2
        PZE ,,1
        LDQ *-1
        HPR 2
        TQP A3.5
        REW 2
        WTB 2
        CPY CODEWD
        WTB 2
        CPY TAPE1
        WEF 2
        REW 2
A3.5    SLT 1
        NOP
        TRA AC
A4      BST 2
        BST 2
        RTB 2
        CPY LIMBC
        TRA *-1
        TRA A3
        IOD
```

```
        RTT
        NOP
        TRA BACK
A5      TSX BELL,4
        TSX PRINT,4
        PZE ,,2
        PZE ,,4
        TSX C3.5,2
        TRA TAPOS
CODEWD  BCD 1F51TAP
LIMBC   PZE
IG      EQU 32562
TAPIN   REW IN
        RTT
N1      NOP 1
        RTB IN
        CPY LIMBC
        TRA *+3
        TRA B2
        TRA B2
        CLA LIMBC
        SUB CODEWD
        TNZ B2
        CPY LIMBC
        TRA B2
        TRA *+2
        TRA B2
        RTB IN
        CPY NAME
B0      RTT
N128    NOP 128
        RTB IN
        CPY QID
        TRA *+3
        TRA B0
        ETT
        TRA B3
        CLA QID
        SUB IC
        TNZ B0
        CPY QSTEP
N1024   NOP 1024
N1020   NOP 1020
        CLA QSTEP
        SUB STEP
        TNZ B0
        LXA N128,1
        CPY IG+1,1
        TIX *-1,1,1
        LXA N1024,1
        CPY Z+1,1
        TIX *-1,1,1
        LXA N1,1
        CLA NBOX
        STD *+3
```

```
        CPY FIELD+1,1
        TXI *+1,1,1
        TXL *-2,1,**
        LXA N1,1
        CLA INDX
        STD *+4
        CPY X+1,1
        CPY Y+1,1
        TXI *+1,1,1
        TXL *-3,1,**
        LXA N1020,1
        CPY BANK+1,1
        TIX *-1,1,1
        RTT
        TRA B1
        TRA BACK
B1      BST IN                  TAPE ERROR
        BST IN
        BST IN
        TSX BELL,4
        TSX PRINT,4
        PZE ,,IN
        PZE ,,3
        TRA BO
B2      TSX BELL,4              IMPROPER TAPE
        TSX PRINT,4
        PZE IN
        PZE ,,1
        TRA TAPIN
B3      TSX BELL,4              NOT FOUND
        TSX PRINT,4
        MZE NAME
        PZE ,,5
        TRA TAPIN
IN      EQU 3
NAME    PZE
CID     PZE
CSTEP   PZE
ID      SYN IG
STEP    SYN IG-1
Z       EQU 32434
BANK    EQU 8760
NBCX    SYN IG-20
FIELD   EQU 31410
INDX    SYN IG-1
BANK    EQU
TAPOUT  WTB 2
        CPY IG
        CPY IG-37
        ETT
        TRA C3
        LXA N128,1
        CPY IG+1,1
        ETT
        TRA C3
        TIX *-3,1,1
```

```
        LXA N1024,1
        CPY Z+1,1
        ETT
        TRA C3
        TIX *-3,1,1
        LXA N1,1
        CLA NBOX
        STO *+5
        CPY FIELD+1,1
        ETT
        TRA C3
        TXI *+1,1,1
        TXL *-4,1,**
        LXA N1,1
        CLA INDX
        STO *+6
        CPY X+1,1
        CPY Y+1,1
        ETT
        TRA C3
        TXI *+1,1,1
        TXL *-5,1,**
        LXA N1024,1
        CPY BANK+1,1
        ETT
        TRA C3
        TIX *-3,1,1
        WEF 2
        BST 2
        BST 2
        RTB 2
        CPY LIMBO
        TRA *-1
        TRA C2
        IOC
        RTT
        TRA C2
        CLA QIC
        STC I6-6L
        CLA QSTEP
        STO IG-67
        CLA NAME
        STC IG-17
        TRA BACK
C2      BST 2
        WEF 2
        BST 2
        TRA TAPOUT
C3      BST 2
        WEF 2
        REW 2
        TSX BELL,4
        TSX PRINT,4
        PZE ,,2
        PZE ,,4
```

```
        TSX C3.5,2
        TRA TAPOUT
C3.5    REW 2
        RTB 2
        CPY LIMBO
        TRA *+3
        TRA C4
        TRA C4
        CLA LIMBO
        SUB CCDEWD
        TNZ C4
        CPY LIMBO
        TRA C4
        TRA C4
        RTB 2
        CPY LIMBO
        TRA *+3
        TRA C4
        TRA C4
        CLA LIMBO
        SUB NAME
        TNZ C4
        TSX BELL,4
        PZE ,,2
        PZE ,,6
        TRA C3.5
C4      REW 2
        WTB 2
        CPY CCDEWD
        WTB 2
        CLA NAME
        ADD PZE1
        STO NAME
        CPY NAME
        TRA 1,2
BACK    LXD X1,1
        LXD X2,2
        LXD X3,3
        TRA 2,4
BELL    WPR
        SPR 5
        SPR 10
        TRA 1,4
        END 0
```

APPENDIX III: BOUNDARY TRAJECTORY SPACE CHARGE PROGRAM

Attached is a listing of the program, which is broken into 13 subprograms, of which the first is the main control program. The first 11 subprograms are coded in the Fortran language, except that the one named PLOT has a few symbolic machine language instructions. The last two are coded in the symbolic machine language and would require rewriting for use on a machine other than the IBM 704. The Fortran language part of the code is nominally compatible with the assemblers for machines other than the IBM 704, but the compatibility has not been tested.

The program requires 14 seconds to step 2000 particles once and recompute the field. Roughly one minute was required to record on tape, the output sequence which consists of roughly 400 numbers and four 8-1/2" by 11" graphs. The nominal add time of the IBM 704 is 24μs and the multiply time is 204μs.

The subroutines MURCD2,[28] MU SAVE,[29] MU SIN4/COS4,[30] MU PLOT1,[31] MU HPLOT,[31] MU SYMBOL[31] and MU LPLOT[31] are required. The first of these reads data from cards into core locations specified on the cards and is used for all input data for the program. The second, a generalized version of the subroutine SAVER included

here, saves the status of the computer on a tape if sense switch 1 is off, allowing a run to be temporarily discontinued. The third computes the sine or cosine of 2π times the argument given it, and last four routines convert their input numbers into output data on tape 9 in the form of increments to be plotted on a Calcomp digital plotter.[32] Such a tape may be interpreted on an IBM 4K1401 computer with attached plotter using MU X25.[33]

The reason for the obscure linkage between the present program and the plotting subroutines is one of compatibility. If subroutine PLOT is replaced by MU PLOT,[34] the output is in the form of graphs simulated by printing asterisks on printer paper by the 1401 computer. No digital plotter is then required, but the information density of the output is reduced.

Points or "particles" on the boundaries and "test particles" are carried in the calculations. The difference is that the test particles do not contribute to the azimuthal density $\rho(\varphi)$ or to the field $\mathcal{E}(\varphi)$, and are included only to allow a small sample of the boundary to be regarded in detail. The test particle coordinates at each output time may optionally be printed out. They are also used to control the size of the time step to assure accurate integration of the motion equations.

The main program initializes the data banks, reads the control parameters, controls the sequence of use of the subroutines and performs a few calculations. All sense switch options occur here. These

allow manual control of the program, and are normally all off. Sense switch 1 (SS1) must be off. If SS2 is turned on, the program is interrupted and SAVE is called. If SS3 is on, the number of integration steps completed is printed on-line as is the total charge in the distribution. If SS6 is on, new control parameters are read through the on-line card reader. At the termination of the calculation, the main program calls SAVER which stops the machine.

Subroutine INPUT specifies the initial distribution of boundary particles and test particles from data read from cards. It has two optional forms. The first provides boundaries either of the form $W(\varphi) = A + B_1 \cos(h_1\varphi + \beta_1) + B_2 \cos(h_2\varphi + \beta_2)$, or in the form of a single closed curve whose shape is that of an oval of Casini. The second gives a boundary in the form of a rectangle in the phase space. The number of complete boundaries is variable but less than 11 and the constant value of the distribution function within each closed curve may have different values. The number of particles must be less than 10001 and of test particles less than 1001 but greater than 1.

Subroutine DENSTY calculates $\rho(\varphi)$ at 128 points in the region $-\pi \leq \varphi \leq \pi$. The boundary is taken to be rectilinear between adjacent points. Periodicity is forced, and the first and last points on a boundary are taken to be adjacent and connected by the boundary. The two types of boundaries used are indicated in Fig. 10. One type is closed on itself in the region $-2\pi n \leq \varphi \leq 2\pi n$, where n is a

finite integer, and the other is periodic. The region bounded by a single curve of the second type extends from the line $W=0$ to the line $W=W_B(\varphi)$ which may be multivalued. These boundaries must then occur in pairs, each having the same value of the distribution function.

Subroutine FIELDS computes a kernel from the control parameters, specifies a field bias of the form $-W_S + V \sin \varphi$, corresponding to a radio-frequency acceleration term, and convolutes the density with the kernel to obtain the net field.

Subroutine STEP integrates the motion equations through one time step for either type of particle. In retrospect, it is seen that five multiplications per particle per time step could have been saved by carrying φ in units of $2\pi/128$ rather than 2π. This would be a saving of roughly 10% in over-all operating time.

Subroutine PLOTSS forms graphs of $\rho(\varphi)$ versus φ, and plots the curve formed by the test particles in the phase space, checking first to see that no points fall outside the range of the graph. If this overflow occurs, the scales are increased accordingly. The graph of $\mathcal{E}(\varphi)$ versus φ may also be made and the boundary curves formed by the particles may be plotted.

Subroutine INPRIN writes the control parameters and the density and field values as output records on tape 9. These are interspersed among the plotting records.

Subroutine WTEST checks to see that the largest movement in φ during one integration step lies between specified limits.

Subroutine PLOT forms the plotter output, placing five graphs on one 7-1/2" by 11" area. These five graphs represent the values of one of the output functions at five instants in the evolution of the system. The graphs are labelled with the function name, the run number, and the integration step number of the first graph included. In general, the known behavior of the system allows them to be distinguished. It should be noted that the subroutine HPLOT causes the next output statement encountered to give written information on the graphs rather than output for the printer.

The function subprogram AMAX/AMIN finds the maximum/minimun of a specified array of numbers, more efficiently and easily than Fortran coding allows.

Subroutine SAVER records the status of the computer on tape 1 at the end of a run. If sufficiently interesting, the run may be continued from this point by reloading it from the tape. The format of the tape is: two records for ordinary SAVE records, $2n$ records containing n SAVER records from n runs and an end of file marker. The program does its own bookkeeping except that an end of file must not be the first record on a tape to be converted to a SAVER tape. Access to the n th run may be obtained by reading $2n+1$ records and loading from the tape.

The usual SHARE disclaimer should be appended here: the program has been extensively tested and was found to operate properly on the MURA computer system early in 1962. No other guarantee is justifiable, since these machines are being continually modified by the manufacturer.

```
C     BOUNDARY TRAJECTORY SPACE CHARGE PROGRAM (MURA F51.5)          DORY
      DIMENSION DATA(100), D(100), SIGMA(10), NUMBER(10), PHIT(1000), WT
     D(1000), PHI(10000), W(10000), P(128), E(128)
      COMMON DATA, NBANDS, SIGMA, NUMBER, PHIT, WT, PHI, W, P, E, NCOUNT
     C, INDEX, NDEX, NPLOTS, NCOUNT, A
      EQUIVALENCE (DATA,D), (D(7),TIME)
     E,(D(3),DT)
      DIMENSION DUMMY (20)

      A=0.
      INDEX=1
      NDEX=1
      NCOUNT=0
      NPLOTS=0
      D(18)=1.
      D(19)=1.E+35
      D(20)=-D(19)
      D(23)=0.
      D(24)=0.
      D(46)=2.
      D(50)=1.
 10   CALL MURCD2 (DATA)
      D(21)=0.
      NBANDS=DATA(4)
      NLINES=D(5)
      NPLO=D(45)
      NLAST=D(46)
      IF (A) 60,50,60
 50   SENSE LIGHT 0
      CALL INPUT (W, PHI, INDEX, SIGMA, NUMBER, NBANDS, D, 10000)
      CALL INPUT (WT, PHIT, NDEX, DUMMY, DUMMY, NLINES, D, 1000)
      INDEX=INDEX-1
      NDEX=NDEX-1
      DO  55 I=1,NDEX
 55   PHIT(I)=(PHIT(I)+2.0)-INTF((PHIT(I)+2.0))
      DO  57 I=1,INDEX
 57   PHI(I)=(PHI(I)+2.0)-INTF((PHI(I)+2.0))
 60   CALL DENSTY
      CALL FIELDS
      CALL INPRIN(1)
      CALL PLOTSS
 200  IF(NCOUNT-NLAST)2020,450,450
 2020 CALL WTEST
      DO 210 I=1,128
 210  E(I)=E(I)*DT
      CALL STEP (WT, PHIT, NDEX, DT/6.2831853, E)
      CALL STEP (W, PHI, INDEX, DT/6.2831853, E)
      CALL DENSTY
      CALL FIELDS
      TIME=TIME+DT
      NCOUNT=NCOUNT+1
      NPLOTS=NPLOTS+1
      IF(SENSE SWITCH 3) 380,400
 380  PRINT 501, NCOUNT , D(44)
 400  IF (SENSE SWITCH 2)410,420
```

```
410   D(21)=1.
      CALL PLOTSS
      CALL SAVE
      D(21)=0.
      CALL INPRIN(1)
420   IF(NPLOTS-NPLO) 440,430,430
430   NPLOTS=0
      CALL INPRIN(1)
      IF (D(6)) 437,438,437
437   WRITE OUTPUT TAPE 9, 502, NCOUNT, (PHIT(I), WT(I), I=1,NDEX)
438   CALL PLOTSS
440   IF(SENSE SWITCH 6) 460,200
450   NUMBER(32452)=D(2)
      D(21)=1.
      CALL PLOTSS
      CALL SAVER
      D(21)=0.
      NUMBER(32452)=NUMBER(32452)
      PAUSE 50505
460   A=1.
      GO TO 10
501   FORMAT (5H STEPI10, 1PE15.7)
502   FORMAT (1H I7/(1H 1P10E13.5))
      END (0,1,1,1,0)


C     INPUT                                                          DORY
      SUBROUTINE INPUT (W, PHI, INDEX, SIGMA, NUMBER, NBANDS, D, MAX)
      DIMENSION W(1), PHI(1), SIGMA(1), NUMBER(1), E(1), D(1)
      DIMENSION PR(20)
      WFCNOF(X)=PR(4)-PR(5)*COS4F(PR(6)+PR(7)*X)
     W-PR(8)*COS4F(PR(9)+PR(10)*X)
      CASINIF(X)=U*SQRTF((SQRTF(ALPHA4+((((X-XO)/V)**2)))) +(SQRTF(ALPHA
     F4+((((X-XO)/V)**2))))-1.-((((X-XO)/V)**2)))

      N1=XMINOF(NBANDS,10)
      IF (D(22)) 200,47,200
47    DO 100 N=1,N1
      CALL MURCD2 (PR)
      NPTS=PR(2)
50    NUMBER(N)=NPTS
      SIGMA(N)=PR(1)*D(18)
60    X=-1./FLOATF(NPTS)
65    DX=-X
      DO 90 I=1,NPTS
      X=X+DX
      WU=WFCNOF(X)
      IF(INDEX-MAX) 70,70,90
70    PHI(INDEX)=X
      W(INDEX)=WU
      INDEX=INDEX+1
90    CONTINUE
100   CONTINUE
110   RETURN
200   DO 260 J=1,N1
      CALL MURCD2 (PR)
```

```
      NPT=PR(2)
      NPTL=NPT-1
      NPT2=NPT+NPT
      NPTS=NPT2+NPT2
      IF(INDEX+NPTS-MAX) 201,201,260
 201  SIGMA(J)=PR(1)*D(18)
      NUMBER(J)=NPTS
 202  XO=PR(3)
      XO=XO
      ALPHA4=(PR(11)**4)/4.
      U=PR(12)
      V=PR(13)
      XMAX=V*SQRTF(1.+PR(11)**2)
      DX=XMAX/FLOATF(NPT)
      X=XO
 230  W(INDEX)=CASINIF(X)
      PHI(INDEX)=XO
      N=INDEX+NPT2
      W(N)=-W(INDEX)
      PHI(N)=XO
      N=INDEX+NPT
      MDEX=INDEX
      W(N)=0
      PHI(N)=XO+XMAX
      N=N+NPT2
      W(N)=0
      PHI(N)=XO-XMAX
 240  DO 250 M=1,NPTL
      X=X+DX
      N=MDEX+M
      F=CASINIF(X)
 243  W(N)=F
      PHI(N)=X
      N=MDEX+NPT2-M
      W(N)=-F
      PHI(N)=X
      N=MDEX+NPT2+M
      W(N)=-F
      PHI(N)=XO+XO-X
      N=MDEX+NPTS-M
      W(N)=F
      PHI(N)=XO+XO-X
 250  CONTINUE
 253  INDEX=INDEX+NPTS
 260  CONTINUE
      RETURN
      END (0,1,1,1,0)

C     INPUT          ALTERNATE VERSION                                  DORY
C     INPUT BOUNDARIES ARE RECTILINEAR
      SUBROUTINE INPUT (W, PHI, INDEX, SIGMA, NUMBER, NBANDS, D, MAX)
      DIMENSION W(1), PHI(1), SIGMA(1), NUMBER(1), E(1), D(1)
      DIMENSION PR(20)
      WFCNOF(X)=PR(4)-PR(5)*COS4F(PR(6)+PR(7)*X)
```

```
      W-PR(8)*COS4F(PR(9)+PR(10)*X)

      N1=XMINOF(NBANDS,10)
      IF (D(22)) 200,47,200
47    DO 100 N=1,N1
      CALL MURCD2 (PR)
      NPTS=PR(2)
50    NUMBER(N)=NPTS
      SIGMA(N)=PR(1)*D(18)
60    X=-1./FLOATF(NPTS)
65    DX=-X
      DO 90 I=1,NPTS
      X=X+DX
      WU=WFCNOF(X)
      IF(INDEX-MAX) 70,70,90
70    PHI(INDEX)=X
      W(INDEX)=WU
      INDEX=INDEX+1
90    CONTINUE
100   CONTINUE
110   RETURN
200   DO 260 J = 1, N1
      CALL MURCD2(PR)
      NPT = PR(2)
      NPT2 = NPT+NPT
      NPTS = NPT2+NPT2
      IF (INDEX+NPTS-MAX) 201, 201, 260
201   SIGMA(J) = PR(1)*D(18)
      NUMBER (J) = NPTS
      XO = PR(3)
      XO = XO
      XE = PR(12)
      YT = PR(13)
      PERIM = XE-XO+YT
      NHFTOP = (XE-XO) / PERIM * FLOATF(NPT-1)
      NHFSID = NPT-NHFTOP-1
      DX = (XE-XO) / FLOATF(NHFTOP)
      DY = YT / FLOATF(NHFSID)
      X = XO
      Y = YT
230   W(INDEX) = YT
      PHI (INDEX) = XO
      N = INDEX+NPT2
      W(N) = -YT
      PHI(N) = XO
      N = INDEX+NPT
      MDEX = INDEX
      W(N) = 0
      PHI(N) = XE
      N = N+NPT2
      W(N) = 0
      PHI(N) = XO+XO-XE
      DO 250 M = 1,NHFTOP
      X = X+DX
      N = MDEX+M
      W(N) = Y
```

```
      PHI(N) = X
      N = MDEX+NPT2-M
      W(N) = -Y
      PHI(N) = X
      N = MDEX+NPT2+M
      W(N) = -Y
      PHI(N) = XO+XO-X
      N = MDEX+NPTS-M
      W(N) = Y
      PHI(N) = XO+XO-X
 250  CONTINUE
      X = XE
      Y = YT+DY
      DO 252 M = 1,NHFSID
      Y = Y-DY
      N = MDEX+M+NHFTOP
      W(N) = Y
      PHI(N) = X
      N = MDEX+NPT2-M-NHFTOP
      W(N) = -Y
      PHI(N) = X
      N = MDEX+NPT2+M+NHFTOP
      W(N) = -Y
      PHI(N) = XO+XO-X
      N = MDEX+NPTS-M-NHFTOP
      W(N) = Y
      PHI(N) = XO+XO-X
 252  CONTINUE
 253  INDEX=INDEX+NPTS
 260  CONTINUE
      RETURN
      END (0,1,1,1,0)


C     DENSTY                                                          DORY
      SUBROUTINE DENSTY
      DIMENSION DATA(100), D(100), SIGMA(10), NUMBER(10), PHIT(1000), WT
     D(1000), PHI(10000), W(10000), P(128), E(128)
      COMMON DATA, NBANDS, SIGMA, NUMBER, PHIT, WT, PHI, W, P, E, NCOUNT
     C, INDEX, NDEX
      EQUIVALENCE (DATA,D), (D(7),TIME)
     E,(D(3),DT)
      DIMENSION PT(256)

      SENSE LIGHT 1
      DO 10 N=1,256
 10   PT(N)=0.
      NORG=0
      DO 340 N=1,NBANDS
      NPB=NUMBER(N)
      SIG=SIGMA(N)*3.1415926
 100  DO 330 K=1,NPB
 110  K1=K+1+NORG
      IF (K-NPB) 130,120,120
 120  K1=1+NORG
```

```
130   KK=K+NORG
      PHI1=PHI(KK)
      PHI2=PHI(K1)
145   DELPHI=PHI2-PHI1
      IF (ABSF(DELPHI)-.5) 180,150,150
150   IF (DELPHI) 160,160,170
160   PHI2=PHI2+1.
      GO TO 145
170   PHI1=PHI1+1.
      GO TO 145
180   N1=PHI1*128.+1.
      N2=PHI2*128.+1.
      IF (N1-N2) 200,300,210
200   NMIN=N1
      NMAX=N2
      PHINT=PHI1
      PHIFIN=PHI2
      WINT=W(KK)
      WFIN=W(K1)
      GO TO 220
210   NMIN=N2
      NMAX=N1
      PHINT=PHI2
      PHIFIN=PHI1
      WINT=W(K1)
      WFIN=W(KK)
220   SLOPE=(WINT-WFIN)/(PHINT-PHIFIN)
      XNITAL=PHINT
      YNITAL=WINT
240   EX=(FLOATF(NMIN-1))*.0078125
      DO 270NN=NMIN,NMAX
      EX=EX+.0078125
      IF (PHIFIN-EX) 250,260,260
250   AREA=SIG * (PHIFIN-XNITAL) * (WFIN+YNITAL) * SIGNF(1.,DELPHI)
      GO TO 270
260   YFINAL=WINT+(EX-PHINT)*SLOPE
      AREA=SIG * (EX-XNITAL) * (YFINAL+YNITAL) * SIGNF(1.,DELPHI)
      YNITAL=YFINAL
      XNITAL=EX
270   PT(NN)=PT(NN)+AREA
      GO TO 330
300   PT(N1)=PT(N1)+SIG*DELPHI*(W(KK)+W(K1))
330   CONTINUE
340   NORG=NORG+NPB
      D(44)=0.
      DO 350 K=1,128
      P(K)=PT(K)+PT(K+128)
350   D(44)=D(44)+P(K)
      RETURN
      END (0,1,1,1,0)

C     FIELDS                                                          DORY
      SUBROUTINE FIELDS
      DIMENSION DATA(100), D(100), SIGMA(10), NUMBER(10), PHIT(1000), WT
     D(1000), PHI(10000), W(10000), P(128), E(128)
```

```
      COMMON DATA, NBANDS, SIGMA, NUMBER, PHIT, WT, PHI, W, P, E, NCOUNT
     C, INDEX, NDEX
      EQUIVALENCE (DATA,D), (D(7),TIME),(D(24),NK)
     E,(D(3),DT)
      DIMENSION RF(128)
      DIMENSION CER(50)

      IF (NK) 40,10,40
 10   DO 15 I=1,128
 15   RF(I)=0.
      DO 20 I=1,30
      CER(I)=D(50)*D(I+50)
      NK=I-1
      IF (CER(I)) 20,30,20
 20   CONTINUE
 30   IF (D(48)) 33,40,33
 33   DO 35 I=1,128
 35   RF(I)=D(49)-SIN4F((FLOATF(I)-.5)/128.)*D(47)
 40   DO 100 I=1,128
 50   E(I)=RF(I)
      DO 100 J=1,NK
      I1=I+J
      IF (I1-128) 70,70,60
 60   I1=I1-128
 70   I2=I-J
      IF (I2) 80,80,90
 80   I2=I2+128
 90   I3=I1
      I4=I2
 100  E(I)=E(I)+CER(J)*(P(I3)-P(I4))
      IF (SENSE LIGHT 1) 110,110
 110  RETURN
      END (0,1,1,1,0)


C     STEP                                                              DORY
      SUBROUTINE STEP (W, PHI, INDEX, DT, E)
      DIMENSION W(1), PHI(1), SIGMA(1), NUMBER(1), E(1)

      DO 330 I=1,INDEX
      PHIF=PHI(I)-DT*W(I)
      PHIBAR=PHIF+PHI(I)
 240  IF (PHIBAR) 250,260,260
 250  PHIBAR=PHIBAR+2.
      GO TO 240
 260  IF (PHIBAR-2.) 285,270,270
 270  PHIBAR=PHIBAR-2.
      GO TO 260
 285  IF (PHIF) 290,295,295
 290  PHIF=PHIF+1.
      GO TO 285
 295  IF (PHIF-1.) 305,300,300
 300  PHIF=PHIF-1.
      GO TO 295
 305  PHI(I)=PHIF
```

```
      ENO=64.*PHIBAR+.5
      DEL=ENO-INTF(ENO)
      NO=ENO
 310  IF (NO) 315,315,320
 315  NO=NO+128
 320  NO1=NO+1
      IF(NO1-128) 326,326,323
 323  NO1=NO1-128
 326  FIELD=E(NO)-(E(NO)-E(NO1))*DEL
 330  W(I)=W(I)+FIELD
      RETURN
      END (0,1,1,1,0)


C     PLOTSS                                                          DORY
      SUBROUTINE PLOTSS
      DIMENSION DATA(100), D(100), SIGMA(10), NUMBER(10), PHIT(1000), WT
     D(1000), PHI(10000), W(10000), P(128), E(128)
      COMMON DATA, NBANDS, SIGMA, NUMBER, PHIT, WT, PHI, W, P, E, NCOUNT
     C, INDEX, NDEX
      EQUIVALENCE (DATA,D), (D(7),TIME)
     E,(D(3),DT)
      DIMENSION S(4)

      NSTEP=NCOUNT
      S(2)=0.
 25   BIG=AMAX(P,128)
      SMALL=AMIN(P,128)
      S(1)=129.
      S(3)=MAX1F(BIG,D(14))
      S(4)=MIN1F(SMALL,D(15))
      DO 30 N=1,128
      EN=N
 30   CALL PLOT (9, EN, P(N), S, 1, 0)
      CALL PLOT(9,0,0,S,1,1)
      WRITE OUTPUT TAPE 9, 503, NSTEP, TIME, (S(I), I=1,4), BIG, SMALL
 5    BIG=AMAX(WT,NDEX)
      SMALL=AMIN(WT,NDEX)
      S(1)=1.
      S(3)=MAX1F(BIG,D(10))
      S(4)=MIN1F(SMALL,D(11))
      DO 10 N=1,NDEX
      EX=PHIT(N)
 10   CALL PLOT (9, EX, WT(N), S, 1, 0)
      CALL PLOT (9, 0, 0, S, 1, 1)
      WRITE OUTPUT TAPE 9, 501, NSTEP, TIME, (S(I), I=1,4), BIG, SMALL
      IF (D(9)) 35,15,35
 35   BIG=AMAX(E,128)
      SMALL=AMIN(E,128)
      S(1)=129.
      S(3)=MAX1F(BIG,D(16))
      S(4)=MIN1F(SMALL,D(17))
      DO 40 N=1,128
      EN=N
 40   CALL PLOT (9, EN, E(N), S, 1, 0)
      CALL PLOT(9,0,0,S,1,1)
```

```
      WRITE OUTPUT TAPE 9, 504, NSTEP, TIME, (S(I), I=1,4), BIG, SMALL
 15   IF(D(8)) 16,45,16
 16   BIG=AMAX(W,INDEX)
      SMALL=AMIN(W,INDEX)
      S(1)=1.
      S(3)=MAX1F(BIG,D(12))
      S(4)=MIN1F(SMALL,D(13))
      DO 20 N=1,INDEX
      EX=PHI(N)
 20   CALL PLOT (9, EX, W(N), S, 1, 0)
      CALL PLOT(9,0,0,S,1,1)
      WRITE OUTPUT TAPE 9, 502, NSTEP, TIME, (S(I), I=1,4), BIG, SMALL
 45   RETURN
 501  FORMAT (31H*TEST PARTICLES-STEP TIME SCALEI6,7F10.5)
 502  FORMAT (31H*BNDY PARTICLES-STEP TIME SCALEI6,7F10.5)
 503  FORMAT (31H*     DENSITY   STEP TIME SCALEI6,7F10.5)
 504  FORMAT (31H*     FIELD     STEP TIME SCALEI6,7F10.5)
      END (0,1,1,1,0)


C     INPRIN                                                          DORY
      SUBROUTINE INPRIN(ISH)
      DIMENSION DATA(100), D(100), SIGMA(10), NUMBER(10), PHIT(1000), WT
     D(1000), PHI(10000), W(10000), P(128), E(128)
      COMMON DATA, NBANDS, SIGMA, NUMBER, PHIT, WT, PHI, W, P, E, NCOUNT
     C, INDEX, NDEX
      EQUIVALENCE (DATA,D), (D(7),TIME)
     E,(D(3),DT), (D(23),JAKE)

      WRITE OUTPUT TAPE 9, 501, ISH, JAKE, NCOUNT
      IF (JAKE) 20,10,20
 10   JAKE=D(2)
      PRINT 501, ISH, JAKE, NCOUNT
 20   WRITE OUTPUT TAPE 9, 505, TIME,NCOUNT,NBANDS,INDEX,NDEX,(SIGMA(I),
     1I=1,10),(NUMBER(I),I=1,10)
      WRITE OUTPUT TAPE 9, 502, (DATA(I), I=1,100)
      WRITE OUTPUT TAPE 9, 503, (P(I), I=1,128)
      WRITE OUTPUT TAPE 9, 504, (E(I), I=1,128)
      RETURN
 501  FORMAT(I1,29HBOUNDARY SPACE CHARGE PROGRAM,20X2I10////)
 502  FORMAT (5H0DATA/(1H 1P10E13.5))
 503  FORMAT (8H0DENSITY/(1H 1P10E13.5))
 504  FORMAT (6H0FIELD/(1H 1P10E13.5))
 505  FORMAT(30H TIME STEP NBANDS NBNDRY NTESTF10.5,4I10/16H SIGMA, NO./
     1BAND/1H 1P10E13.5/10I13)
      END (0,1,1,1,0)


C     WTEST                                                           DORY
      SUBROUTINE WTEST
      DIMENSION DATA(100), D(100), SIGMA(10), NUMBER(10), PHIT(1000), WT
     D(1000), PHI(10000), W(10000), P(128), E(128)
      COMMON DATA, NBANDS, SIGMA, NUMBER, PHIT, WT, PHI, W, P, E, NCOUNT
     C, INDEX, NDEX
      EQUIVALENCE (DATA,D), (D(7),TIME)
```

```
      E,(D(3),DT)

      BIGEST=AMAX(WT,NDEX)
 10   IF (BIGEST-D(19)/DT) 50,50,20
 20   DT=DT/2.
 30   IF (BIGEST-D(19)/DT) 40,40,20
 40   RETURN
 50   IF (BIGEST-D(20)/DT) 60,60,40
 60   DT=DT*2.
 70   GO TO 50
      END (0,1,1,1,1)


C     PLOT LINKAGE FOR BSCP AND THIRTY INCH PLOTTER                    DORY
      SUBROUTINE PLOT (NTAPE, EX, WY, S, NO, IND)
      DIMENSION S(4), BANK(200), SW(4), ORG(4), LABL(1)
      COMMON DATA, NBANDS, SIGMA, NUMBER, PHIT, WT, PHI, W, P, E, NCOUNT
     C, INDEX, NDEX, NPLOTS, NCOUNT, A, BANK
      DIMENSION DATA(100), D(100), SIGMA(10), NUMBER(10), PHIT(1000), WT
     D(1000), PHI(10000), W(10000), P(128), E(128)
      EQUIVALENCE (DATA,D), (D(7),TIME), (D(3),DT)

SLOCP DEC 10441
SLOCE DEC 10313
SLOCT DEC 31441
SLOCW DEC 20441
SMASK OCT 77777
SL4   ALF   W*PHI
SL3   ALF   E*PHI
SL2   ALF   WT*PHI
SLABL ALF   P*PHI

      N=N
      IF(N)5,5,60
S5    CLA *57
S     ANA MASK
S     ALS 18
S     STO IWY
      IF(D(21)) 9,9,6
 6    IF (D(21)-1.5) 7,7,220
 7    D(21)=2.
      M=0
      IF (NP) 200,200,140
 9    N=1
      IF(IWY-LOCP) 10,40,10
 10   N=2
      IF(IWY-LOCT) 20,40,20
 20   N=3
      IF(IWY-LOCE) 30,40,30
 30   N=4
      IF(IWY-LOCW) 200,40,200
 40   IF (NP) 50,50,60
 50   ORG(1)=0.
      ORG(2)=7.5
      ORG(3)=7.5
      ORG(4)=7.5
```

```
      NORUN=D(2)
      M=2
      IF (D(9)) 52,54,52
 52   ORG(3)=15.
      M=M+1
 54   IF (D(8)) 56,58,56
 56   ORG(4)=ORG(4)+7.5
S57   CLA WY
      M=M+1
 58   CALL PLOTS (BANK(200), 200, 11.)
 60   IF (IND) 70,70,120
 70   IF (SW(N)) 80,80,110
 80   EXMAX=MAX1F(S(1), S(2))
      EXMIN=MIN1F(S(1), S(2))
      WYMAX=MAX1F(S(3), S(4))
      WYMIN=MIN1F(S(3), S(4))
      IF(N-1) 87,83,87
 83   NP=NP+1
      NDUMMY=NO
      NDUMMY=NTAPE
 87   NPEN=3
      IF DIVIDE CHECK 90,90
 90   AX=10./(EXMAX-EXMIN)
      BX=.5-AX*EXMIN
      AY=6.5/(WYMAX-WYMIN)
      BY=-AY*WYMIN
      IF DIVIDE CHECK 200,100
 100  SW(N)=1.
      IF (NP-1) 110,102,110
 102  CALL PLOT1 (.5, ORG(N), 3, -1)
      CALL PLOT1 (.5, ORG(N)+6.5, 2, -1)
 110  X=AX*EX+BX
      Y=AY*WY+BY
      X=MIN1F(X,10.5)
      X=MAX1F(X,.5)
      Y=MIN1F(Y,6.5)
      Y=ORG(N)+MAX1F(Y,0.)
      IF (ABSF(XLAST-X)-2.5) 113,112,112
 112  NPEN=3
 113  CALL PLOT1 (X, Y, NPEN, -1)
      NPEN=2
      XLAST=X
      GO TO 220
 120  SW(N)=0.
      IF (NP-1) 127,123,127
 123  CALL PLOT1 (10.5, ORG(N), 3, -1)
      CALL PLOT1 (.5, ORG(N), 2, -1)
      HALF=.5
      CALL HPLOT (HALF, ORG(N)-.25, .01)
      WRITE OUTPUT TAPE 9, 501, NORUN, NCOUNT, LABL(N)
 127  IF (NP-5) 200,130,130
 130  M=M-1
      IF (M) 140,140,200
 140  NP=0
      CALL PLOT1 (11.,0,3,1)
```

```
200   N=0
220   RETURN
501   FORMAT(8HBSCP RUNI6,5H PLOTI6,4XA6)
      END (0,1,1,1,0)

      REM FUNCTION SUBPROGRAM AMAX/AMIN (SAP ASSEMBLER LANG.)      DORY
      REM            MAXA(ARRAY,NUMBER)
      REM            AMIN(ARRAY,NUMBER)
      REM            MINA(ARRAY,NUMBER)
      FUL                  PROGRAM CARD
      MZE ,,10
      PZE
      PZE INDEX+1
      PZE
      BCD 1AMAX
      PZE AMAX
      BCD 1MAXA
      PZE AMAX
      BCD 1AMIN
      PZE AMIN
      BCD 1MINA
      PZE AMIN
      REL
      REM FIND MAXIMUM OR MINIMUM OF THE FIRST
      REM NUMBER DATA STORED IN ARRAY THROUGH
      REM ARRAY+1-NUMBER.  AC CONTAINS MAXIMUM OR
      REM MINIMUM AS CALLED AND MQ CONTAINS VALUE
      REM OF INDEX FOR LAST DATUM EQUAL TO MAX OR MIN
      ORG 0
AMAX  SXD IRSAV,1          SAVE A
      CLA 1,4              GET ARGS
      ADD *-1              GET ARGS
      STA INST1            GET ARGS
      STA INST2            GET ARGS
      CLA 2,4              GET ARGS
      STA *+1              GET ARGS
      LXD **,1             NUMBER OF TEST VALUES
      CLS BIG              PUT -BIG IN AC
INST1 LDQ **,1             GET TEST VALUE
      TLQ *+3              Q. ** BIGGER THAN -BIG
      SXD INDEX,1          YES, SAVE INDEX
INST2 CLA **,1             PUT ** IN AC
      TIX INST1,1,1        NO, CONTINUE
      STO RESULT           STORE LARGEST
      ADD BIG              SEE IF -BIG
      TNZ RETURN           IF NOT, FOUND AN ANSWER
IRSAV TXI NONE,,**         IF SO, -0 IN AC, JUNK IN MQ
AMIN  SXD IRSAV,1          SAVE A
      CLA 1,4              GET ARGS
      ADD *-1              GET ARGS
      STA INST3            GET ARGS
      STA INST4            GET ARGS
      CLA 2,4              GET ARGS
      STA *+1              GET ARGS
      LXD **,1             NUMBER OF TEST VALUES
```

```
        LDQ BIG                 PUT +BIG IN MQ
 INST3  CLA **,1                GET TEST VALUE
        TLQ *+3                 Q. ** SMALLER THAN BIG
        SXD INDEX,1             YES, SAVE INDEX
 INST4  LDQ **,1                PUT ** IN MQ
        TIX INST3,1,1           NO, CONTINUE
        STQ RESULT              STORE SMALLEST
        CLS RESULT              SEE IF BIG
        ADD BIG                 IF NOT, FOUND AN ANSWER
        TZE NONE                IF SO -0 IN AC, JUNK IN MQ
RETURN  CLA RESULT              FOUND AN ANSWER-TO AC
        LDQ INDEX               SUBSCRIPT OF ANSWER TO MQ
 NONE   LXD IRSAV,1             RESTORE A
        TRA 3,4                 RETURN TO CALLER
 BIG    OCT 377777777777
RESULT  PZE **,,**
 INDEX  PZE ,,**
        END 0


        REM SUBROUTINE SAVER    (SAP ASSEMBLER LANGUAGE)                DORY
        REM SAVES STATUS OF 704 ON TAPE 1
        REM TWO RECORDS + END OF FILE REPLACE 1ST EOF ON TAPE 1
        REM UNLESS NO EOF FOUND  THEN THESE REPLACE THE 3RD TAPE RECORD
        FUL
        MZE ,,4
        OCT
        PZE FADER+1
        PZE
        BCD 1SAVER
        PZE 0
        REM
        REL
        ORG 0
 SAVE   SXD IX1,1
        SXD IX2,2
        SXD IX4,4
        STO AC1
        ARS 35
        STO AC2
        STQ MQ
        LXA H1,1
        SLT 1
        TXI *+1,1,1
        SLT 2
        TXI *+1,1,2
        SLT 3
        TXI *+1,1,4
        SLT 4
        TXI *+1,1,8
        SXD SLT,1
        CLA WTB
        RTT
        CLA WTD
        STO WRITE
```

```
        DCT
        ARS 2
        ALS 1
        STO DIV
        CLA NOP
        TOV *+2
        CLA TOV
        STO ACOV
        CLA LOW
        TQO *+2
 H8187  PXD 32763,0
        STO FADER
        CLA RTB1
        STO RTB1+1
 REWTB  REW 1
 RTB1   RTB 1
        HTR **
        RTB 1
        CLA TRARD1
        CPY -1
        TRA *-1
        TRA BST1
        ETT
        TRA REWTB-1
        TRA REWTB+3
TRARD1  TRA READ1
 BST1   BST 1
        BST 1
 READ1  RTB 1
        CPY -1
        TRA *-1
        HTR READ1-1
        IOD
        RTT
        NOP
 WTB    WTB 1
        LXA H5,1
        CPY RESTO,1
        TIX *-1,1,1
        LXA H8187,1
        CPY 0,1
        TIX *-1,1,1
 WRITE  HTR **
        CPY 0
        WEF 1
        BST 1
        BST 1
        BST 1
        BST 1
        RTB 1
 CHECK  RTB 1
        CPY -1
 IX1    TXI *-1,,**
        TRA REWTB-2
        REW 1
        IOD
```

```
        RTT
        TRA REWTB-1
        REM
        HPR 0
        REM
IX2     TXI RESTO,0,**
        LXA 0,4
        CPY 2,4
        TXI 1,4,-1
H1      HTR 1
IX4     TXI RESTO,0,**
RESTO   RTB 1
        CPY 0
        CLA WRITE
        DVP DIV
        CLA FADER
        FAD FADER
        CLA *
        ALS 35
        CLA AC2
        ALS 35
        ADD AC1
ACOV    HTR **
LDQ     LDQ MQ
        LXD SLT,1
        SLF
        TIX *+2,1,8
        SLN 4
        TIX *+2,1,4
        SLN 3
        TIX *+2,1,2
        SLN 2
        TIX *+2,1,1
        SLN 1
        LXD IX1,1
        LXD IX2,2
        LXD IX4,4
        TRA 1,4
AC1     HTR **
AC2     HTR **
MQ      HTR **
SLT     HTR 5,0,**
WTD     WTD 1
DIV     HTR **
NOP     NOP
TOV     TOV LDQ
LOW     OCT 010400000000
FADER   HTR **
H5      SYN SLT
        END SAVE
```